Proceedings of the 6th Meeting of Japan CF Research Society

Edited by Hiroshi YAMADA

April 27-28, 2005

Tokyo Institute of Technology, Japan

Preface

This is Proceedings of the 6th Meeting of Japan CF-Research Society, JCF6, which was held at Tokyo Institute of Technology, 27-28 April 2005.

Japan CF-Research Society (JCF) was established in March 1999, with its first scientific and general assembly meeting JCF1 at Osaka, aiming at the promotion of CF researches in Japan and sending information to the world. CF researches stand for investigating new kinds of nuclear reactions which are supposed to take place in the environment of condensed matter. In 1999 to 2004, we could successfully organized JCF meetings JCF1 through JCF5, in almost every year. We started to issue the printed and electronic (via internet) versions of Proceedings of JCF meetings since JCF4.

Submitted papers to JCF6 meeting were peer-reviewed by the JCF Editorial Board (Chairman; Professor Hiroshi Yamada, Iwate University). One or two reviewers were offered to review each of submitted papers, who kindly sent back comments, questions, corrections to authors via Editorial Board. After receiving revised versions, papers were accepted to publish.

The book of Proceedings JCF6 does not necessarily contain all of presentations at the JCF6 meeting. Abstracts of all presentations are available at our web-site http://wwwcf.elc.iwate-u.ac.jp/jcf/ The electronic version of the Proceedings is also available in the same web-site.

CF-Researches in the world is now called as Condensed Matter Nuclear Science (CMNS), since the establishment of the International Society ISCMNS (http://www.iscmns.org/). Accumulation of research efforts by researchers in the world since 1989, especially concrete results obtained in latest reports, has revealed the existence of new nuclear reactions in condensed matter, under strong linkage between nuclear physics and condensed matter physics and chemistry. Clean deuteron-related fusion with ^{4}He ash and cold transmutations of host and added metal nuclei in metal-deuterium and metal-proton systems are actual consequences of latest CMNS studies, both in experiments and theories. JCF has been keeping in touch with linkage and collaboration with ISCMNS and world researchers.

We thank you all participants of JCF6.

Akito Takahashi (Prof. Emeritus, Osaka University), Director-in-Chief of JCF

Hiroshi Yamada (Prof., Iwate University), Chairman of JCF Editorial Board

August 2005

CONTENTS

THEORY

FURTHER STUDIES, ABOUT NEW ELEMENTS PRODUCTION, BY ELECTROLYSIS OF CATHODIC PD THIN–LONG WIRES, IN ALCOHOL-WATER SOLUTIONS (H, D) AND TH-HG SALTS. NEW PROCEDURES TO PRODUCE PD NANO-STRUCTURES.

FRANCESCO CELANI[(1)], A. SPALLONE[(1)], P. MARINI[(2)], V. DI STEFANO[(2)], M. NAKAMURA[(2)], E. TODARELLO[(2)], A. MANCINI[(3)], P. G. SONA[(4)], E. RIGHI[(1)], G. TRENTA[(1)], C. CATENA[(1)], G. D'AGOSTARO[(1)], P. QUERCIA[(1)], V. ANDREASSI[(1)], F. FONTANA[(5)], L. GAMBERALE[(5)], D. GARBELLI[(5)], E. CELIA [(6)], F. FALCIONI[(6)], M. MARCHESINI[(6)], E. NOVARO[(6)], U. MASTROMATTEO[(7)].

(1) INFN-LNF Via E. Fermi 40, 00044 Frascati (Rome)-Italy; (2) EURESYS, Via Lero 30, 00129, Rome-Italy; (3) ORIM Srl, Via Concordia 65, 62100 Piediripa (Macerata)-Italy; (4) Via S. Carlo 12, 20090 Segrate (Milan)-Italy; (5) Pirelli Labs SpA, Viale Sarca 222, 20126 Milan-Italy; (6) CSM SpA, Via di Castel Romano 100, 00129 Rome-Italy; (7) STMicroelectronics SpA, Via Tolomeo 1, 20010 Cornaredo (Milan)- Italy.

Abstract

They were continued, at National Institute of Nuclear Physics, Frascati National Laboratories-Italy, the systematic studies about detection of new elements, some even with isotopic composition different from natural one, after prolonged electrolysis of Pd wires.
The electrolytic solution adopted is the, unusual, used from our experimental group since 1999.
In short, it was a mixture of both heavy ethyl alcohol (C_2H_5OD at 90-95%) and water (D_2O, at 10-5%), with Th salts at micromolar concentration and Hg at even lower concentration (both of spectroscopic purity). The liquid solutions, before use, were carefully vacuum distilled (and on line 100nm filtered) at low temperatures (30-40°C) and analysed by ICP-MS. The pH was kept quite mild (acidic at about 3-4).
The cathode is Pd (99.9% purity) in the shape of long (60cm) and thin wires (diameter only 0.05mm). Before use, it is carefully cleaned and oxidised by Joule heating in air following a (complex) procedure from us continuously improved (since 1995). Before and after use, some pieces of it, about 50% of total length, are ICP-MS analysed.
The anode is a Pt wire (purity>99.99%), 0.250mm diameter.
The cell adopted is usually a borosilicate chemical glass (like SCHOTT-DURAN, Germany), filling volume about 750cc. Recently (since July 2004) an ultra-pure quartz cylinder (volume about 1050cc) was adopted in order to rule out possibilities of corrosion effects from the cell.
The sample older and details of cell are made only of PTFE, as detailed at ICCF10 and ICCF11.

In respect to previous experiments, we made the following progress:
* It was studied, for long time and at a current density about 2 times larger than usual adopted, a solution of light ethyl alcohol and water instead of heavy one. It was used the usual borosilicate glass cylinder.
* It was made a very long experiment (8 months) using the quartz cylinder, "heavy" solutions.
* It was developed an innovative circuitry (under patent procedures) aimed to produce nano-structures at Pd cathode surface during electrolysis. Experiment planned to "emulate" the Y. Arata procedure of Pd nano-particles. Experimentally proved, by D_2 gas, excess loading in respect to thermodynamic limit values.
* It was developed, very recently, a procedure to promote nano-structure since the beginning of experiment, even in a gas atmosphere.
* It was also experimentally demonstrated, for the first time in the world, the effect of "confinement" of D_2 gas (the so called "Preparata effect"): increase of loading, over thermodynamic equilibrium, due to a voltage drop longitudinal to wire length. Work in progress.

** During the Workshop it was discussed, in details, only some of key results obtained.

Keywords: PdDx-Hx, electrolytic hydro-alcoholic solution, Pd thin-long wire, Th-Hg 'transmutation', colloidal silica stabilised nanostructures.

1. INTRODUCTION

1.1. Heavy/light experiments, borosilicate/quartz cells

In order to detect anomalies in Pd-Deuterium systems, and rule-out possible mistakes during measurements, they were performed (at Frascati National Laboratories of National Institute of Nuclear Physics), during the year 2004 two kinds of main experiments, one with almost "light Hydrogen" solution and another with "heavy Hydrogen".
In order to rule out some source of contaminant coming out from the beaker, the light experiment, used as reference one, was performed with the same borosilicate glass used by us from over 4 years. In

total, were made over 8 experiments with deuteride solution (all the previous experimental results, analysed by ICP-MS instruments, were reported also at JCF4, JCF5, ICCF10, ICCF11; Ref. 1).
About the last heavy experiment, we used a new (virgin) ultra-pure quartz glass, properly aged/cleaned by pure, warm, aqua regia solution.

1.2. New interpretation of *all* positive experiments.

Analysing (from a new specific point of view), several "Cold Fusion" experiments that give positive results, we were convinced that almost all worked "well" just because "spontaneous but uncontrolled" growing of nano-structures or fractal at surface.
For what we know, only Yoshiaki Arata (Osaka University, Ref. 2) make some specific experiments with nano-particles. Almost all of the other Researchers, starting even from M. Fleischmann-S. Pons, get such kind of geometry just because by chance. Among others, we considered some of the positive results obtained by: S. E. Jones, A. Takahashi, E. Storms, M. McKubre, F. Celani, A. B. Karabut, G. Preparata-E. Del Giudice-A. De Ninno, G. Miley, V. Violante, Y. Iwamura (Ref. 3), T. Mizuno.

Because the previous reason, we specifically investigated the possible rule of fractal surface (and/or nano-structure at Palladium surface) by the use of an innovative electronic circuitry (developed by our Group) able to induce continuously, ***fresh*** specific geometry during the electrolysis.

2. Cell description and experimental results.

The cell geometry and experimental set-up was detailed in our previous reports, especially at ICCF10 one.

2.1. ICP-MS results.

The results about main new elements, detected by a high resolution ICP-MS, are reported in Tab. 1. The composition of solutions, refillings included during the long experiments, were the following:

a) Light experiment: main solution 750cc (C_2H_5OH 95%, H_2O 5%); $Th(NO_3)_4$ =5cc; Hg_2SO_4 = 7cc.

b) Heavy experiment: main solution: C_2H_5OD=1005cc, D_2O=89cc; $Th(NO_3)_4$=6cc; Hg_2SO_4=8cc; NH_4OD (0.16M), in D_2O=6cc.

Element	Light Exp. Counts	Heavy Exp. Counts	Comments
P	0	**6.4E6**	BKG=4E3
^{39}K	0	1.8E7	BKG=1E6
Cu	2.3E6 63/65=2.20	**2.5E7** **63/65=2.11**	Nat. 63/65 =2.25
Zn	6.2E6	**4.9E7**	
Rb	3.1E4	8.2E4	
^{108}Pd (26.5%)	Normal	**Depleted of 5%**	
Ag	6.5E4	2.6E5	
^{140}Ce(88.5%)	1.86E4	1.31E5	
W	1.16E4	4.42E4	
Tl	80	**900**	
Pb	4.5E5	**1.38E7**	
U	1.1E3	**1.0E4**	
^{195}Pt(33.8%)	4.3E7	10.8E7	Marker Anode dissolution

Tab1. Main new elements detected in light alcohol-water (Pyrex type) and heavy alcohol-water (quartz) cell; all reagents $Th(NO_3)_4$ (at 1mg/ml concentration) and Hg_2SO_4 (10^{-3}M) are in D_2O. BKG and reagents subtracted. 1 Count = about 5E10 Atoms.

2.2. Deuterium self-loading after electrolysis and SEM analysis.

In previous electrolytic experiments we get, several times, evidence (although not fully reproducible) of spontaneous deuterium self-loading, in liquid solution, without applied electrolytic current. The

deuterium was absorbed from the gas dissolved in the solution due to previous electrolysis.
The effect was increased, and made almost reproducible, after prolonged "specially cycled" electrolysis.
The gaseous loading-unloading can be controlled just changing the kind of gas (D_2-->Ar-->D_2-->Ar) dissolved in the solution (Fig.1).

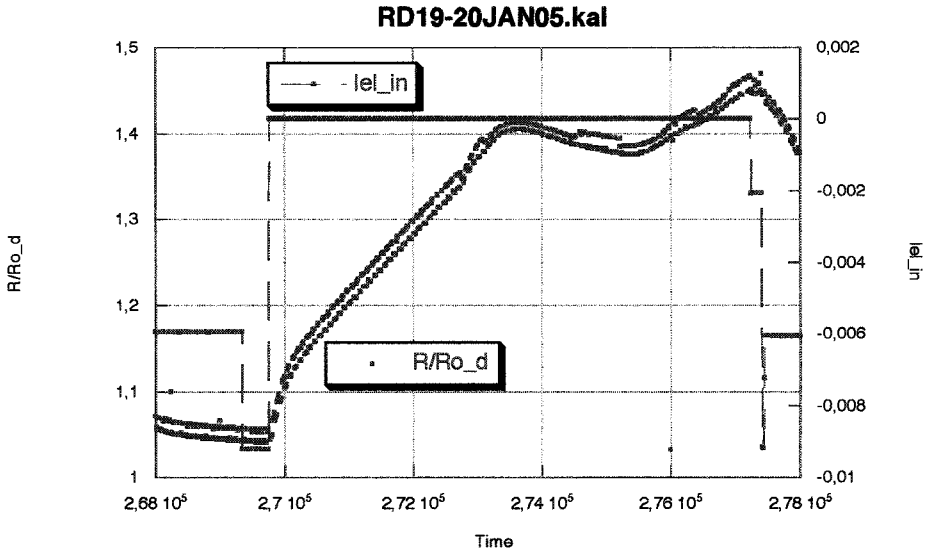

In Fig 1, at time about 269500s, the anodic stripping was ended (the current, from –9mA returned to 0mA). The wire, almost immediately, started to absorb the deuterium dissolved in the solution and the R/Ro increased from about 1.05 to about 1.405. At time 273500s was introduced large amount of Argon gas, by bubbling it inside the solution. Immediately, the R/Ro started to decrease. At time 275500, after the R/Ro decreasing (because Argon effect) from 1.405 to 1.375, it was added again D_2 gas by external bottle. The R/Ro value again increased, showing reversible and controllable effects. At time 277300, when the R/Ro increased to 1.45, was stopped the intake of D_2 and added again Argon. At the least, was made again anodic stripping (at –6mA) in order to deload fully the wire.

We would like to remember that in almost our experiments, since 2003, we introduced an innovative procedure that allows evaluating, together with R/Ro value, the Resistive Thermal Coefficient of Palladium versus the Hydrogen or Deuterium content. Such procedure is based on cyclically injecting, along the wire, a current of low (typically 15mA) and high intensity (typically 120mA). This is the reason because we observe 2 parallel lines in R/Ro measurements.

Moreover, we get experimental evidence of spontaneous self-loading **over the thermodynamic**, well-known, **limit**. In other words, we expected a R/Ro ratio less than 1.8 but we observed a value much larger, close to 1.95—2.0. Such value is equivalent to a deuterium pressure of about 8—10 times larger then 1bar (Fig. 2).

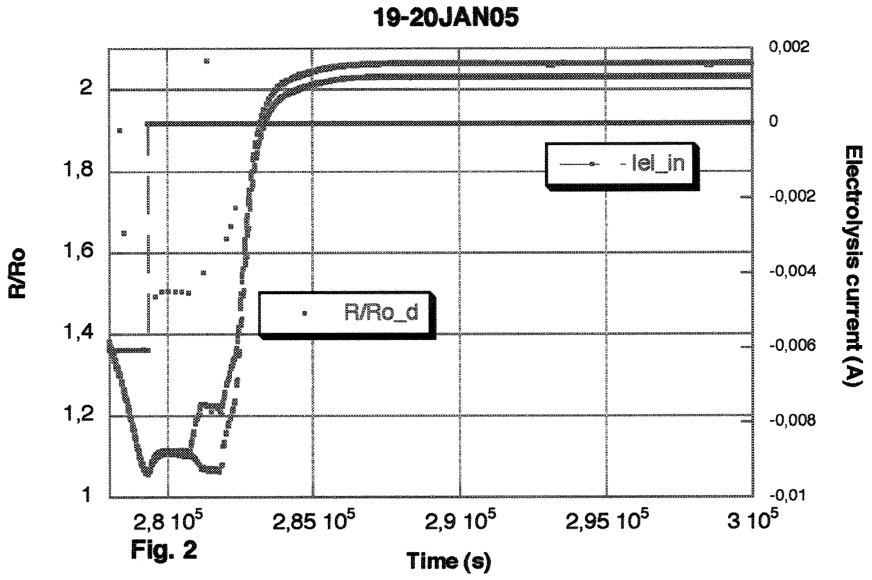

Fig. 2

In Fig.2 it is shown the spontaneous loading by deuterium gas dissolved in solution (time 282000s →over 300000s). At time 279000s was ended the anodic stripping. in Argon atmosphere. At the end of anodic stripping was observed a weak self-loading. Later (time 281000s) was added again Argon, because calibration purposes. At time 282000s was finally added Deuterium gas and self-loading started immediately.

The R/Ro values are >2.0 (time 290000) because effect of residual stress (R/Ro at D/Pd=0 is increased to about 1.05 in respect to 1.00 at time 0 of beginning the experiment). In other words, the wire was deloaded (at time 282000) and intentionally we didn't correct (by mathematic calculation) the value in such experiment because we would like to "monitor" the value of residual stress over time.

In Fig.3, 4, 5, are shown some pictures, by SEM microphotography, of Pd wire before (Fig. 3) and after (Fig.4, Fig. 5) heavy solution electrolysis.

Elemental analysis (by microprobe) of some «white» area of Fig 5 are shown in Fig. 6.

The wire analysed was about 10cm long in respect to 60cm total. The new elements are concentrated at about 15% of total length, in a random like distribution.

It is clearly shown the problem coming out from anode dissolution and its deposit at Pd cathode surface. Such deleterious effect, in respect to H, D absorption in Pd, is not yet solved (despite our deep efforts). We recall that, unfortunatelly, the overvoltage of H,D at Pt surface is close to zero. We are convinced that one of most important reasons of poor Deuterium loading into Palladium, as reprted from several Researchers, is just the Platinum coating (from the anode) at Palladium cathode surface.

It is interesting to note that, apart sensitivity, the some elements are detected from both SEM and ICP-MS. In other words, the ICP-MS results are "safe" and aren't instrumental fakes.

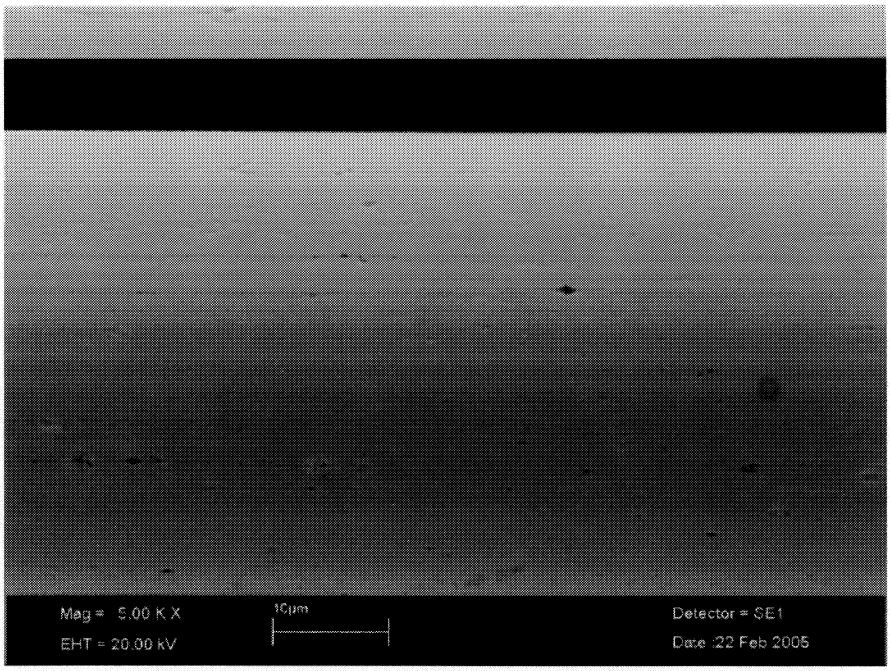

Fig. 3. SEM picture of Pd virgin wire, before electrolysis. The wire is contiguous to used one of Fig. 4.

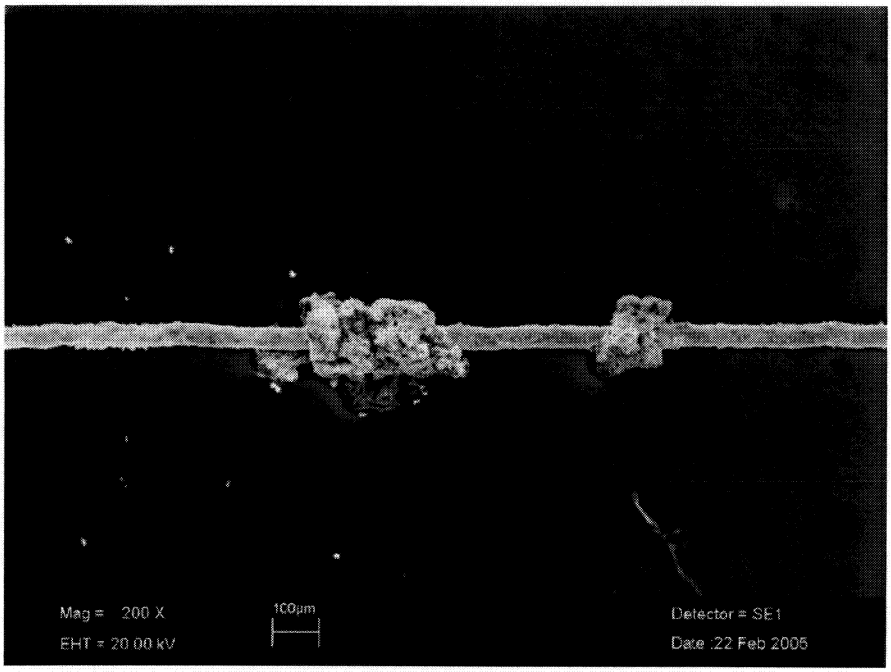

Fig. 4 SEM picture of a used wire, heavy solution electrolysis. The "new" elements and Pt deposit (from anode) are concentrated in few spot area (about 15% of wire length).

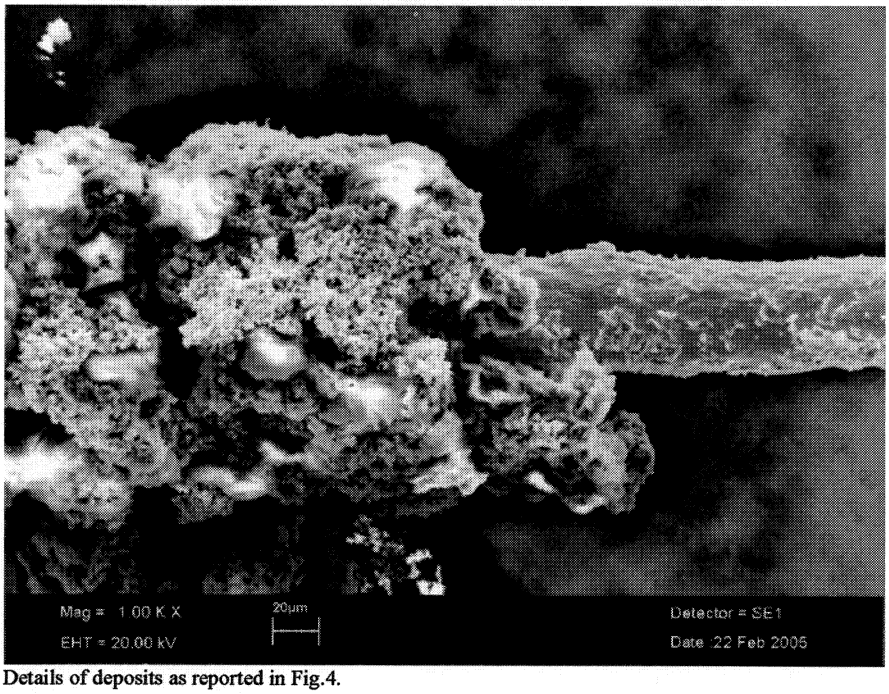

Fig. 5. Details of deposits as reported in Fig.4.

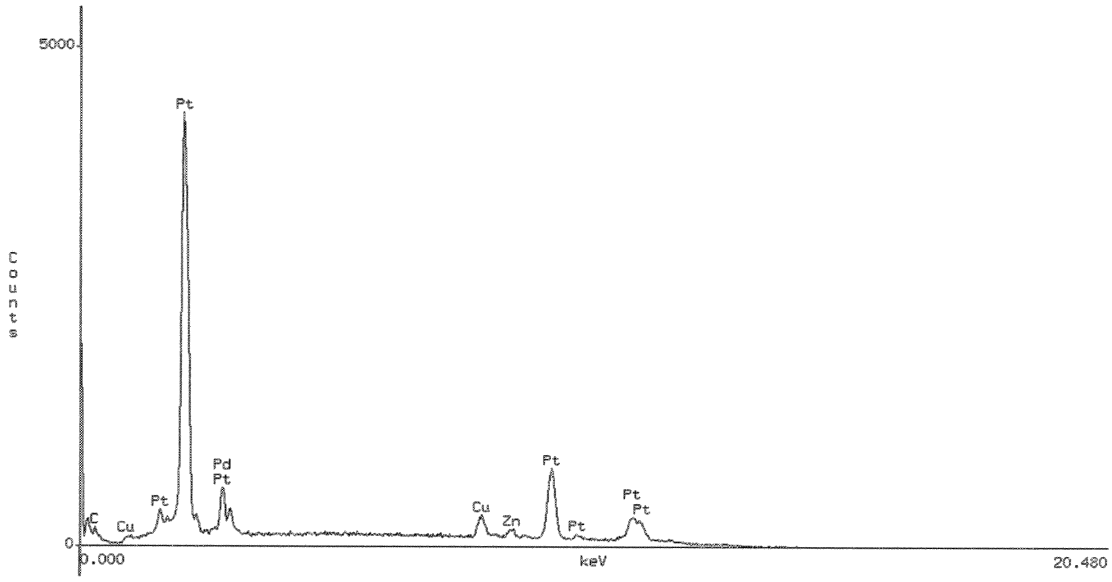

Fig. 6. SEM elemental analysis of one of "white" area has shown in Fig. 5. The, unwanted, large deposition of Pt at Pd surface is clearly detected.. Moreover, also Zn and Cu, detected by ICP-MS analysis, are re-confirmed.

3. Four experiments to understand the effect nanostructure on deuterium absorption

The key points and experimental steps/drawbacks of nanostructure growing can be resumed as following.

3.1. Wire just after electrolysis.

The first experiment started using the wire used for over 6 months in electrolysis which ICP-MS results are reported in tab 1. We emphasise that previous long lasting electrolysis was performed using a new special circuitry to enhance nano-structures (under patent procedure). Electrolysis was performed at low current intensity (5-20mA/cm^2). The operation sequence was as following:

a) Wire overloaded in liquid solution (C_2H_5OD 90%, D_2O 10%) with very few amounts of salt dissolved (about 10mg/liter) was left without electrolysis for few hours.
b) After about 2 hours, the wire was still loaded. In order to unload we applied proper anodic stripping (up to complete unloading, R/Ro=1). When anodic current was removed, we observed that R/Ro increased spontaneously up to about 2.0 in about 10,000s. (note that usual gas loading up to D/Pd=0.75, i.e. R/Ro=2, requires 10atm).
c) The stability was poor: R/Ro decreased from 2.0 to 1.8 (i.e. D/Pd=0.55, equivalent to a gas loading at 1atm) in about 10h.
d) The wire was completely deloaded, in solution, by usual anodic stripping (j=2mA/cm^2).
e) Liquid solution was removed from the cell and the cell was filled by D_2 gas (p=1030mbar).
f) The wire spontaneously loaded up to maximum (R/Ro=2) in 3,000s. See Fig. 2 for further details about.
g) The stability, in respect to point c) improved: R/Ro=2, was maintained stable more than 20h.

* About the self-loading effect described at point b), it is easy to evaluate that the Deuterium dissolved into the solution is enough large to refill the wire after deloading. Although we can't find specific data about deuterided solutions, we can estimate that the reported values on hydrogenated liquids are similar each other between a 20% indetermination.
* The Pd wire used (diameter 0.05mm, length 60cm, density 12g/cm^3, atomic mass about 106g) is equivalent to about 133 microM (Moles=volume*density/atomic mass).
* The solubility in H_2O (at 293K and 1013mbar) of O_2 and H_2, are respectively 31ml/l and 18ml/l (when divided by Avogadro number i.e. 1 Mole=22.4l, such values are equivalent to 1384 and 800 microMole/l). The values in C_2H_5OH are respectively 143ml/l and 80ml/l (equivalent to 6384 and 3571 microMole/l).
* Considering that at the end of experiment, because selective evaporation of alcohol in respect to water, we will have about 950ml of C_2H_5OD and 109ml of D_2O, we can estimate the total amount of D_2 dissolved as following:

- in D_2O, 800 microMole*0.109=87.2 microMole;
- in C_2H_5OD, 3571 microMole*0.950=3392 microMole.

* In conclusion, even supposing that some of the Deuterium dissolved is recombined with Oxygen to heavy water because catalytic effects of Pt anode and Pd itself, the amounts of D_2 dissolved is over a factor 50 larger (i.e. (3392+87)*2/133=52.3) of what necessary to load the Pd wire at a value of D/Pd as large as 1.

3.2. Three other experiments without previous electrolysis.

In order to elucidate the phenomena of large self loading after the end of electrolysis, three different experiments were performed using three different virgin wires never electrolysed.
The samples were coming from the same batch used for our previous electrolytic experiments, i.e. wires with a diameter of 0.05mm and length of 60cm.
Aims of such systematic studies were the promotion of stable (>24h) nano-structures at Pd surface in a way as simple as possible.
There will be shown results about R/Ro loading behaviour versus time.
We anticipate that we obtained both a very large diffusion speed (about 0.5 micron/s) and deuterium concentration over thermodynamic limit. The **improvements** were, respectively, over **1,000** times and about **8** times in comparison to reference one.

3.3. The second experiment

The second experiment started using a virgin wire. Several different tests performed on this wire are detailed in the following:

a) Virgin Pd wire, no acetone washing, only distilled water washing and drying. Loading in D_2 gas at 1030mbar.
b) Time to reach maximum loading (R/Ro=1.82) about 230,000s. Such time doesn't include the "activation time" of virgin Pd (about 60,000s). These values are in agreement with literature results. The results are shown in Fig.7.

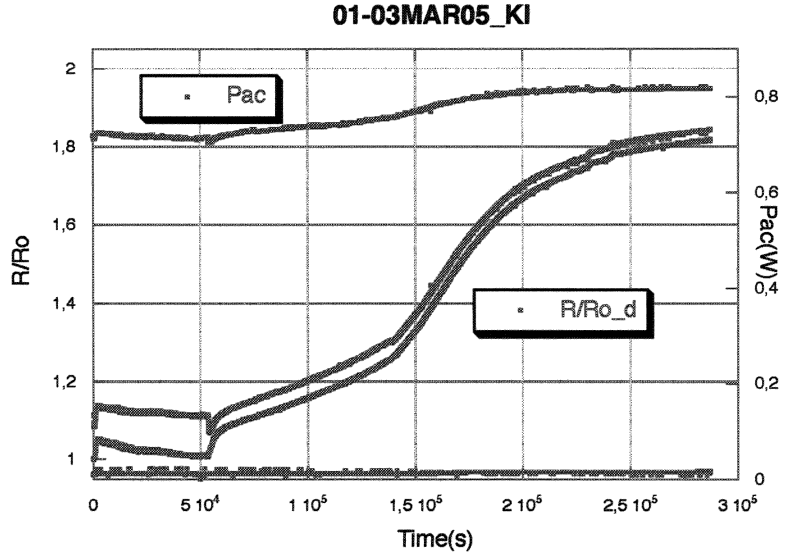

Fig. 7. Loading characteristic of a virgin Palladium wire: loaded at room temperature with 1bar of Deuterium gas. In order to "activate" the Pd surface, it was made a preloading cycle (from time 0 to about 60000s) with D2 gas, 293K, 1 bar and later allowed to decrease, very slowly, the Deuterium content in the cell. Even neglecting the activation time, the time needed to reach the thermodynamic limit of R/Ro=1.82 is as large as 220000s. Such values (i.e. R/Ro and time) are in agreement with data usually reported in the literature. As standard in our procedure from about 2 years, we cyclically inject electromigration ac current (square wave, 10KHz) with low (about 10-15mW) and high power (700-800mW) in order to calculate the Resistive Thermal Coefficient versus D/Pd ratio.

c) Stability (at R/Ro=1.82), is obviously very good: (over 100h) at the thermodynamic limit.
d) Wire deloaded by Joule heating in ^{4}He atmosphere
e) **Colloidal silica was hand-painted ex-situ on the wire surface** (silica characteristic: diameter 3-4nm, normalised surface 500m^2/g,, low sodium content. Specially developed (patenting) for our purposes: fabrication tests started since 2000.
f) Time to reach maximum loading (R/Ro=1.78) about 80,000s. The loading ratio was a little bit worse than the experiment a), Fig. 7, but loading time was about 3 time shorter than a).
g) Please note that applying DC electro-migration current (100mA), after other 20,000s, R/Ro reached 1.86 and was stable (demonstration of ***"Preparata effect"***, although "weak"). Removing electro-migration, after about 20h, R/Ro slowly decreased to 1.82 (usual thermodynamic value). In other words the Preparata effect improved the resistance ratio from 1.82 to 1.86.
h) **Joule heating, i.e. oxidation, of wire in situ** (600°C, 60s, 3 times) in dry ultrafiltered air atmosphere.
i) Time to reach maximum loading (R/Ro=1.95), 600s.
j) Stability over 2h. The wire was again deloaled, without checking long-time stability, in order to check reproducibility of the fast loading.
k) **Another Joule heating, i.e. oxidation, of wire in situ** (600°C, 60s, 3 times) in dry ultrafiltered air atmosphere.
l) Time to reach maximum (R/Ro=1.95), 700s.
m) Stability: at R/Ro=1.95 for about 12h; later, after 15h, R/Ro decreased to 1.93. Please, note that the combined effect of colloidal silica and later oxidation improved largely the loading ratio and the loading time.

3.4. Third wire experiment

The effect of Joule heating oxidation was studied using a new virgin wire. The operations were the following.

a) Virgin Pd wire, acetone washed.
b) **Joule heating, i.e. oxidation, of wire in situ** (600°C, 60s, 3 times) in dry ultrafiltered air atmosphere.
c) Time to reach R/Ro=1.90: 200s.
d) Time to reach R/Ro=1.95: 1,000s.

e) Stability was not excellent at long time: after 20h, R/Ro decreased from 1.95 to 1.93; after 100h, R/Ro decreased to 1.87.
f) No further data allowable: wire broke during operation of D_2 gas refilling (pressure gauge damaged)

3.5. Fourth wire experiment

A new virgin wire was used to check the sequential combined effects of oxidation and silica stabilisation as following:

a) Virgin Pd wire, acetone washed, outside cell:
b) **Joule heating in free air** (600°C, 60s, 3 times)
c) **Painting with colloidal silica in free air**
d) **Joule heating in free air** (600°C, 60s, 3 times)
e) **Painting with colloidal silica in free air**
f) **Joule heating in free air** (600°C, 60s, 3 times).
g) **Operation b-c-d-e-f were performed sequentially in about 30 minute taking care of cleanness.**
h) Wire inserted in the cell
i) Short time Joule heating in dry ultrafiltered air (600°C, 30s, 1 time) in order to burn possible uncontrolled contaminants affecting the wire during the set-up of the experiment
j) **Time to reach R/Ro=1.90: 50s.** See Fig. 8.
k) Time to reach R/Ro=1.95: 300s
l) Stability, at R/Ro=1.95, over 3h.
m) No further data allowable: wire broke during operation of D_2 gas refilling (due to pressure gauge damaged, same problem of experiment 3.4.f).

Please note the "giant" diffusion speed, Calculations give diffusion speed about 0.5 micron/s

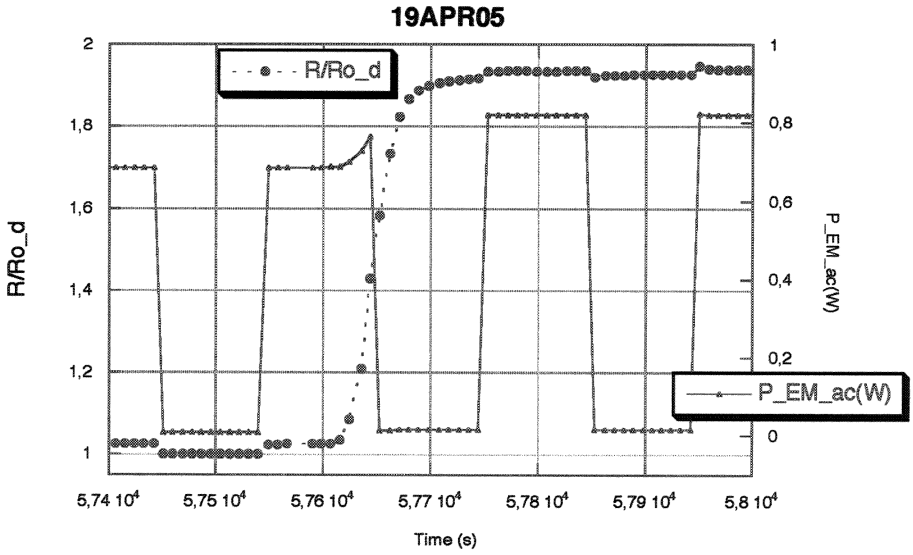

Fig. 8. Behaviour of R/Ro and electromigration AC power in the wire oxidised and painted by colloidal silica, experiment # 4.The time to reach R/Ro=1.90, from beginning of experiment, was as low as (less than) **100 seconds**.

4. CONCLUSIONS

It was found that the anomalous effects, about the amount of new elements detected by ICP-MS analysis, are over one order of magnitude larger in deuteride solution in respect to hydrogenated one.
Moreover, we argued that surface condition of cathode, especially at nanometric size, make a key rule in the production of anomalous effects.
It was exsperimentally proved that it is possible to improve both the diffusion speed of deuterium inside palladium and value of the thermodynamic limit, just providing the surface of a **stabilised nano-metric geometry**. The method that we developed (before oxidation of Pd surface by Joule heating and immediately later stabilisation by colloidal silica of nanometric dimension) looks quite simple and reliable.
The results we found are, obviously, in agreement with the (very impressive) experimental results

obtained by Prof. Yoshiaki Arata at Osaka University (deuterisation of PdO-ZrO powders of nanometric size: subsequent fusion induced by proper triggers like laser or ultrasounds).
About theoretical models, we think that the "Tetrahedral Symmetric Condensation" model developed by Prof. Akito Takahashi (Osaka University, Ref. 4) is a good tool to explain several of our results.
Further, systematic, work is obviously necessary to study the long-term stability of the procedure adopted and the effects due to the increasing the pressure and/or changing the temperature.
Finally, can be very interesting to make some experiments were before the "special" Pd wire (prepared according to such new procedure) is gas loaded and just after the cell is filled with some proper liquid to perform electrolysis.
As a general comment, we are almost optimistic about the fate of Researches named "Condensed Matter Nuclear Science". We feel that some application in real life (like remediation of some radioactive fission products coming out from nuclear power plant) is quite near. Perhaps, a proper "mixing' of the very elegant methods introduced by Dr Yasuhiro Iwamura (at Mitsubishi Heavy Industries) about transmutation of natural Strontium and Caesium and "nanometric point of view" will be the winner in the field of long waited "application" of "Cold Fusion" effects.

5 ACKNOWLEDGEMENTS.

*
We are indebted with Prof. Akito Takahashi (Osaka University) and Dr. Yasuhiro Iwamura (Mitsubishi Heavy Industries, Yokohama) because very detailed discussion on surface effects about Cold Fusion phenomenology.

- Moreover, the critical reading of our manuscript, and patience, of Prof. Hiroshi Yamada and Shinya. Narita (both at Iwate University) were really useful to us.
- The help of Dr. Giannantonio Cibin (at INFN-LNF) about data analysis (by kaleidograph program) was crucial to minimise the "dead time" between experiments.

REFERENCES

1) F. Celani, A Spallone et al. Proc. of ICCF10, 24-29 August 2003:http://www.lenr-canr.org; and JCF4, JCF5 at http://wwwcf.elc.iwate-u.ac.jp/jcf/

2) Y.Arata, Y.Chang Proc. of ICCF10, 24-29 August 2003: http://www.lenr-canr.org

3) Y. Iwamura et al Proc. of ICCF10, 24-29 August 2003: http://www.lenr-canr.org ; and JCF4, JCF5 at http://wwwcf.elc.iwate-u.ac.jp/jcf/

4) A, Takahashi Proc. of ICCF10, 24-29 August 2003: http://www.lenr-canr.org ; and JCF4 , JCF5 at http://wwwcf.elc.iwate-u.ac.jp/jcf/

Novel Reaction Induced by Light Water Critical Electrolysis

Yu TORIYABE, Tadahiko MIZUNO[1], Tadayoshi OHMORI[2], Yoshiaki AOKI[3]

Division of Quantum Science and Engineering, Hokkaido University
1: Division of Energy and Environmental System, Hokkaido University
2: Hokkaido Institute of Technology
3: Technology and Electronics College of Hokkaido
torigoya@pop.qe.eng.hokudai.ac.jp

Abstract

Tungsten and nickel electrodes were critically electrolyzed in 1M K_2CO_3 or Na_2CO_3 solutions for 15 days. After electrolysis, we analyzed electrode surface and deposition in electrolyte by EDX, and we detected a strong platinum peak from both of the samples. Though we have not checked the isotopic ratio for the platinum, the element probably originated from a counter electrode. In general, the Pt anode may not dissolve in alkaline solutions, especially K_2CO_3 or Na_2CO_3 solutions. Nevertheless, the experimental result suggests the novel reaction might be occurred in restricted conditions. Consequently, when we discuss the nuclear transmutation reaction during electrolysis, we should consider the contamination from the counter electrode.

1. Introduction

Since Ohmori et al. reported a nuclear transmutation reaction in his light water electrolysis system[1)], many researchers still have claimed various kinds of low energy nuclear reactions[2~4)]. Yet, it is quite difficult to replicate that reaction on normal electrolysis condition. There are some papers to report a positive correlation between current density and excess heat[5~7)]. If we increased current density (or cell voltage) to get the excess heat or the transmutation products, the normal electrolysis would brake down, and then Plasma Electrolysis would start[8, 9)].

It is well known that, plasma electrolysis can produce a large amount of excess heat, and the nuclear transmutation products. In most cases, this electrolysis, however, cannot continue over 30 min due to the breakage of the cathode material with rare nuclear transmutation products. Therefore Ohmori et al. proposed a new type of electrolysis which is referred to as Critical Electrolysis[10, 11)].

2. Plasma Electrolysis

2.1 Time Variation

Fig.1 shows time variation of current and cell voltage during plasma electrolysis. A tungsten rod (1.5mm diameter, approximately 1cm^2 surface area) is used for the discharge electrode, namely cathode material with 0.2M K_2CO_3 electrolyte solution.

When a temperature of electrode exceeds the boiling temperature of electrolyte due to the intense polarization, a thin vapor layer is formed at the metal / electrolyte interface in which high electric field ionize vapor molecules to generate the plasma state. Generation of this vapor film is the first key factor to achieve the plasma electrolysis condition.

2.2 IV Relation

A current-voltage relation during this electrolysis is shown in Fig.2, which is converted from Fig.1. Axis of ordinates means not only current but also current density because the surface area of cathode is ca. 1cm^2 in this case. If the current density increased over approximately 2.5 A/cm^2, the type of electrolysis could change to the plasma. This critical value also supports the experimental result reported by Ohmori et al[8)].

We defined six electrolysis regions from the start of normal electrolysis to the end of plasma

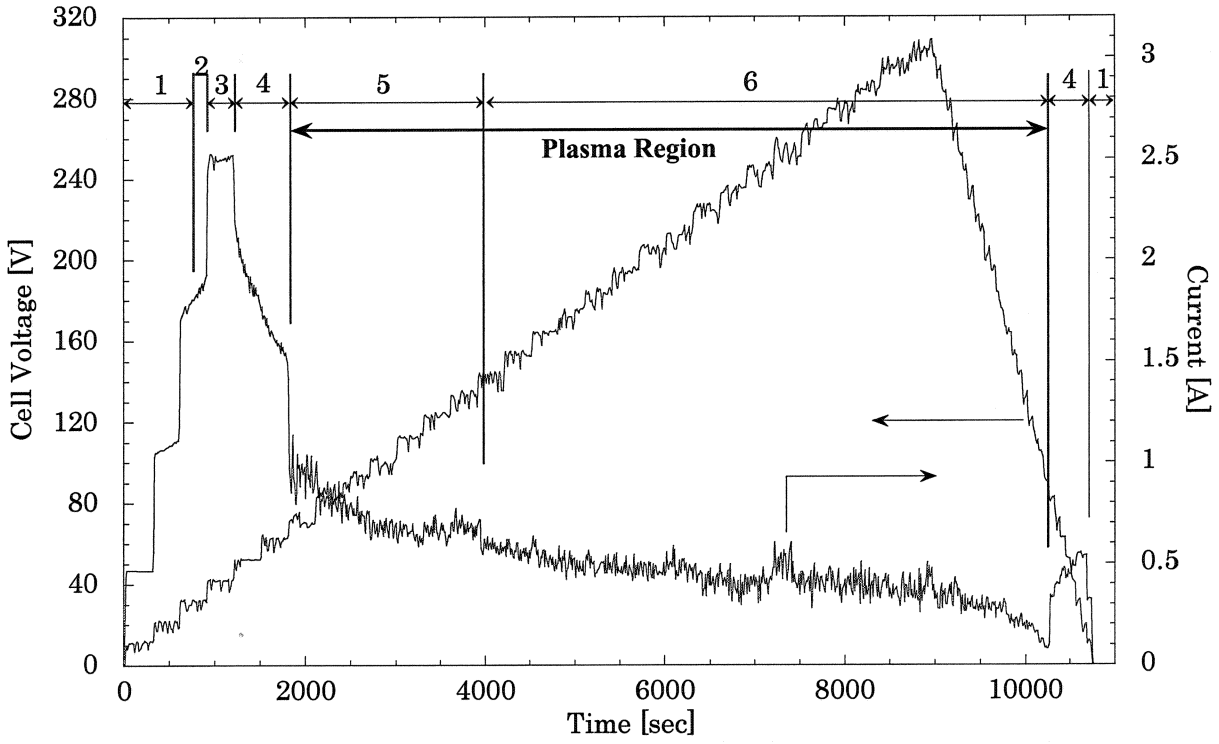

Fig.1 Time variation of cell voltage and current during Plasma Electrolysis; 1, Normal region; 2, Critical region; 3, Breakdown point; 4, Transitional region; 5, Partial plasma region; 6, Full plasma region; region5 and 6 are plasma region in this case.

electrolysis shown in Fig.1 and 2.

Region-1 and 2 are conventional electrolysis regions, which are described at section 3.1. Point-3 is a breakdown point at which the sheath of vapor film is generated. Because the electrolyte cannot touch the electrode directly, current immediately drops down through a transitional region (region-4).

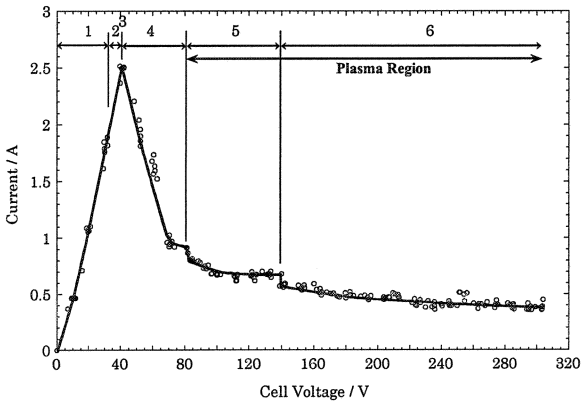

Fig.2 IV relation of plasma electrolysis. This relation is converted from Fig.1 and region 1~6 are same as Fig.1.

If cell voltage is sufficiently high, some atoms or molecules could be ionized (region-5). Thus current doesn't become zero and the electrode temperature can keep high due to the high electro conductivity and the less thermal loss of the gas phase. From this partial plasma region, light emission is occurred, whose color depends on the solution. Light emission area is being expanded with increasing the cell voltage. Finally, this area fill all surface of electrode and the intention of light become strong (region-6). Through this full plasma region, spark discharge with whitish light is happened and sometimes the electrode is melted. We defined these two regions, region-5 and 6, as plasma region.

2.3 Shortcomings

Although the plasma electrolysis usually induces large excess heat and anomalous nuclear transmutation, this type of electrolysis has some and fatal shortcomings.

At the boundary between region-5 and 6, namely at the time when whole area of the

electrode surface is covered with plasma, the temperature of surface rises up to 1,400 degree Celsius. Furthermore local temperature exceeds the melting point of the electrode at the sparks happen due to the generation of current flow paths between the electrode and the electrolyte. Therefore the electrode cannot stand over 30 min without being melted or broken.

This is the most serious problem for plasma electrolysis experiments. Cathode material is required quite high melting point to obtain continuous excess heat. Even if that experiment lasted over 30 min, the rare nuclear transmutation products on the electrode surface, would be lost and the electrolyte solution also would be pyrolyzed.

3. Critical Electrolysis

3.1 Optimum region

In order to evaluate the nuclear transmutation products after any kind of electrolysis, it is required that two conditions, quite low level impurities and an electrode without damage, have to be fulfilled. However, we cannot avoid damage of electrodes after plasma electrolysis.

From the six regions described above, we have to select an optimum region for nuclear transmutation. Here, we suppose that there exist a positive correlation between excess heat and current density, or cell voltage in case of the conventional region, or the plasma region, respectively. Hence, Ohmori et al. specified that region-2 is most favorable region to obtain the excess heat and the transmutation in electrolysis system[10, 11]. They referred to this type of electrolysis as Critical Electrolysis and this region is shown in Fig.3.

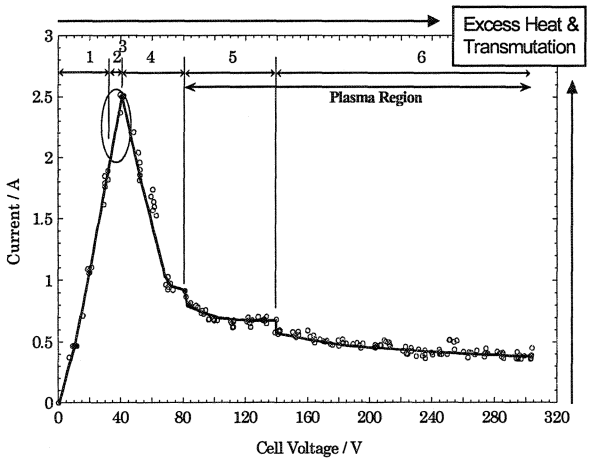

Fig.3 Optimum region for condensed matter nuclear science experiments, Critical region on the Fig.2.

3.2 Experimental Set-up

A schematic view of experimental set-up is shown in Fig.4. In this study, tungsten (99.95%) and nickel (99%) electrodes were used for a critical cathode whose length, diameter, surface area are 5mm, 1.5mm, apparent 0.5cm^2, respectively. Upper area of the working electrode was covered with a Teflon (PTFE) tube. A counter electrode was platinum mesh (50mm × 100mm) welded with 1.6mm platinum wire. An electrolytic cell whose capacity is 300ml, was also made by Teflon (PFA), in which the working and the counter electrode were located at each side.

There were two thermo couples to measure an electrolytic temperature at the center and the edge in the cell. This cell was capped with a

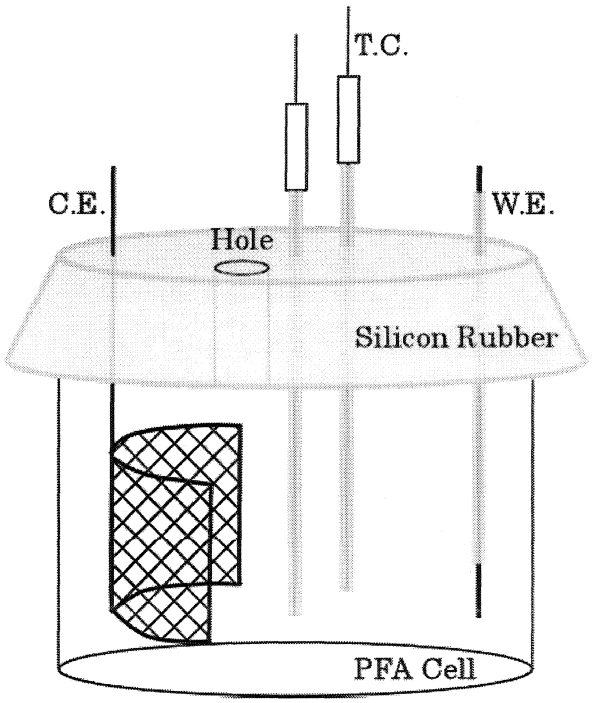

Fig.4 A schematic view of the experimental set-up; the PFA cell, the silicon rubber with a hole, the working and the counter electrode and thermo couples.

silicon rubber to avoid impurities, which has a hole to add water with another silicon rubber.

The electrolyte was 150ml, 1mol/dm^3 K_2CO_3 or Na_2CO_3 (99.95%) solution prepared with Milli-Q water. The cathode materials were washed by acetone and mixed acid (H_2SO_4 and HNO_3) and rinsed by the Milli-Q water, after having been polished up by an emery paper (#1500). The cell was also cleaned by the same routine.

Those electrodes were critical electrolyzed for 15days, namely current density was ca. 2.6 A/cm^2. Although vapor cannot leak from this system, hydrogen and oxygen can easily. Therefore we added Milli-Q water every 24 hours to restore the volume of the solution to the original level, which decreased due to the decomposition.

3.3 Results

During this electrolysis, the current density was kept around 2.6 A/cm^2, and mean voltage was ca. 14V, thus an input power is 20W at maximum, and solution temperature rose up to 81~83 degree Celsius, which depends on the volume of the electrolyte decreasing due to the decomposition.

After electrolysis we analyzed the cathode materials by EDX: Energy Dispersive X-ray Spectrometry. Some black powders that deposited at the bottom of the cell, were collected and also analyzed.

Figure 5 shows the one EDX spectrum before the experiment and spectrums of two different areas after that in the case of tungsten electrode. The detected elements which didn't exist before the experiment, are magnesium, aluminium, copper, and iron that might be the impurities.

Here, it is notable that there are obvious peaks of platinum at shoulders of tungsten peaks, although they are overlapped each other. The detected elements except Pt can be interfused frequently from everywhere. However, it is clear that the Pt is not impurities but an electrodeposition of the counter electrode or the nuclear transmutation.

In order to determine the origin of this Pt, we changed a working electrode from tungsten to nickel, because characteristic X-rays from the nickel cannot overlap with that of the platinum, and fission channels of nickel atoms whose atomic number is smaller than tungsten, are so less than that of tungsten, that analysis of fission products, namely nuclear transmutation products, is greatly simplified if photofission[12] were induced by the critical electrolysis.

The EDX spectrums in the case of nickel electrodes are shown in Fig.6 in which the similar elements to the above case, magnesium, iron, zinc are detected. Furthermore, the amazingly strong platinum peaks from each place, tip and side, are confirmed.

Two certain particles of deposition after the

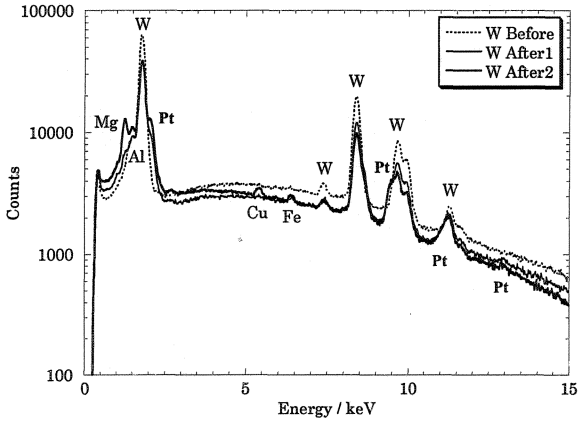

Fig.5 EDX spectrum of tungsten electrode which was analyzed before and after the critical electrolysis. Pt peaks are overlapped with W peaks.

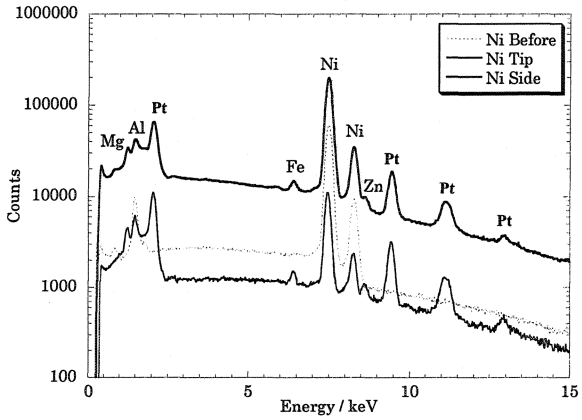

Fig.6 EDX spectrum of Nickel electrode which was analyzed before and after the critical electrolysis. Amazingly strong Pt peaks are detected.

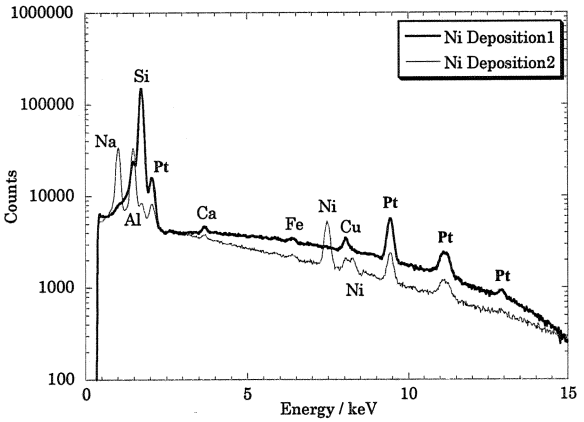

Fig.7 EDX spectrum of depositions after the critical electrolysis. Strong Pt peaks are also detected as Fig.6.

experiment are also analyzed and results are shown in Fig.7. The anomalous platinum peaks are detected from both samples. The elements which are different from that on the electrode, are sodium, silicon, calcium, copper. In particular the peak of silicon is quite high.

Although we didn't check an isotopic yield of the detected elements, those results are clear evidences for the electrodeposition of the counter electrode, the platinum. In general, the platinum anode is seldom, if ever dissolved and electrodeposited in alkali solution, especially in K_2CO_3 or Na_2CO_3 solution, while this reaction is usually occurred in acid. In order to determine the origin of this platinum, the electrode has to be analyzed by other method, for example SIMS which can discriminate the isotopic yields.

It is strongly required to check the isotopic yields of depositions to determine an existence of the nuclear transmutation. Therefore we can't judge the origin, whether the impurities or the transmutations, of all elements deposited in this experiment. Nevertheless we assume that all detected elements may be impurities except for the platinum, which might be the electrodeposition of the counter electrode.

4. Conclusion

Tungsten and nickel electrodes were critically electrolyzed. After the electrolysis, we analyzed the electrode and the deposition by only EDX, and detected strong Pt peak from both of the samples. We assume the Pt would originate from the counter electrode where meniscus was formed at the time the electrolyte decrease abundantly.

However, it is still difficult to conclude that the origin of the deposition, because we have to check the isotopic ratio for the elements and needs a series of experiments. Furthermore, it needs the analysis for the anode electrode. It would be a next subject.

In consequence, when we discuss the nuclear transmutation reaction during electrolysis like the photofission[12], it needs to consider the effect of the counter electrode on the cathode.

References

1) T. Ohmori and M. Enyo, Proceedings of ICCF4, Vol.1, N2.3, 1993
2) T. Mizuno et al., Proceedings of ICCF10, 2003 (not published)
3) Y. Iwamura et al., Jpn. J. Appl. Phys., **41**, 4642, 2002
4) H. Yamada et al., Proceedings of JCF5, 69, 2004
5) T. Ohmori and T. Mizuno, Current Topics in Electrochemistry, **5**, 37, 1997
6) M. C. H. McKubre et al., Proceedings of ICCF3, 5, 1993
7) K. Kunimatsu et al., Proceedings of ICCF3, 31, 1993
8) T. Ohmori Current Topics in Electrochemistry, **7**, 102, 2000
9) T. Mizuno et al., Jpn. J. Appl. Phys., **39**, 6055 2000
10) T. Ohmori et al., Proceedings of JCF4, 22, 2003
11) T. Ohmori et al., Proceedings of JCF5, 36, 2004
12) A. Takahashi et al., Jpn. J. Appl. Phys., **40**, 7031, 2001

A Simple Method to Check the Purity of D_2O at Your Hand

M. Koda* and Y. Takeuchi**
*Independent researcher/music composer, **Kagoshima University
y.takeuchi@ieee.org

Abstract: The purity of D2O is a crucial factor in D2O solution CF experiments. In this paper a simple and reliable method to estimate H2O contamination of D2O is presented with instrumentation. It bases on sound (ultrasound) speed difference in D2O and H2O.

Keywords: D2O, H2O, Purity, Sound Speed.

(1) Problem or issue to be solved:
It has been known that, if the D_2O in experiment is impure less than about 90% to 95%, the experiment turns out all in vain, at large. Fig.1 is a hand sketch of known success rate versus purity of D_2O (1). However, there given is no practical method and means to measure the purity of D_2O instantly in situ. The wanted method (or needle/probe-like device (fig.2)) must be able to check it instantly in situ, as well as without withdrawing and/or contaminating the sample.

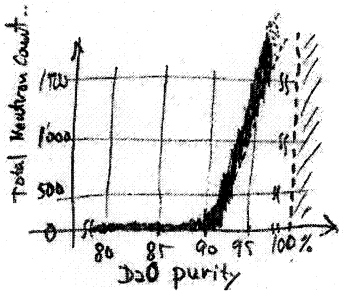

Fig. 1: How bad if D2O is H2O contaminated.

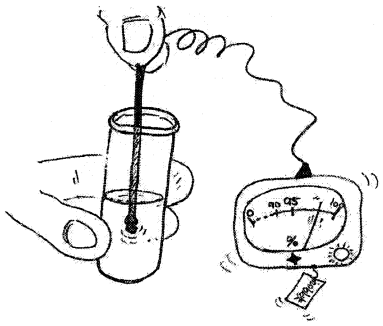

Fig. 2: Wanted D2O purity tester.

(2) Method and its theory of operation:
Since the sound velocity of liquid at given temperature is given likewise;

sound speed is given as; $C = \sqrt{\frac{K}{\rho}}$ C : sound speed, K : volume elasticity, ρ : density

Sound speed C is inverse proportional to density ρ if volume elasticity K remains same. It could be supposed K is common for H2O and D2O because inter-atomic structure and their coulomb force relations are same. Measuring the C allows to suppose ρ, and hence purity of D2O or mixing ratio of D2O and H2O. The known C of D2O and H2O are 1360m/s and 1524m/s respectively at 300K (2)(3), the ratio will make a good inverse-approximation of their densities 1.105 and 1.000, correspondingly.

(3) Experimental Device;
For feasibility study of system concept a small volume (0.06cc+-) parallel wall test chamber (fig.3) is made by clear acrylic resin, which is also ultrasonically transparent. A 2.25MHz 19mm diameter focused concave single element transducer (GE) is placed to make its sound beam at focal zone coincide tangential to the chamber walls. Impulse driven echo displayed on oscilloscope as sketched in fig. 4 is measured for roundtrip sound transit time in between posterilal surface of anterial wall to anterial surface of posterial wall. Since the physical dimention of the chamber is known, sound speed in the material filling the chamber is easily known. In our test three acrylic substrate (t=3m) are stacked with specific adhesive solvent (dichrolomethane) while the middle one having d=5mm hole to form the

test chamber. As seen in photo two of them are jaxtaposed, one for D2O to be evaluated and the other for H2O for reference.

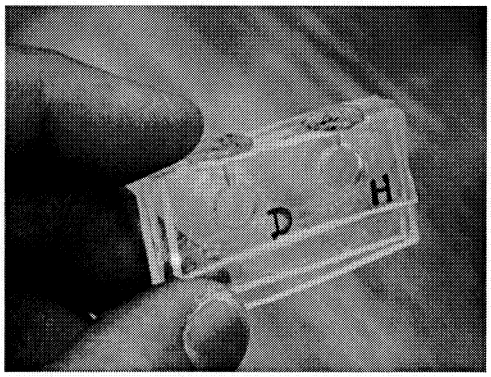

Fig. 3: Chamber assembly. Note that two identical chamber jaxtaposed for D2O and H2O.

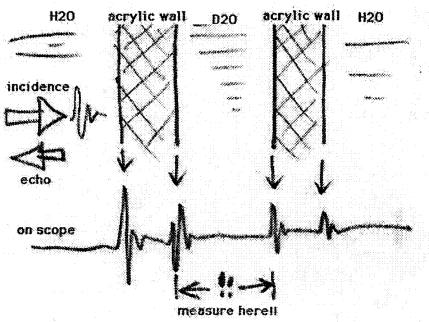

Fig. 4: Method tomeasure echo transit time.

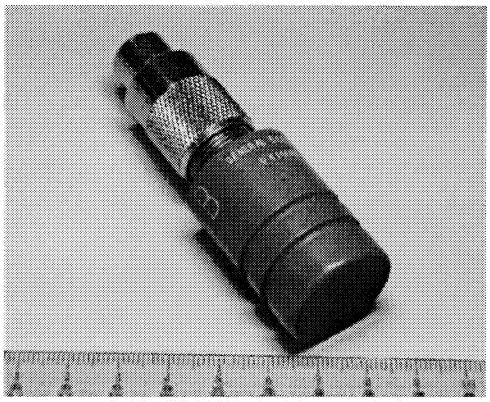

Fig. 5: Single element focused transducer used in this study (General Electric type B)

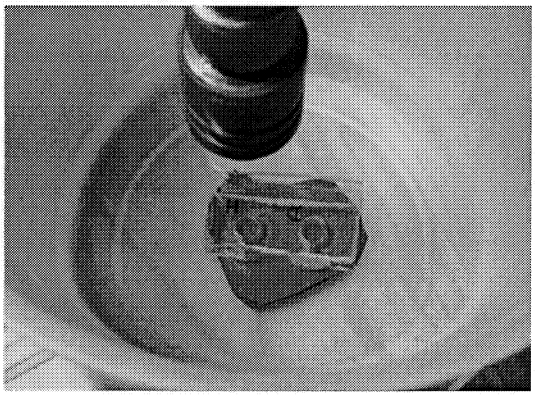

Fig. 6: Measurement setup in water vessel with sound absorber behind the chamber assembly.

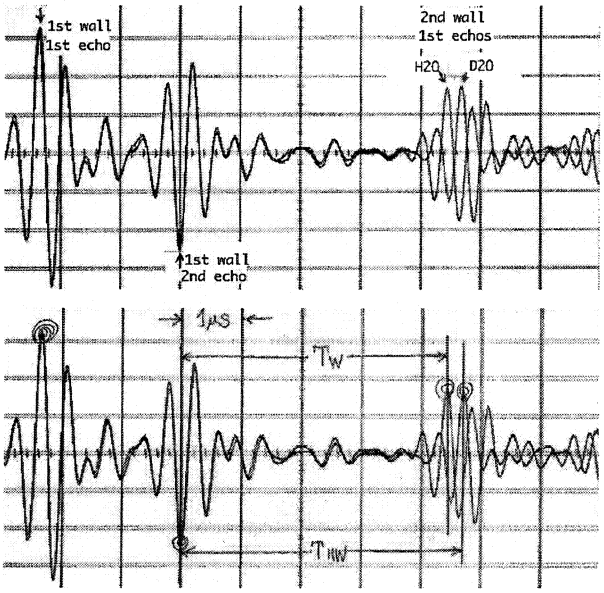

Fig. 7: Detail of echo and intra-chamber transit time measurements for H20 (TW) and D20 (THW).

(4) Result and consideration for instrumentation:
In spite of known old published data @300K(27deg.C) (2)(3),

	Density (g/cc)	C (sound speed)
H2O	1.000	1.524Km/s
D2O	1.105	1.360Km/s

our earliest measurement using this device gives such as;@293K(20deg.C)

	Echo transit time for (3x2=)6mm	C(sound speed)
H2O	TW=4.4369 μS	CW=1.3523Km/s
D2O	THW=4.7016 μS	CHW=1.2762Km/s

This suggests that the measurement itself works, however, with some unknown bias which may need compensation or calibration. Suggestively the chamber size should be measured in situ again exactly. Here the signal to noise ratio (S/N) determines measurement resolution. In simple oscilloscopy it gives at least 40dB or more in transmission drive level 5 to 10Vpp. S/N=40dB corresponds to measurement accuracy or resolution 1%. With medical imaging level signal processing and measurement on this echo it is known to reach to 80 or more dB, 0.01% resolution can be easily available. Since the sound speed difference in between H2O and D2O is about 5% (and is proportional to mixing (=contamination) ratio) 0.01% overall resolution for this 5% corresponds to 0.2% resolution for such contamination. System so far could be said having required capability for contamination measurement.

(6) Cost consideration:
D2O is a very expensive material for pocket-money research challengers, in Japan, costs 200yen/cc as market available 1% class purity lot. The method proposed here needs a needled syringe injection to the 5mm-dia. 3mm span chamber about 0.06cc D2O, the cost is 12 yen a measurement if the D2O is for waste. This could be an acceptable level for our lean-budget challenging laboratories.

(7) Limitation of this method:
Since the sound speed in liquid also depends on temperature and pressure, they must be accurately measured and included in density estimation process. Also it depends on salt or other soluble organic and inorganic materials solved with, the system as is now is applicable to fresh D_2O (and H_2O) only. However, it is expected that a proper data-base for co-existing of other salts will permit the system workable case by case.

(8) Conclusion:
Authors expect that this method will offer another small-but-effective tool for our challenging community to maintain quality of experiment, as expected device outlook sketched like the final figures below.

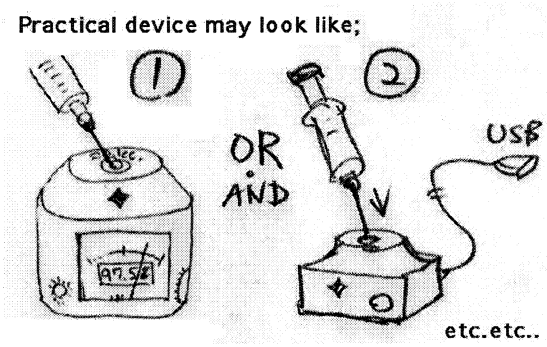

Fig. 8: Practical device may look like such.

(9) Acknowledgement:
Authors thanks for Prof. K. Kishi of the University of Electro-Communication, Chofu Japan for his introduction of oldest generation data of D2O sound speed measurement. This work has been supported privately by authors and their families.

(10) References:
(1) Prof. A. Takahashi, personal communication
(2) C. T. Chen and F. J. Millero, "Speed of sound in deuterium oxide relative to normal water as a function of temperature and pressure": J. Acoust. Soc. Am., 62, 3, pp553-557 (1977)
(3) W. D. Wilson, "Speed of sound in heavy water as a function of temperature and pressure": ibid, 33, 3, pp314-316 (1961)

Anomalous energy and elements generation in conventional electrolysis

Tadahiko Mizuno and Yu Toriyabe, Akito Takahashi[1] and Akihiro Takada[2]
Laboratory of Nuclear and Environmental Materials,Division of Energy and Environmental Systems, Graduate School of Engineering, Hokkaido University, Kita-ku, North 13, West-8, Sapporo 060-8628 JAPAN, Tel:81-11-706-6689, Fax:81-11-706-7835, E-mail:mizuno@qe.eng.hokudai.ac.jp
1; Emeritus Professor of Osaka University
2; Daikin Ind. Ltd.

1.Summary

We have experienced an explosive energy release during conventional electrolysis experiment. The cell was a 1000 cc Pyrex glass vessel that has been in use for 5 years. It contained 700 cc of 0.2M K_2CO_3 electrolyte; a platinum mesh anode; and a tungsten cathode wire 1.5 mm in diameter, 29 cm long, with 3 cm exposed to the electrolyte. The estimated heat out was 800 times higher than input power by the remaining output data. There were many elements deposited on the electrode surface. The major element was Ca, S and the total mol was roughly estimated as 10^{-6}.

2.Introduction

The event occurred in the first stage of the experiment before plasma normally forms. Soon after ordinary electrolysis began, voltage was increased to 20 V and current rose up to 1.5 A. Within 10s later, the cell temperature steeply rose up to 80 degree and a bright white flash was surrounded around the cathode. The light expanded to the solution and at the same instant the cell exploded. The explosion blew off the Plexiglas safety door and spread shards of Pyrex glass and electrolyte up to 5 ~ 6 m into the surrounding area.

The effluent hydrogen and oxygen were mixed in the cell headspace. (Note that the inverted funnel described in Ref. 1 was not in use during this experiment.) There were 2 ~ 3 cc of hydrogen at the time, although this is an open cell so only minimal amounts of gas remain in the headspace. Oxygen gas and hydrogen gas were also mixed in with the electrolyte solution. It is likely that the platinum mesh anode catalyzed the hydrogen and oxygen to recombine rapidly in the electrolyte, triggering the explosion in the headspace.

The vessel was old and may have had a scratch on the inner surface. It is possible that the tungsten cathode may have been exposed to the gas in the headspace.

3.Experiment

3.1 Electrolysis cell

Figure 1 shows the experimental set up. The experimental setup is described in Ref. 1 and 2. We measure many parameters including sample surface temperature, neutron and x-ray emission, mass spectrum of gas, input and output power, and so on. Figure 2 shows the schematic sketch of the cell and gas measurement system [1-2]. The cell is made of the Pyrex glass 10 cm diameter and 17 cm in height and 1000 cc in solution capacity. It is closed with a Teflon rubber cap, 7 cm in diameter. The cap has several holes in it, three for platinum resistance temperature detectors (RTD) (Netsushin Co., Plamic Pt-100Ω), two for the inlet and outlet of the flowing coolant water, and one to hold a funnel that captures the effluent gas from the cathode. The funnel is made of quartz glass, and is 5 cm in the diameter at the top of the cell, and 12 cm in length. Gas leave from the top of the funnel flows and goes into a water-cooled condenser, which is connected to the funnel with another Teflon rubber cap.

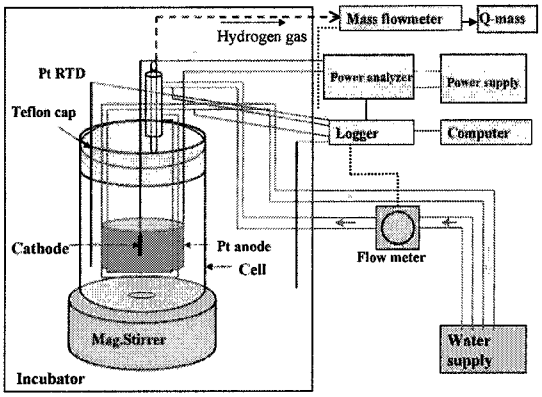

Fig.1 Experimental set up.

We measured several parameters, rate of gas flow, temperature of the sample surface, mass spectrum of gas and input power. Measurement system was described in elsewhere [1,4]. The electrolyte was composed by basic K_2CO_3 solution and the volume was 700cc. Plasma discharge was change by input voltage up to 350V. The gas generated by the plasma discharge was continuously analyzed by the Quadra pole mass spectra system.

3.2 Measurement of hydrogen gas

A mixture of steam, hydrogen and oxygen (from pyrolysis) passes from the cell to the condenser. The steam condenses and falls back into the cell. An 8-mm diameter Tigon tube is coupled with the gas exit of the condenser, connecting it to a gas flow meter (Kofloc Co., model 3100, controller: Kofloc Co., model CR-700).

The flow to voltage transformer element is a heated tube of thermal flow meter system, the minimum detection rate of hydrogen gas flow is 0.001 cc/s, and the resolution is within 1%. The power output from the measurement system was led to the computer through a logger.

After path through the flow meter, the gas goes to a mass spectra analysis system. A small amount of constant volume of the gas such as 0.001 cc/s paths continuously through a needle valve and was analyzed by a quadruple mass analysis method.

The main composition of gas released from the cathode was then continuously analyzed by above-mentioned method.

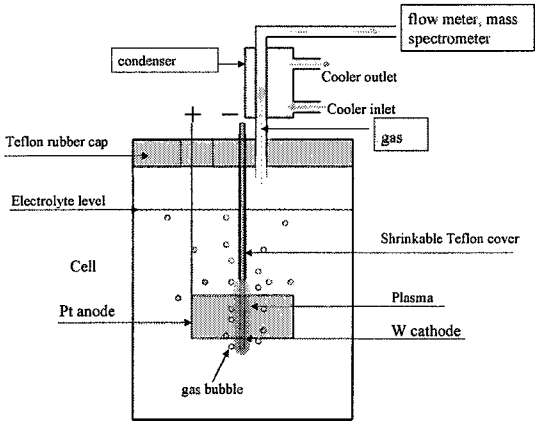

Fig.2 Detail of gas measurement

3.3 Calorimetry

Temperature measurements were made with 1.5 mm diameter RTDs. Calorimetry was performed by combining the flow and isoperibolic method. Flow calorimetry is based on the temperature change of the cooling water. The cooling water is tap water flowing through Tigon tubing. It passes first through a constant temperature bath to keep the temperature constant. From there, it flows through the outer jacket of the condenser, and then through the coil of tubing wrapped around the funnel. (The outside of this cooling water coil is covered with the anode, a platinum mesh). The flow rate is measured with a turbine meter (Japan Flow Control Ltd., model T-1965B). The inlet temperature is measured before the cooling water enters the condenser, and outlet temperature is measured where it exits the cell. Heat from both condensation and glow discharge electrolysis are combined together.

Isoperibolic calorimetry is performed by placing three other RTDs in the cell electrolyte at different depths in the solution to measure the temperature. The solution is mixed with a magnetic stirrer.

Figure 3 shows the notional sketch for heat measurement. Heat out can be divided into several factors. These are energy for water decomposition, heat of electrolyte, heat bring by the coolant, heat releasing from the cell wall and heat releasing with the vapor through the cell plug.

The heat balance is estimated by input and output formulas, input and output power is given in the following equations:

· **Input** (J) = **I** (current) · **V**(Volt) · **t**,
· **Out** = Hg + Hw + HC + Hr,

here,

Hg = Heat of decomposition = $\int 1.48 \cdot dI \cdot dt$

Hw = Electrolyte heat = $\int Ww \cdot Cw \cdot \delta T$; *Ww*:electrolyte weight,*Cw*:heat capacity, δT:temperature difference

Hc = Heat of coolant = $\int Wc \cdot Cc \cdot \delta T$; *Wc*:coolant weight, *Cc*:heat capacity, δT:temperature difference

Hr = Heat release = $\int (Ww \cdot Cw + Wc \cdot Cc) Tr$; *Tr:* temperature change

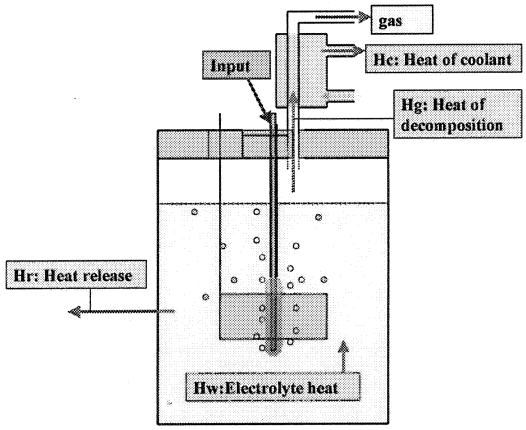

Fig. 3. Schematic representation of heat balance

The heat balance is calculated in straightforward. Input power is only from the electric power source. Output is divided into several parts. The first factor is heat of water decomposition (designated Hg). It is easily calculated from the total electric current. The second factor is electrolyte enthalpy (Hw). It is easily derived from the solution temperature difference. The third factor is heat removed by the coolant (Hc). This is measured from the temperature difference between the coolant inlet and outlet, and the coolant flow rate. The fourth factor is heat release from the cell (Hr). This is rather complicated and can be estimated with a semi-empirical equation. We have measured most of the heat in the condenser directly by monitoring the inlet and outlet temperature of the cooling water that passes through the condenser outer jacket.

If there were various gases, we have to measure the gas composition precisely, because even a small volume of gas generated, it may remove a large amount of enthalpy. This was done with the precision gas flow meter and mass analysis. The first factor, water decomposition (Hg) has a large effect on the rest of the equation.

3.4 Electrode and solution

The electrode is tungsten wire, 1.5 mm in diameter and 15 cm in length. The upper 13 cm of the wire is covered with shrink-wrap Teflon and the bottom 2 cm is exposed to the electrolyte and acts as an electrode. After the electrolysis, the sample wire was consumed. The electrolyte solution was made from high purity K_2CO_3 reagent at 0.2M concentration.

3.5 Power supply

Power supply was used a model of EH1500H made by Takasago Co. Ltd.. The electric power was collected with a power meter (Yokogawa Co., model PZ4000) in every 5 seconds. And the electric power was measured in each 40μs and accumulated for 100k numbers during 5 seconds.

3.6 Data collection

All data, including the mass of cooling water flow from the flow calorie measurement, the temperature of coolant entrance and exit, electrolyte temperature measured by three RTDs, input voltage, current, electric power and the amount of the hydrogen gas generated were collected by a data logger (Agilent Co., model 34970A), and stored in a personal computer.

3.7 element analysis

The sample electrodes and the electrolyte were subjected to element detection by means of energy dispersion X-ray spectroscopy (EDX), Auger electron spectroscopy (AES), secondary ion mass spectroscopy (SIMS) and electron probe micro analyzer (EPMA).

3.8 Mass analysis

The generated gas was continuously analyzed a Quadra –pole mass analysis. Few amount of gas was once introduced into a differential evacuation system and then bring to the mass analysis measurement system. We used mass analysis of Ulvac Rega-201 that is a mass filter type of Quadra-pole mass analyzer. The analyzer can measure mass number from 2 to 400.

4.Results and Discussion

Figure 4 shows changes of input voltage, cell temperature and current for the usually case of

experiment. Input voltage was usually increased as stepwise from 0V to more than 100V and then decreased to 0V. The input current raised usually a maximum value of 4.3A at conventional electrolysis by using the $1cm^2$ area of W electrode, but it usually decreased once plasma started and stayed around 1.6A from 120V to 220V.

The time expanding graph of fig.4 is shown in fig.5. It indicates input voltage, current and temperature changes for the first 250s in the fig.4. Here, input voltage is increased at 182s and reached to 40V at 220s,at the same time, current increased to 1.8A. Meanwhile, electrolyte temperature raise is within 1degree, it can be say almost constant.

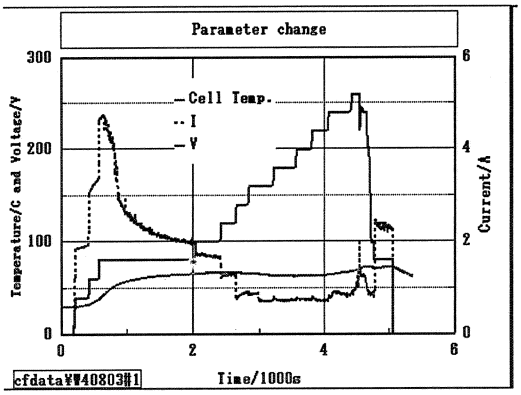

Fig.4 Changes of voltage, cell temp. and current

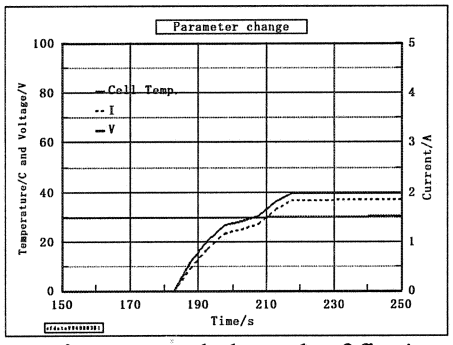

Fig.5 Time expanded graph of fig.4

However, changes of temperature for the case of explosive reaction was differed from the usual experiment. The input voltage and current were supplied by 15V and 1.5A at 40s; that means 22.5W shown in fig.6. The input power was supplied for 10s; total input was roughly calculated as 300J. The electrolyte temperature raise up steeply from 40s to 60s within 20s. After that, the electrolyte cell was broken by steep increase of inner pressure. The heat out was estimated 800 times higher than the input power by the remaining output data.

There were many elements deposited on the electrode surface. The major element was Ca, S and the total mol was roughly estimated as 10^{-6} shown in fig.10.

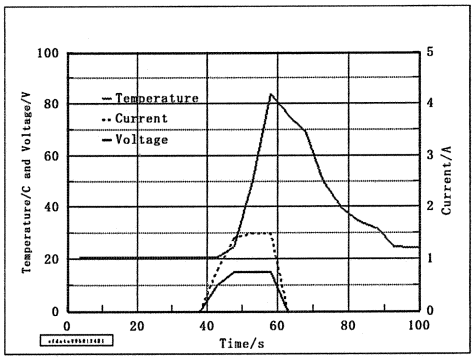

Fig.6 Changes of voltage, cell temp. and current

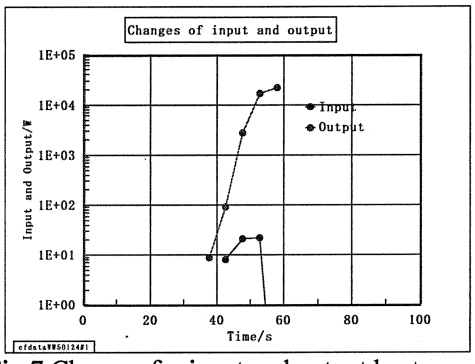

Fig.7 Changes for input and output heat.

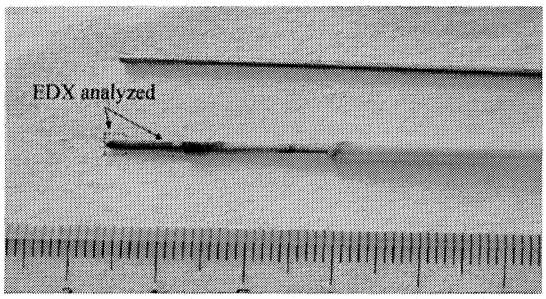

Fig.8 Electrode; above: before, bottom: after

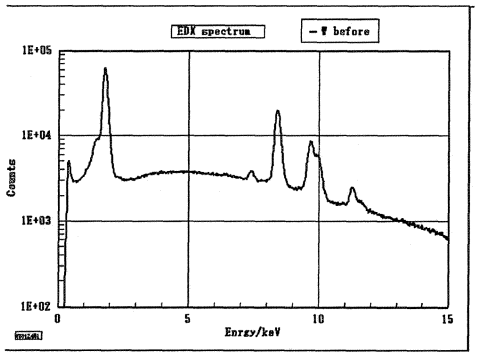

Fig. 9 EDX spectra for before W.

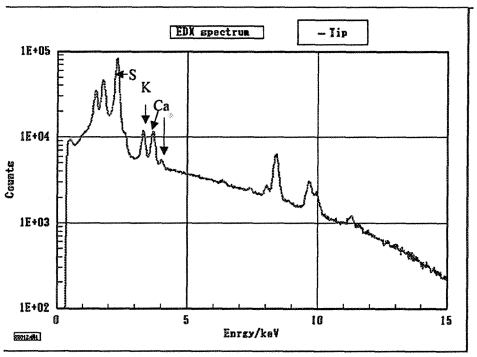

Fig. 10 EDX spectra for after W.

If we can assume the reaction would be occurred by the TSC mechanism, then the reaction products by a typical isotope of tungsten can be shown by follows.

$^{182}W + 4^{1}H \rightarrow {}^{130}Te + {}^{56}Fe + 128.6MeV$
$\rightarrow {}^{136}Xe + {}^{50}Cr + 117.4MeV$
$\rightarrow {}^{138}Ba + {}^{48}Ti + 117.4MeV$
$\rightarrow {}^{142}Ce + {}^{44}Ca + 107.2MeV$
$\rightarrow {}^{154}Sm + {}^{32}S + 79.2MeV$
$\rightarrow {}^{158}Gd + {}^{28}Si + 72.7MeV$

However, it is still difficult to explain the reaction by the mechanism, because of the absence of heavier pair elements.

References

1,Tadahiko Mizuno, Tadayoshi Ohmori, Tadashi Akimoto and Akito Takahashi; "Production of Heat during Plasma Electrolysis in Liquid", Jpn. J. Appl. Phys. Vol.39 (2000) pp.6055-6061.

2,Tadahiko Mizuno, Tadashi Akimoto, Kazuhisa Azumi, Tadayoshi Ohmori, Yoshiaki Aoki and Akito Takahashi, " Hydrogen Evolution by Plasma Electrolysis in Aqueous Solution"; Japanese Journal of Applied Physics Vol. 44, No. 1A, 2005, pp.396-401.

ICP - MS Analysis of Electrodes and Electrolytes after Light Water Electrolysis

S. Taniguchi, S. Shimadu, H. Yamada, S. Narita, T. Odashima*, N. Teshima* and T. Ohmori**

Department of Electrical and Electronic Engineering, Iwate University, Ueda 4-3-5, Morioka, 020-8551 Japan, *t5304007@iwate-u.ac.jp*
*Department of Chemical Engineering, Ichinoseki National College of Technology, Hagiso, Takanashi, Ichinoseki, 021-8511 Japan
**Advanced Technology Inc., Hokkaido Institute Technology, Maeda 7-15, Teineku, Sapporo, 006-8585 Japan

Abstract:

In this study, we carried out light water electrolysis with Pd cathode and Pt anode. The composition of both electrodes and the electrolytes was analyzed by ICP-MS to search for the evidence of the nuclear transmutation. B, Mg, Cu, Zn, Rb and Ba were detected in the analysis as candidates of transmutation products.

1. Introduction

In light water electrolysis experiments, elements production has been reported [1]. In most of them, only the surface composition of the electrodes were analyzed. In addition to analysis of the electrodes, it is desirable to investigate electrolytes since elements on/in the electrodes can be dissolved in it. In this study, both solutions of electrodes and electrolyte were analyzed by ICP-MS.

The sample solution introduced into the ICP-MS should be acid, in general. Then, we utilized HNO_3/H_2O and H_2SO_4/H_2O as electrolytic solution instead of Na_2SO_4/H_2O or K_2SO_4/H_2O, that we previously used in our experiment so that the electrolytes can be directly introduced into the device.

2. Experimental

Figure 1 shows the cell used. The cell is 90 mm in diameter, 110 mm of height and cylindrical shape quartz glass with volume capacity of 550 ml.

The Pd foil (99.95% pure) for cathode is 0.1×5×10 mm in size and the Pt foil (99.98% pure) for anode is 0.1×5×10 mm in size. The gap is about 3 cm. A Pd lead wire (ϕ 1 mm) and a Pt lead wire (ϕ 1 mm) were used for connecting cathode and anode to a power supply, respectively. They were coated with the Teflon heat-shrinkable tube.

Before the electrolysis, the electrodes were washed with acetone and aqua-regia to remove the impurity. The electrolytes used were ultrapure nitric acid (Kanto kagaku, Ultrapure reagent) and ultrapure sulfuric acid (Kanto kagaku, Ultrapure reagent). The volume of electrolyte solution was 500 ml.

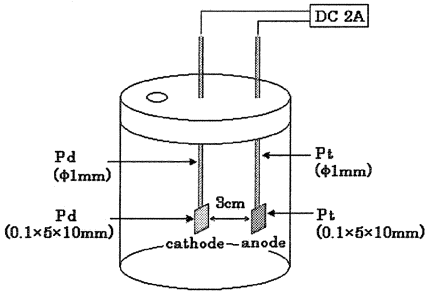

Fig. 1 Electrolysis cell

In the electrolysis, 0.1M HNO_3/H_2O or H_2SO_4/H_2O was used and DC 2 A was applied for 14 days[2]. The cell was replenished with ultra pure water of 100—200ml every day. Table 1 summarizes the condition. We prepared reference sample which was just soaked into each electrolyte for 14 days (we call it "before sample"). The pressure inside cell was kept to be slightly higher than atmospheric pressure during the electrolysis [3].

Table 1 Condition of the electrolysis

Current (A)	Electrolyte	Days
2.0	HNO_3/H_2O	14 days
2.0	H_2SO_4/H_2O	14 days

Table 2 Elements newly detected and increased after HNO_3/H_2O electrolysis

	Pt (before) (ppb)	Pt (after) (ppb)	Pd (before) (ppb)	Pd (after) (ppb)	Electrolyte (before) (ppb)	Electrolyte (after) (ppb)
B	1.170	0.428	0.613	0.622	0.174	94.862
Mg	0.343	4.570	0.189	2.870	-	9.230
Cu	0.134	1.716	0.176	1.522	-	0.406
Zn	0.173	1.463	0.130	17.439	-	5.610
Rb	-	1.301	-	1.157	-	1.288
Ba	-	0.137	-	0.100	-	15.063

The elemental analysis of the electrodes and electrolyte was examined by ICP-MS (SII:SPQ9000). It can detect the most of elements with high sensitivity (ppb to ppt) and measure the density in the sample for specified elements. It can also evaluate the isotopic abundance.

We also analyzed the surface composition of electrode used in HNO_3/H_2O experiment by TOF-SIMS (ULVAC-PHI:TFS-2100). The Ga^+ was utilized as the primary ion. We randomly selected three areas of 40 μm square and measured them. Since the uppermost surface of the sample can be contaminated by many kinds of organic and inorganic compounds in environment, we analyzed those areas after 10 s Ga^+ sputtering to remove such impurities.

3. Results and Discussion

3.1 Electrolysis experiment of HNO_3/H_2O

For ICP-MS analysis, Pd and Pt electrodes were dissolved by 1 ml of ultra pure nitric acid, diluted by 50 times with pure water and sample solutions were prepared. In the electrolysis, a semi-quantitative analysis was done by ICP-MS in this research. Six elements that have been surely detected are shown in Table 2. In our analysis, the signal stands out when the corresponding element exists with the density above 0.1ppb.

Marked increase in density of Mg was observed. For Pt electrode it has increased from 0.343 to 4.570 ppb. For Pd electrode it has increased from 0.189 to 2.870 ppb. For electrolyte it was detected only for the sample after electrolysis. An increase of Zn in the density is also remarkable. For Pt electrode it has increased from 0.173 to 1.463 ppb. For Pd electrode it has increased from 0.130 to 17.439 ppb. For electrolyte it was detected only for the sample after electrolysis as well as Mg. Rb and Ba were also detected after electrolysis in electrodes and electrolyte as shown in Table 2. Especially for electrolytes, a large amount of Ba was detected. Both Rb and Ba hardly exist in the air (Rb: $0.6\text{-}20\times10^{-6}$ ppb and Ba: $0.2\text{-}90\times10^{-6}$ ppb)[4]. Therefore, these elements Rb and Ba are not considered to be impurities from air environment.

Table 3 shows amounts of the Rb and Ba converted by quantitative analysis by ICP-MS. The amounts of Rb and Ba in electrolytes are much more for both electrodes.

Table 3 Rb and Ba density in HNO_3/H_2O and the electrodes

	Pt (after) (μg)	Pd (after) (μg)	Electrolyte (after) (μg)
Rb	3.25	2.89	64.40
Ba	0.34	0.25	753.15

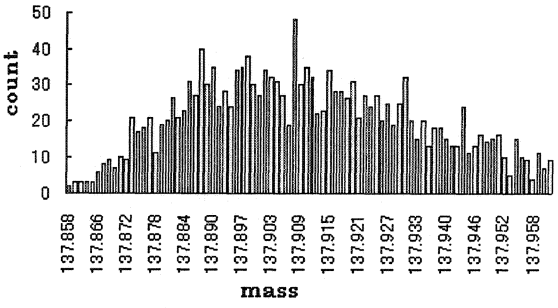

Fig. 2 TOF-SIMS mass spectrum

Comparing weight of electrode between before and after dissolving for processing ICP-MS sample solution, we estimated how deep the electrode dissolved. As a result, we found that about 8.3 μm thickness for "before sample" Pd and 2 μm for Pd after electrolysis were dissolved.

Table 4 Elements newly detected and increased after H_2SO_4/H_2O electrolysis

	Pt (before) (ppb)	Pt (after) (ppb)	Pd (before) (ppb)	Pd (after) (ppb)	Electrolyte (before) (ppb)	Electrolyte (after) (ppb)
B	0.232	1.036	0.229	0.670	0.082	19.551
Mg	0.157	6.894	0.122	3.972	-	10.001
Ti	-	0.031	-	0.024	1.638	756.006
Ni	-	0.122	-	0.110	-	0.373
Cu	0.034	0.841	0.041	1.230	-	54.630
Zn	0.067	1.458	0.043	0.836	0.586	18.549
Pb	0.024	0.058	-	0.300	-	0.161
Rb	-	1.087	-	0.938	-	0.086
Ba	-	0.410	-	0.119	-	3.152

The former value is four times as large as the latter one. If all the elements detected had been contaminants from the Pd, the densities of these elements for electrodes and electrolyte of "after sample" should have been less than those of "before Sample". Thus, it is unlikely that these elements are impurities from Pd electrode.

Figure 2 shows mass spectrum by TOF-SIMS for Pd cathode around mass 138. The peak corresponding to ^{138}Ba was observed. The Ba was thought from this spectrum to exist on the surface of the Pd.

3.2 Electrolysis experiment of H_2SO_4/H_2O

The elements identified by ICP-MS are shown in Table 4. Elements B, Mg, Cu, Zn, Rb and Ba were observed commonly to results for HNO_3 case. In addition to these elements, Ti, Ni, and Pb were detected only in H_2SO_4 experiment. Cu increased from 0.034 to 0.841 ppb for Pt anode and from 0.041 to 1.230 ppb for Pd cathode, respectively. It was detected with 54.630 ppb in electrolyte although not detected in "before sample". Zn increased from 0.067 to 1.458 ppb for Pt anode and from 0.043 to 0.836 ppb for Pd cathode, respectively. It was detected with 18.549 ppb in electrolyte although very little detected in "before sample". It should be noticed that Rb and Ba were detected only after electrolysis for every sample solution. Considerable increase in density of Ti from 1.638 to 756.006 ppb is seen for electrolyte.

Table 5 shows amounts of Rb and Ba for electrodes and electrolyte estimated by quantitative analysis by ICP-MS. The Rb density detected in each sample solution was almost same. A large amount of Ba was detected in electrolyte as well as the experiment with HNO_3/H_2O.

Table 5 Rb and Ba density in H_2SO_4/H_2O and the electrodes

	Pt (after) (μg)	Pd (after) (μg)	Electrolyte (after) (μg)
Rb	2.72	2.35	4.30
Ba	1.03	0.30	157.60

We estimated how thick the Pd sample dissolved into the sample solution in pre-processing of ICP-MS analysis, as well as doing for the sample used in HNO_3 experiment. About 4 μm Pd ("before sample") and 0.1 μm Pd after electrolysis were dissolved. The former value is nearly 40 times as large as the latter one. If all the elements detected had been contaminants from the Pd, the densities of these elements for electrodes and electrolyte of "before sample" should have been 40 times as large as those of "after sample". Consequently, the elements including Rb and Ba could not be impurities from Pd electrode with HNO_3/H_2O electrolysis as well as the experiment with H_2SO_4/H_2O.

4. Conclusions

We performed light water electrolysis using HNO_3 and H_2SO_4. By ICP-MS analysis, we observed significant increase for the elements B, Mg, Cu and Zn in electrodes and electrolyte after electrolysis. Furthermore, Rb and Ba were newly detected. These elements are possible candidates of products resulting from

nuclear transmutation.

References

[1]T. Ohmori, H.Yamada, S. Narita and T, Mizuno, Proceedings of the 9th International Conference on Cold Fusion, pp. 284-294, 2003

[2] H. Yamada, S. Narita, Y. Fujii, T. Sato, S. Sasaki and T. Omori, Proceedings of The 9th International Conference on Cold Fusion, pp. 420-423, 2003

[3] T.Sato, S. Sasaki, T. Kubozono, S. Narita, H. Yamada and T. Ohmori, Proceedings of the 4th Meeting of Japan CF Research Society, October 17-18, 2002, pp.9-12.

[4] The periodic table of the elements, http://home.hiroshima-u.ac.jp/er/Rmin_GL.html#anchor64130

HEAT MEASUREMENT DURING PLASMA ELECTROLYSIS

K.Iizumi, M.Fujii, S.Mitsushima, N.Kamiya and K.Ota
Department of Energy and Safety Engineering, Yokohama National University
79-5 Tokiwadai Hodogaya-ku, Yokohama 240-3501 JAPAN

Abstract

It is important to establish an accurate heat measurement system to confirm the excess heat owing to the cold fusion phenomenon at the plasma electrolysis. Input power is much higher than normal electrolysis. In this condition, an accurate heat measurement is difficult due to the evaporation of electrolyte and the heat loss to the environment from a body of an electrolytic cell. In this study, a flow calorimetry system was used in a flow cell system. The heat balances were from 86% to 94% in our accurate 18 experiments this time, and the clear excess heat was not detected.

1. Introduction

Since 1989, many people have reported on the excess heat production during water electrolysis. However, most of them had not enough reproducibility, and a theory for the excess heat has not been established, yet. Mizuno et al reported the excess heat during their plasma electrolysis [1]. Considering the quantity of excess, we can consider the application. In this study, we have developed, a flow calorimetry system using a flow cell system, and the heat balance during the plasma electrolysis has been measured.

2. Experiment

Figure 1 shows the electrolytic flow cell which was used in this study. The body of the cell was 27cm length of an acrylic pipe. The inside and outside diameter were 2cm and 5cm, respectively. The anode was a platinum mesh (99.99% purity, 55meshs) with 2cm diameter of a cylindrical shape. The cathode was tungsten rod (Φ 1.0mm, 99.95% purity) and was placed at the center of the cylindrical anode. The distance between the two electrodes was set to be 1cm. Electrolyte was 0.2M K_2CO_3 light water solution, and it was circulated in this system passing through a reservoir. The temperature of electrolyte at the cell inlet was kept at 296K. The flow rate of electrolyte was fixed at the range of 571~831ml min^{-1}. The temperature difference between inlet and outlet of the electrolyte was measured by Pt resistance thermometers. Hydrogen and oxygen that generated during electrolysis were collected in the reservoir and measured the rate of gas generation.

The electrolysis was conducted at the constant voltage of 95~125V. During

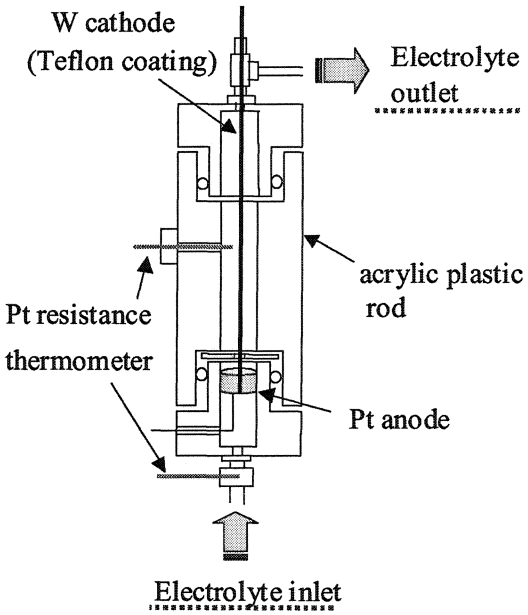

Fig.1 Plasma electrolytic cell.

electrolysis, we measured the cell voltage, the cell current, the electrolyte inlet temperature, the electrolyte outlet temperature, room temperature, reservoir temperature, the electrolyte flow rate and the gas flow rate of the gaseous product (H_2 + O_2) were measured.

3. Results and Discussion

3.1 Typical characteristics of plasma electrolysis.

Figure 2 shows the cell voltage and the current as a function of time. The cell voltage was controlled by a step function with 20 sec interval. At the beginning, the current increased with the cell voltage; however the current decreased with the increase of the cell voltage from 80 to 130V. Plasma discharge was started in this region. The bright plasma was observed above 130V. The current increased with the cell voltage above 130V. When the plasma stopped at 90V, the current increased from 2A to 13A. Plasma might have a role of an electrical resistant effect.

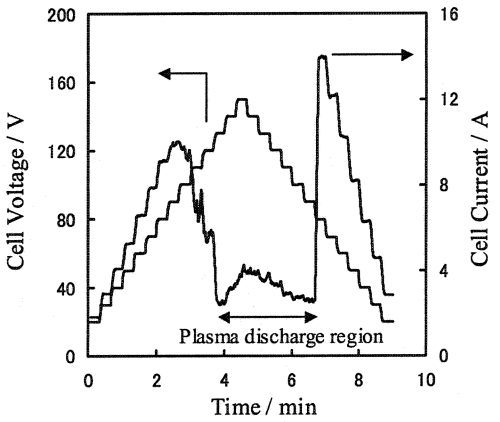

Fig.2 Trend of input voltage and current during normal and plasma electrolysis in 0.2M K_2CO_3 light water solution.

3.2 Heat measurement during plasma electrolysis.

Input energy was determined by the product of the cell voltage and the current. The output energy was the sum of sensible and latent heat. The sensible heat was determined by the temperature difference between the outlet and input of the electrolyte. The latent heat was determined from the flow rate of the gasous product. The heat loss through the wall of our system was neglected in this study. The loss was considered to be very small compared to two factors, since the electrolyte temperature was kept very close to the room temperature and the cell was insulated.

The heat balance was calculated by the following equations.

$$W_0 = U \times I$$
$$W_1 = FR \times \Delta T \times d \times Cp$$
$$W_2 = (2/3) \times V_g \times Q$$
$$HR = W_1 / W_0$$
$$HB = (W_1 + W_2) / W_0$$

Where W_0 is the input energy, W_1 is the output energy that was used obtained by the for temperature increase of the electrolyte, W_2 is the output energy that included the energy of H_2 and O_2 was used for electrolysis, HB is heat balance when output energy is only W_1, HR is heat balance when output energy is the sum of W_1 and W_2, U is the cell voltage, I is the cell current, FR is the electrolyte flow rate, ΔT is the temperature difference from the electrolyte inlet temperature to the electrolyte outlet temperature, d is electrolyte density, Cp is the heat capacity, V_g is the gas flow rate of the gaseous product, and Q is the reaction enthalpy of water electrolysis.

Figure 3 shows trend of output power, input power and temperature difference between inlet and outlet of the electrolyte The experimental condition was as follows; the electrolyte was 0.2M K_2CO_3 light water solution, the flow rate of the electrolyte was 825ml/min, the room temperature was 295K, the time during

heat measurement was 30 minutes, and the electrode length were 1.5cm, respectively. Since the inlet temperature of the electrolyte was 296K, the output temperature of the electrolyte was about 301K constantly during plasma electrolysis. Figure 4 shows the trend of the heat balance that was calculated these data. Current efficiency for gaseous production (hydrogen gas and oxygen gas) was 93%, 96%, 97%, respectively. HR becomes 90%, and HB becomes 91. However, excess heat could not be detected.

Table 1 shows results of the heat balance in our 18 experiments this time. In these runs, the time of heat measurement was 30 minutes. The current efficiency of gaseous production (hydrogen gas and oxygen gas) was from 93% to 98%, and the heat balances were from 86% to 94%. In these experiments, the input power and the temperature range were limited. Therefore, the higher input power and temperature experiment would be required to determine the plasma electrolysis.

4. Conclusion

The calorimetry system which we developed showed a high-performance. However, the heat balances were from 86% to 94% and excess heat could not be detected in our 18 experiments this time. In order to get excess heat, other experimental conditions might be studied.

Reference

1) T.Mizuno, T.Ohmori, and T.Akimoto, A.Takahashi, "Production of Heat during Plasma Electrolysis in Liquid", Jpn J. Appl. Phys.,Vol.39, No.10 (2000) 6055-6061

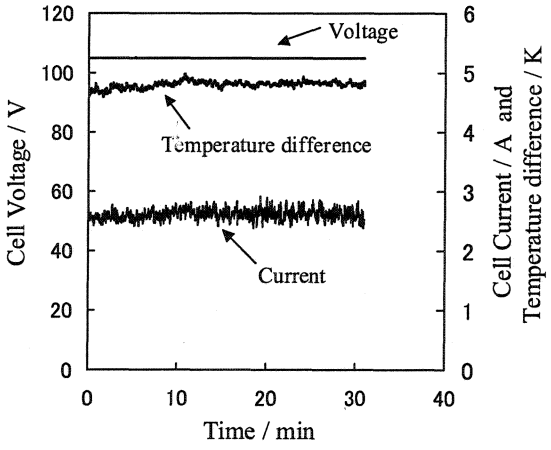

Fig.3 Trend of output power, input power and temperature difference during plasma electrolysis in 0.2M K_2CO_3 light water solution at 825ml/min. (Electrode lengths were 1.5cm, respectively.)

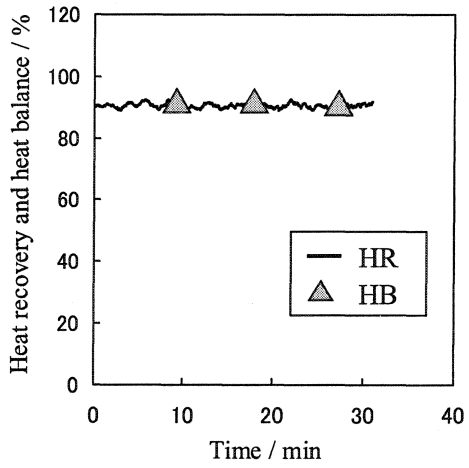

Fig.4 Trend of heat balance during plasma electrolysis in 0.2M K_2CO_3 light water solution at 825ml/min. (Electrode lengths were 1.5cm, respectively.)

Table 1 Heat balance of plasma electrolysis in 0.2M K_2CO_3 light water solution.

	Cell voltage [V]	Cell current [A]	Electrode Length [cm]	Flow rate [ml min^{-1}]	discharge Voltage [V]	HR	HB
h1	95	2.0 ~ 2.7	2	576	125	0.89	0.90
h2	105	2.5 ~ 3.1	2	583	122	0.89	0.90
h3	123	2.5 ~ 3.5	2	577	123	0.90	0.91
h4	95	2.2 ~ 2.9	2	818	125	0.89	0.90
h5	105	2.4 ~ 3.4	2	813	130	0.91	0.92
h6	122	2.5 ~ 3.7	2	824	122	0.92	0.93
h7	95	1.9 ~ 2.5	1.5	579	121	0.89	0.90
h8	105	2.1 ~ 2.7	1.5	593	123	0.90	0.91
h9	125	2.3 ~ 4.1	1.5	599	125	0.86	0.87
h10	95	1.9 ~ 2.5	1.5	831	125	0.92	0.93
h11	105	2.1 ~ 3.0	1.5	825	121	0.90	0.91
h12	120	2.7 ~ 4.1	1.5	829	120	0.85	0.86
h13	95	1.4 ~ 2.6	1	571	120	0.89	0.90
h14	105	1.6 ~ 2.4	1	574	118	0.86	0.87
h15	120	1.2 ~ 3.0	1	586	120	0.87	0.88
h16	95	1.4 ~ 2.0	1	818	120	0.92	0.93
h17	105	1.4 ~ 2.2	1	803	120	0.91	0.92
h18	120	1.9 ~ 2.8	1	819	120	0.83	0.94

Simulation approach to elucidate evolution mechanism of vortex appeared on Pd electrode surface after long-term evolution of deuterium in 0.1M LiOD

Hiroo NUMATA[1†] and Masanobu BAN[2] :† numata @mtl.titech.ac.jp
1 Graduate School of Metallurgy and Ceramics Science, Tokyo Institute of Technology
1-12-1, O-okayama, Meguro-ku, Tokyo 152-8552 Japan
2 Technology evaluation section, Tokyo Metropolitan Industrial Technology Research Institute
3-13-10, Nisigaoka Kita-ku, Tokyo 115-8586 Japan

Abstract: Long-term electrolysis for well annealed thick Pd rod (9.0 mm ϕ) in 0.1M LiOD was performed. High count rate of neutron appeared after the current increased to c.a. 100 mA/cm^2 and the temperature of the electrolyte rose to 50 °C. Microscopic observation of post electrolysis Pd showed that long-term electrolysis did not resulted in any cracking but surface voids, two long faults, voids arranged in a straight line and peculiar surface traces: vortex. In-situ measurement of the hydrogen/deuterium evolution of the Pd-H (D) system and the measurement of solid-state properties of post electrolysis Pd revealed the micro structural model inside the solid, which improves reproducibility of cold fusion related phenomena. An important process in that model is the motion of deuterium from a vessel to other ones, which might occur the observed vortex patterns on post electrolysis Pd surface. However, there has been remained unsolved yet a phenomenological explanation for the process of the vortex formation.

The lattice gas cellular automata method was utilized for simulating the Poiseuille flow with the boundary conditions incorporating the motion of the hypothetical particle fluid. The Poiseuille flow and the flow pattern of the vortex were obtained in a simple 2D flow. More precise 2D model simulating the vortex pattern was presented adopting the advanced inflow and outflow boundaries under particle generation and disappearance conditions.

Keywords: Computational fluid dynamics, Lattice Gas Cellular Automata, Pd, Electrolysis in 0.1M LiOD, Nuclear reaction cycle model, Vortex

Introduction

Ever since the announcement of Fleischmann and Pons, and Jones et al.[1-2] of the generation of neutron and thermal energy accompanied with electrolysis on Pd in 0.1M LiOD, there still has been remaining the questions about the mechanism of the cold fusion reaction. For example, the observed ratios of neutrons to protons in cold fusion experiments are smaller than that of normal D-D fusion, therefore, this discrepancy will be explained by fusion of deuterated metals occurring an extraordinary approach of neuclei in dynamic state. Jones et al.[2] have suggested that cold fusion of deuterons in the earth might cause anomalous ^{3}He release from magmatic water and an abrupt T increase in air synchronized with the volcano erruptions[3]. What kind of phenomenon occurs when deuterium is absorbed in Pd metal by electrolysis, it is believed, one of the reasons never expelled from the above doubt. With respect to the phenomena accompanied with the cold fusion experiment at ambient temperatures, similarity is sought at this time in a phenomenon of the earth's activities assuming that the cold fusion reaction is considered to construct a cyclic process [4-8]. In this paper explanation of the phenomena accompanied with the cold fusion reaction as a cyclic process was attempted. One of the phenomena is the vortex pattern appeared on Pd electrode surface after long-term electrolysis in 0.1M LiOD. To elucidate the vortex formation mechanism computational fluid simulation method was applied to analyze the motion of hypothetical particle mass through the electrode/electrolyte interface.

Experimental

Long-term evolution of deuterium on thick rod Pd electrode in 0.1M LiOD

Substantially cold fusion experiment at ambient temperatures has been conducted by electrolysis of heavy water on a Pd electrode or the other stable metal, e.g., Ni or Au electrode. In Fig.1 the electrolysis equipment, especially the geometrical shapes and arrangement of the electrode, the counter electrode and an electrolyte are shown, and the measurement systems with respect to excess

heat, neutron emission, and an isothermal water bath are not drawn. Using a potentiostat (or current supply) a constant cathodic current was applied to a Pd electrode on which an evolution of deuterium gas was occurred. By continuing a state where deuterium is strongly absorbed in a Pd electrode, heat generation or emissions of neutrons or charged particles is observed. We successfully performed non-intermittent electrolysis for 2 and ca. 6 months with two experimental runs, referred to Exp.1 and Exp.2, respectively. The characteristics of the experimental apparatus and procedures are: (1) Quartz cell (2) Cast rod Pd electrode (3) Thicker rod Pd electrodes (usually rods with a diameter of ca. 3mm and plates with approximately 0.5mm thickness are used, but rods with 9mm and 21mm diameters were used here[4-5]) (4) Preparatory absorption of deuterium in the D_2 gas atmosphere (D/Pd 0.36) (5) Increase in electrolysis current density in a form of stepwise (6) Long-term continuous electrolysis (ca. 6 months) (7) Temperature cycling. The experiment was conducted in accordance with the following measurement procedures (1) Neutron count rate by means of NE213 scintillation counter where the signal was treated with n-γ discrimination, and neutron energy spectrum (2) Bath temperature (3) Continuous measurement of the Pd electrode potential. In addition, the temperature and humidity around the measurement equipments were controlled. The experimental runs were conducted twice in 0.1M LiOD by using the rod Pd electrodes with a diameter of 9mm referred to Exp.1[9], and a diameter of 21mm referred to Exp.2[4-5], both of which were made by casting. Further details of surface pretreatment and electrolysis conditions are shown in Table 1. The results of neutron measurement are described elsewhere[4-5].

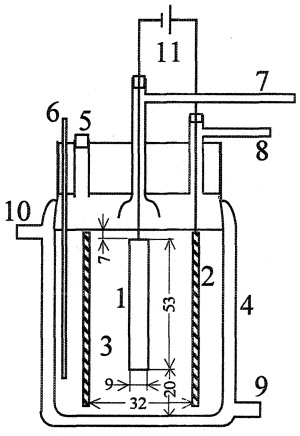

1 Pd rod cathode
2 Anode
3 0.1M LiOD electrolyte
4 Double jacketed transparent quartz cell
5 Addition tube
6 Thermocouple
7 Guide for Deuterium gas
8 Guide for Oxygen gas
9 Circulating water inlet
10 Circulating water outlet
11 Current supply

Fig.1 Schematic diagram of electrolytic cell for deuterium absorption on a Pd electrode in 0.1M LiOD.

Table1 Experimental conditions of Exp.1

Run No.	Current, $mAcm^{-2}$	Pretreatment
1 st	0.05-40	Cast, 800°C anneal(10^{-6}Torr)
	40-500	Acid treatment
2nd	40	Polishing, Acid treatment, Evacuation, D_2 gas charge
3rd	40	Evacuation, Polishing, Acid treatment
4th	40	Evacuation, Polishing, Acid treatment

Results and Discussion

Descriptions with respect to microscopic observation and an expansion of the electrode are made with the result of Exp.1. The electrode expansion during the period of 1st to 4th run of Exp.1 was determined by measuring the diameters at three positions of the electrode after interruption of electrolysis. Then, the electrode was carefully re-installed. In the period of 1st run the largest expansion occurred (1st ca.6%, 1st-4th total 7.8-8.3%), during which significant count rate of neutron over the background was appeared. No explanation with respect to the relation between a neutron emission and an expansion of the electrode was made at that time[4, 9].

Figure 2 shows an optical micrograph of the transverse cross sectional area (shown as rectangular in the left), where the sample was taken from the apex of the electrode, embedded in epoxy resin and lightly etched. In metallographic aspect the specimen as a whole is consisted of columnar crystals (also see Fig.4), which is supposed to be grown inside from a crucible wall

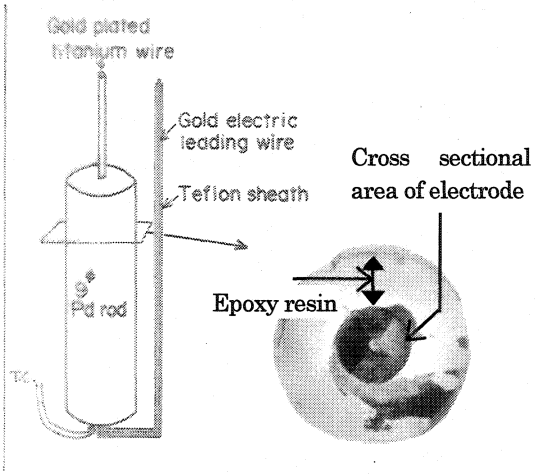

Fig.2 Schematic of Pd electrode and optical micrograph of cross sectional surface area of electrode.

during cooling. The picture of the specimen exhibits a peculiar grain structure, quadrified by two straight grain boundaries. Long prisms grew longitudinally along the electrode center. However, these results are unexpected, since the temperature of the electrode and that out side of the counter electrode showed no significant change corresponding to heat bursts. Hence, this is well acceptable, only when the small heat evolution in the interior of the electrode lasted long time so as to promote abnormal grain growth. Coupland et al.[10] found the recrystalline grain near the area of electrical connection. However, there has not been hitherto reported such kind of anomalous grain structure. This suggests that during emission of neutron, the heat evolution in the interior occurred slowly showing the symmetrical crystal structure. However, there is no experimental evidence relates neutron emission to the increase of the temperature assuming huge heat burst introduced by Fleischmann and Pons[1].

Since the above result obtained by microscopic observation is, different from electrode potential, neutron count rate, and bath temperature, not the information with which electrolysis was in progress, it is impossible to give an answer to the matter when such a microscopic structure appeared or to the time correlation with neutron count rate. However, it was possible to estimate such problems by an analogy with natural phenomena, as shown below.

Nuclear reaction cycle model

So far, endeavors have been exerted on understanding the individual phenomenon accompanied with the cold fusion reaction, which is a complicated phenomenon as a whole. At the next stage, by considering phenomena as an energy engine, a model is proposed from a point of view of its continuous operation (4 reciprocating cycle). Thus, taking into account of the correspondence to the long-term electrolysis experiment of a thick rod Pd, the hindered factors might come to the surface. Numata[7-8] proposed a nuclear reaction cycle model (thereafter shortened to N-cycle model) illustrated in Fig.3 with a view to making explanation with the cold fusion reaction. It was insisted that a key point for reproducibility of the cold fusion experiment resides in continuation of the cycle. In case of long-term electrolysis of a thick rod Pd in 0.1M LiOD conducted by our group, the result was explained as the N-cycle occurred, as shown before[11-12]. Furthermore the reaction vessels are either the regions formed so many in the whole Pd electrode or the rod Pd electrode itself. Here, brief explanation is made to grasp the idea of N-cycle model.

Let the correspondence be examined with the model in question to the phenomena of the experiment. In the absorption and compression processes of the reactants of the reaction (see Fig.3), a barrier layer of deuterium migration by compression stress (also corresponds to the B side of the single-side electrolysis referred to the report[8]) is formed as absorption in progress, resulting in formation of a vessel composed of the interior and blanket as the barrier layer. In the compression process, the interior appears to make expansion owing to the continued absorption, i.e., a part of the generated deuterium is contributed to further slow absorption. However by the compression pressure of the blanket, a kind of enhanced pinch effect is brought about resulting in an increase of the internal pressure (in otherwise an increase in stress). In the reaction process a reaction should be caused by an external trigger that is applied to the inside (i.e., injection of high-energy particles from the outside) or by an internal trigger. As an actual internal trigger, case I and II (also shown in the report[8]) can be considered depending on a manner whether the role of the fault formation should be regarded as the final step of the reaction process or a reaction is induced by allowing the fault

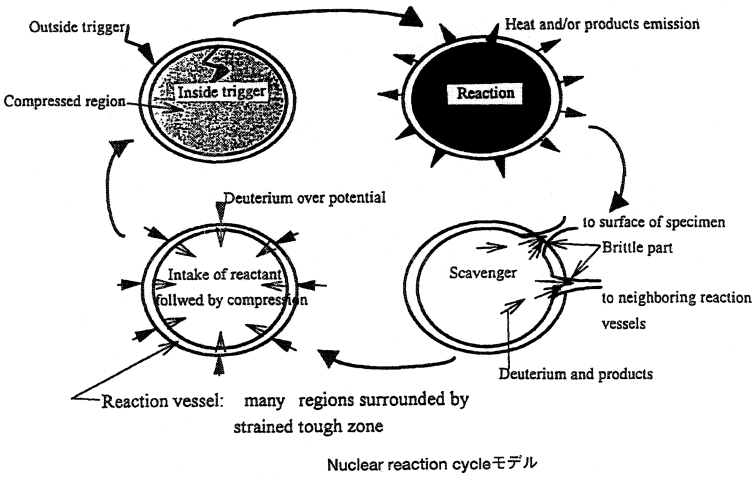

Fig.3 Schematic of a nuclear reaction cycle model.

formation to provide the blanket with a path to expedite further absorption[11]. Very many holes concentrated on both the sides of the fault found in the experiment[4] were discharge ports of the reaction products in the process of scavenging. At this stage, discharge is made with the products of the reaction together with unreacting deuterium[11-12]. In case of the internal trigger I, emission of the neutrons and charged particles at first occurs as a precursor phenomenon of the cold fusion reaction similar to an earthquake as listed in[8]. Secondly fault is formed simultaneously with reaction. In case of the internal trigger II, vessel is formed in the compression process, although the D/Pd ratio could be insufficient to the reaction. Therefore fault is formed through a barrier layer (formation of this layer makes it for either absorption or desorption to occur), which allows the absorption to take an easy route. Thus, it is inferred that the D/Pd ratio is raised, resulting in occurrence of the cold fusion reaction.

Considering again the absorption reaction in Exp.1, the resulting ca. 6% expansion confirmed during 1st run (also see the left of Fig.4) suggests the occurrence of considerable internal pressure increase corresponding to the absorption/compression process of N-cycle model. Apart from the identification of the reaction vessels and the (once this particle was defined as charged particles, deuterium or reaction products) occurrence of the reaction, the subsequent outflow of the hypothetical particle mass might occur toward 360° radial direction as the scavenger process of N-cycle model (also see the right of Fig.4). Such motions of the particle mass might be realized from the geometry of the reaction vessel formed during the absorption/compression process shown in the left. That is, in a long prism crystal absorbed reaction products or deuterium under high pressure coincidently spout out with sufficient energy where the motion of the flows are expressed as vectors normal to the electrode interface as shown in the right. Importantly all the flows synchronize with the occurrence of the reactions. In addition obstacles might adhere on the surface due to its inhomogeneity. Thus, N-cycle model predicts that the flows occur coincidently through the electrode /electrolyte interface (this is formerly shown in Fig.3 as the motion of reaction products and deuterium to neighboring vessels and surface of the electrode), however, phenomenological evidence has not yet been shown, which is substantiated next by numerical simulation of the fluid flow.

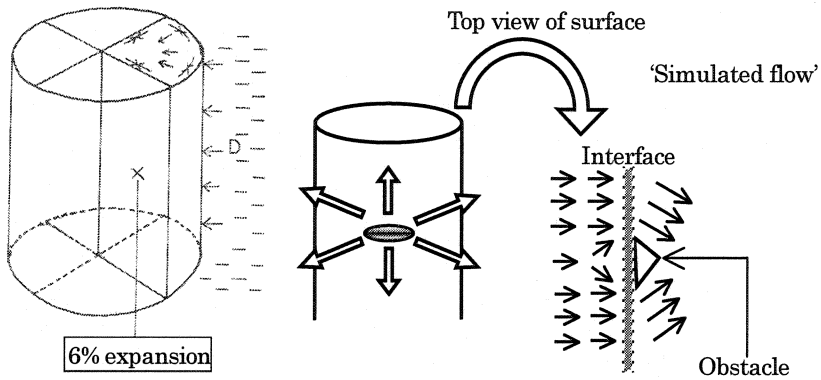

Fig.4 Absorption of deuterium and resultant outflow of hypothetical particle mass.

Vortex appeared on Pd electrode surface

Figure 5 shows a significant morphology of a thick rod Pd electrode in 0.1M LiOD observed on

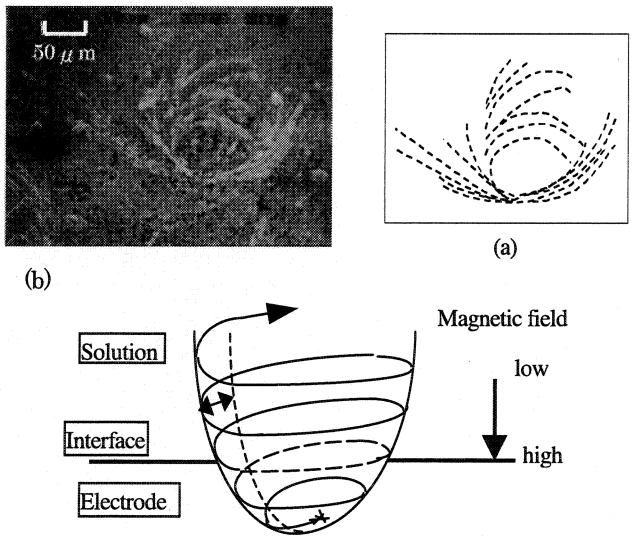

Fig.5 Vortex appeared on Pd electrode surface after long-term electrolysis in 0.1M LiOD, (a) Duplicate of SEM picture (b) Vortex evolved normal to electrode surface. Dashed line shows locus of vortex.

the surface after long-term electrolysis. This is not the substance adhered on the surface, but is a material on which the pattern was deeply impressed in a shape of a ditch. In (b) of Fig.5, vortex is shown as masses of the high energy particles discharged (deducing from the electric potential gradient of the electrode/solution interface, they might be electrons if charged particles) taking a locus of vortex on the electrode surface. It is imagined that due to an electro-magnetic interaction with a magnetic field (i.e., a magnetic field generated by varying current) attenuating from the electrode surface toward the bulk of the electrolyte, the pattern of the conicals (depicted in dots) different from each other in their sizes were left on the surface. Thus, the locus of the vortex observed on the Pd surface after long-term electrolysis in 0.1M LiOD is considered to be an occurrence of energetic particles emission. At this stage the mechanism of such vortex evolution stayed in the guess. Precise experimental proof is needed before definitive conclusion can be reached.

Lattice Gas Cellular Automata method

Briefly summarizing the above discussion, it is shown that from N-cycle model the coincident fluid flow motion through the interface is reasonably deduced, which might be evidenced by the locus of vortex appeared on Pd electrode. Since the mechanism of the vortex evolution remains unknown, the substance attributable to such phenomenon is defined as hypothetical particle mass in this paper (once this particle was defined as charged particles, deuterium or reaction products). In the scavenging of N-cycle model the hypothetical particle mass move coincidently from the reaction vessel to the surface and/or the other one. To understand the mechanism of the vortex evolution computational simulation of the vortex pattern is performed, where an unknown principle governing the motion, the physical meaning and properties of the fluid element can be elucidated. In the following, LGCA method is employed for computational calculation of the fluid flow.

Lattice Gas Cellular Automata method (LGCA) is a kind of computational simulation of an incompressible hydrodynamic fluid, which is equivalent to solving the Navier-Stokes equation. In LGCA calculation identical particles possessing unit mass and unit velocity (also obeying Pauli's exclusive principle) are set on a hexagonal lattice plane whereby particles move engaging in collisions and propagation obeying the mass and

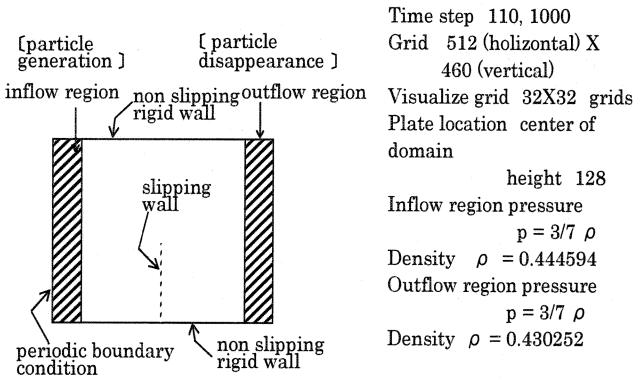

Fig.6 Schematic of boundary conditions and rectangular domain.

momentum conservation rules in one time step advance. The advantage of LGCA method is in providing a microscopic atomistic model because of its simplified principle. On the contrary averaging many particles motion or a large number of time steps of calculations is requested to describe the motion of macroscopic flow. In this study a 2D LGCA model incorporating the obstacle plate at the center of a rectangular domain was employed for simulation of the above mentioned hypothetical fluid motion through the electrode interface (also see Fig.4). Figure 6 shows a LGCA model, together with miscellaneous numerical constants of simulation.

Simulations were carried out on a usual PC for a 512 x 460 lattice with the boundary conditions as shown in Fig.6, and preliminary upto 1000 time steps. The actual development of the program has been achieved in two steps, in order to confirm the

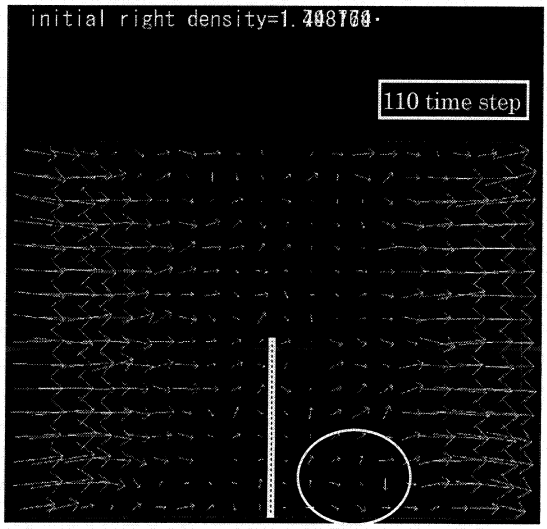

Fig.7 LGCA simulation result of vortex evolved behind flat plate on 512 x 460 grids at t=110.

research progress step by step; first a simple 2D fluid simulation was performed resulting the Poiseuille flow and the flow pattern of the vortex, afterwards more precise 2D model simulating the vortex pattern is developed adopting the advanced inflow and outflow boundaries under particle generation and disappearance conditions[13].

Figure 7 shows the flow behind a flat plate at t=110 by using a FHP-III model in a rectangular domain, where stationary flow from left to right is given by the pressure difference of the inflow and outflow boundary regions. The result of the simulation qualitatively well agrees with those of the other reports. This simulation shows that the flow creates a vortex behind a flat plate as shown in the area enclosed with a circle. In this case the flat plate is considered as an obstacle for the first approximation. Although the coarser simulation is unable to fully describe the phenomenon, it is shown that a vortex exists in the downstream as

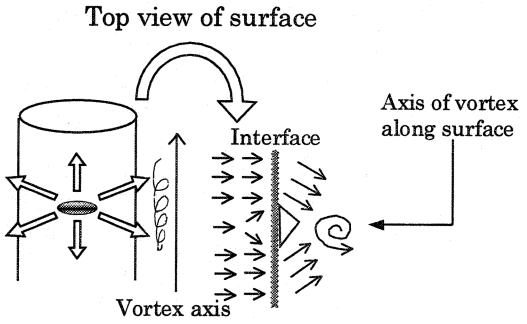

Fig.8 Schematic view of vortex with axis along electrode obtained by numerical simulation.

schematically re-drawn in Fig.8.

In the simulation calculation the vortex appeared in the vicinity of an electrode /electrolyte interface through which the hypothetical particle mass flow in parallel avoiding an adherent obstacle on the surface, as shown in Fig.8. Importantly the fluid elements might move coincidently and the resultant vortex evolves normal to this page with axis along to the electrode. Figure 9 shows vortex appeared on Pd electrode surface and that evolved normal to the electrode surface (not normal to this page as shown in Fig.8) where the latter was deduced from the fact that the charged particles or uncharged particles move through the electrified interface, i.e., electric double layer. By comparing both the vortex patterns the vortex with axis normal to the electrode surface might be far from the experimentally obtained one. This result suggests that comparing merely the vortex axis the vortex with the leaned axis can only be consistent with that of experimentally obtained

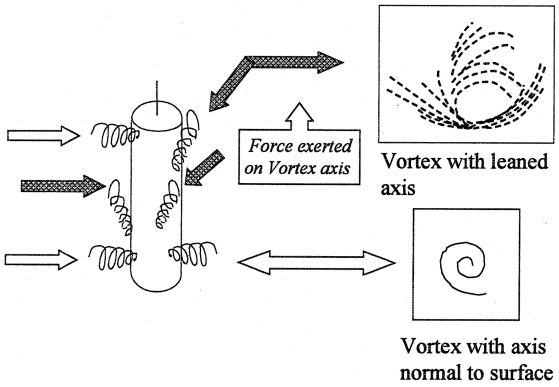

Fig.9 Schematic view of vortex with axis normal to electrode surface and locus of vortex appeared on electrode surface.

one. More accurate simulation might be needed to establish the physical model to describe the motion of the hypothetical particle mass. Even though it is useful to evaluate the force exerted on the motion of the hypothetical particle mass due to a significant magnetic field change at the interface (also see Fig.9).

At the electrode surface, strictly the interface between the electrode surface and the bulk of the electrolyte, there is a potential difference, where electrons flow toward outside in the electrode and ions in the same magnitude transfer in the

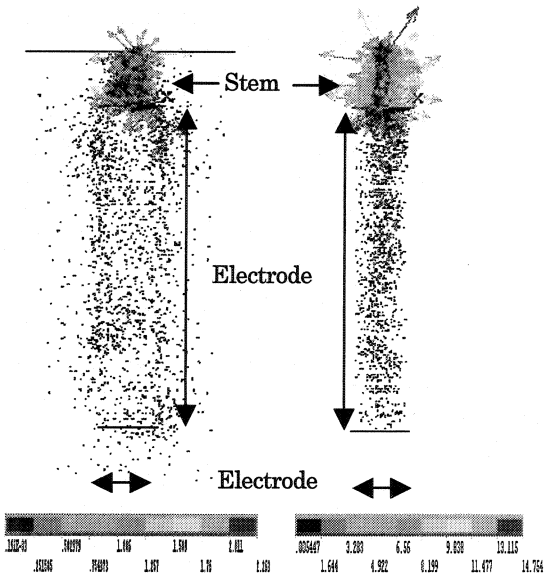

Fig.10 Perspective view of magnetic flux density of the electrolyte (left) and the electrode (right). The color and length of arrows show the amplitude of vector.

electrolyte. Under the circumstance of a constant current the induced magnetic field (obeying the Maxwell equation) was numerically analyzed using Finite Element Method (FEM). The full 3-D FEM program (ANSYS) was used for the analysis of magnetic field density in the vicinity of the electrode surface and of the electrolyte bulk in the electrolytic cell where the geometrical model (Fig.1) was made for the boundary conditions. Figure 10 shows perspective vector views of the electrolyte (left) and the electrode (right). In the view of original data those vectors exhibited the vectors representing the value of an electrode element and that of an electrolyte element so that the separation of those coexistence or close existence of vectors was needed. Ignoring the irregular vectors at the stem with abnormally large amplitude, the values of the magnetic field density of the electrolyte were in the range of 1.91×10^{-3} with some regional scattering, while those of the electrode in the range of 0.0055 within narrowed region. Apparently the amplitude of the electrode vectors exhibits almost 3 times higher value than that of the electrolyte. In due course the influence of the magnetic field density difference on the fluid motion will be evaluated.

Conclusions

The reality of the scavenging in N-cycle model (proposed by H.N) was proved by LGCA and FEM numerical simulation methods. We investigated vortex pattern appeared on Pd surface after long term electrolysis in 0.1M LiOD. The N-cycle model predicted that the hypothetical particle mass flow coincidently through the electrode surface/electrolyte interface. By LGCA method simulating the motion of such particle mass the formation of vertex along the electrode (not normal to the electrode surface) was proved. From the comparison of these vortexes from simulation and the result of experiment it is elucidated that the magnetic field density difference at the interface has the influence on the motion of those particle mass.

Acknowledgement

The authors thank Dr. Naoki Takada at AIST for helpful discussion. He (H.N) thanks valuable discussion with Drs. Mikio Fukuhara and Tadahikiko Mizuno. He also thanks supportive encouragement in the early stage of this work with Profs. Shiro Haruyama and Izumi Ohno at Tokyo Inst. of Technol.

References

1) M. Fleischmann and S. Pons, "Electrochemically Induced Nuclear Fusion of Deuterium," J.Electroanal.Chem., 261,301(1989), and errata, 263,187(1989).

2) S.E. Jones et al.,"Observation of Cold Nuclear Fusion in Condensed Matter," Nature, 338, 737(1989).

3) F.Goff, A.I.Adams, G.M.McMurty, L.Shevenell, D.R.Pettit, J.A.Stimac, C.Werner, "Magmatic Tritium," LA-UR-97-1516, DOE Office of Scientific and Technical Information (OSTI), pp.1-11 (1997).

4) R.Takagi, et al., Neutron Emission During a Long-term Electrolysis of Heavy Water; Fusion Technol., 19, 2135-2139 (1991)

5) H. Numata et al., "Neutron Emission and Surface Observation During a Long-Term Evolution of Deuterium on Pd in 0.1M LiOD," Proc. Conf. Science of Cold Fusion, Vol.33, p.71-79, T.BRESSANI, E.DEL GIUDICE, and G.PREPARATA eds., SIF, Bologna, Italy (1991).

6) H. Numata and M. Fukuhara, "Low-Temperature Elastic Anomalies and Heat Generation of Deuterated Palladium," Fusion Technol., 31,300-310 (1997).

7) H. Numata and I. Ohno, "In situ Potentio, Resisto and Dilatometric Measurement of Repeated Hydrogen Absorption in Pd Electrode by Electrochemical Cathodic Loading Method," Proc.of the 6th Int. Conf. on Cold Fusion, "Prog.in New Hydrogen Energy", Toya Japan, 13 Oct., 1996, Vol.1, p.213, NEDO, The Inst.of Appl. Energy, (1997).

8) H. Numata and I. Ohno, "In situ Potentiometric, Resistance and Dilatometric Measurements of Pd Electrode During Repeated Electrochemical Hydrogen Absorption," Fusion Technol., 38, 206-223 (2000).

9) H. Numata, et al. "Neutron Emission During Deuterium Evolution on Pd in Heavy Water," Proc.of Mini Sympo. on Cold Fusion, Tokyo Metropolitan Univ. pp.129(1990).

10) D.R.Coupland et al., Proc. of 1st Annual Conf. on Cold Fusion, pp.299, Utah (1990).

11) H.Numata , "Cold fusion considered as solid state earthquake ?" in book "Cyber X" No.11, pp.37-51 (1999) Kougakusha.

12) A.Takahashi et al., "Nuclear Reaction Study In Condensed Matter No.1," Chapter 4, p.124 (1999) Kougakusha.

13) Y.Matsukuma and R.Takahashi, Trans. JSME, 61-588, B, 2826-2832 (1995)

Appendix

Actual loading of deuterium on a thick rod Pd electrode was made by adding the exhausted electrolyte solution twice per day, taking-in of data, and visual observation of the cell during electrolysis. In case of electric power failure, an auxiliary generation of electricity using a midget engine was made. Using an advanced electrolytic cell in the Exp.2, more stabilized experiments were conducted with an incorporation of the heavy water recovery instrument involving catalysts for exhaust gas.

Despite the above mentioned care, cell detonation occurred several times while the electrolysis was in progress. This occasion is more or less anticipated because D_2 and O_2 generated from electrolysis were in coexistence in the room over the liquid surface of the cell, which might induce the catalytic recombination of both the molecules, so called hydrogen detonation. Although it was unclear how the ignition of the gas mixture broke out. The weak portions had been incorporated with the electrolytic system, which allowed the detonation to prevent bad effect on the experimental continuation. One day the experimenter was able to witness the detonation. Large amount of deuterium gas was accumulated in the room, where electric discharge would be produced between the lead portion extruded from the liquid surface and the counter electrode. However, it was perceived that noise of the detonation was heard simultaneously with the instant when a pale flash was emitted from the Pd rod surface in contact with alkali heavy water toward the counter electrode. After the detonation was experienced, a countermeasure for safety was intended.

Preliminary Test for Decay Rate Measurement of Radioactivity Embedded in Host Materials

Takayoshi AOKI and Nobuharu YOSHIKAWA*

Isotope Center, The University of Tsukuba, Tsukuba-shi, Tennoudai 1-1-1, 305-8577, Japan
*KEK, Tsukuba-shi, Ouho 1-1, 305-0801, Japan

Abstract: Preliminary test for observing small change of beta-decay rate of radioactivity ^{197}Pt, embedded in different host materials Au and Al, was made. Difference of decay constant was found to be $|\lambda - \lambda'| < 5.2 \times 10^{-5}$.

Keywords: Lifetime, host material, implanted ^{197}Pt.

1. Introduction.

If the cold fusion phenomena are really happened, some quantum mechanical effects may play a major role. The effects may be arisen from leakages of wave functions of nuclei and statistics of the wave functions (bosons and fermions). It has been thought that in the usual nuclear physics, these effects are too small to observe. However, realization of the cold fusion may lead us to an idea that such very small effects may be detectable in traditional nuclear physics field other than special field of the cold fusion. If we can find the effects of this kind, that will help analysis of the cold fusion phenomena (if exists). One candidate of the detectable phenomenon might be found in half-life measurement of radioactivity. Rate of beta decay may be changed due to the small effect that is realized by surroundings of parent nuclei. Electron capture decay (EC) is not the candidate because EC rate depends strongly on atomic electron density at the position of the parent nucleus[1,2,3] while the beta decay is purely internal nuclear process and is not dependent on atomic electron density.

Preliminary test for observing small change of beta-decay rate of radioactivity ^{197}Pt, embedded in different host materials Au and Al, was made. A parent ^{197}Pt nucleus decays to a daughter ^{197}Au nucleus with half-life of 18.3 h [4]. Natural abundance of stable ^{197}Au nucleus is 100%. If a parent ^{197}Pt nucleus is put as close as possible to daughter Au nuclei in the gold foil, some unknown quantum mechanical effects might accelerate or decelerate the beta-decay rate. The effect may arise from leakage of wave functions of both parent and daughter nuclei, position periodicity of daughter nuclei, statistics the nuclei obey, and so on. It may be interesting to compare the decay rate of ^{197}Pt embedded in Au foil to that of embedded in another host (Al) foil.

2. Experiment.

2.1 Source preparation.

To produce the parent nucleus ^{197}Pt, neutrons were used to irradiate two pieces of Pt wires with 1 mm diameter and 4 mm length. The neutron-activated wires were set in a sputtering negative heavy ion source in RI Center of University of Tsukuba. The ^{197}Pt activity was sputtered by Cs ions and extracted. The activity ion beam was accelerated to energy of 147 keV. Mass of the beam was analyzed by passing the beam through a magnet. Implantations of ^{197}Pt beam were made by stopping the beam on a Au foil and a Al foil, respectively. The foils were fixed on square frames. Thickness of the foils was 0.05 mm.

2.2 Rotating source system with two detectors:

Half-life measurements were performed using an alternate rotating source system, which consisted from a stepping motor with a rotating bar, two NaI(Tl) detectors A and B with Be windows, and lead and copper inner radiation shield block. Similar radiation shield wall encapsulated the whole elements. Fig.1 shows schematically rotating source system inside the shield wall(top view).

The foils frames were put on separately at end edge of the rotating bar. The bar was fixed to a shaft of the stepping motor and was rotated 180 degree to change source positions. The time necessary to rotate the bar to change position was

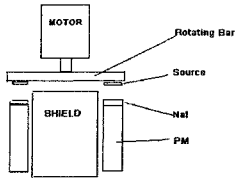

Fig1. Schematical top view of rotating system. The Au source and the Al source were put on end edge of the rotating bar. Lead and copper shield block were put between counter A and counter B.

3 minutes. Stopped position of the bar and fixed position of the detectors were adjusted so as to coincide the source frames with the front face of the NaI(Tl) detectors. The distance between the source and the front face was 1.5cm. The crystal size was 14 mm in diameter and thickness was 2 mm. Radiations (Gamma-, X- and beta-rays) emitted from the sources were measured by the detectors, which were set in the shielded block separately. The photo-multiplier used was R647 PM. Electronic signals form the PM were fed to model 460 Delay Line Amplifiers (DLA). Model 551 Single Channel Analyzers (SCA) were used to produce logic signals, which were fed to model 994 Counter and Timer(CT) to record the radiation events. Measured energy spectrum was shown in Fig.2. The beta continuum, 12 keV x-ray and 77 keV gamma-ray emitted from ^{197}Pt are seen. Discrimination level of SCA was set just below the energy of 12 keV X-ray.

Cross contamination of counting number detected by each detector was checked and contamination factor was found to be less than 0.014%. The factor was time independent. Therefore, in final analysis to get time dependence of the ratio as a linearly time dependent function, the correction was factored out and did not contribute to time dependent part. Lifetime measurement was controlled by a personal computer with GPIB network.

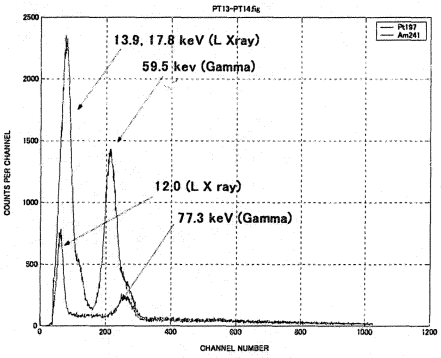

Fig.2 Observed energy spectrum form source ^{197}Pt(lower) and calibration source ^{241}Am(upper). The beta continuum, 12 keV x-ray and 77 keV gamma ray are seen.

3. Lifetime measurement.

When the system was initiated, first count collection (named by HH mode measurement) was made for 27 minutes and then the forward 180-degree rotation was followed for 3 minutes to change source. After that, second 27 minutes collection (name by HT mode measurement) was performed. Then the backward 180-degree rotation for 3 minutes was made to return original source position. These actions constituted one cycle (HH mode measurement, forward rotation, HT mode measurement and backward rotation). Cycle time was 1 hour. Using this system, both A and B counters with each CT's were able to collect the radiation from the Au foil source and Al foil source, alternatively. In HH measurement mode, the A detector recorded Au foil source events while the B detector recorded Al foil source events. In HT mode, the A detector counted Al source events contrarily and the B detector counted Au source events.

A test for preliminary lifetime measurement was

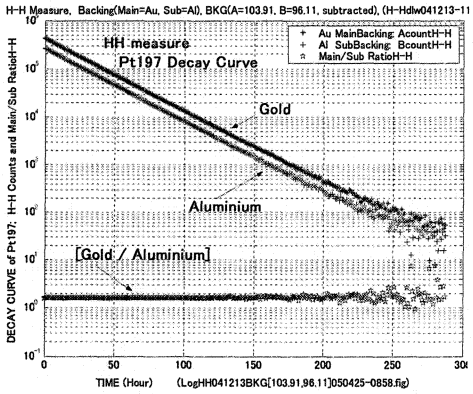

Fig.3 HH mode measurement. Symbol (*) represents decay curve of the Au foil source recorded by the detector A. symbol (+) represents the decay curve of Al foil source detected by the detector B.

tried to get time distribution of decay event. The cycle number was 288 (for 12 days). Successive measurement also tried to get time distribution of back ground event. Fig.3 shows time distribution measured in the HH mode. Ratio of the Au count to the Al count is also shown. Fig.4 shows the background measurement in the

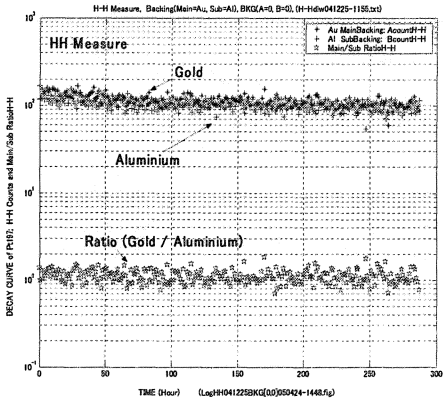

Fig.4 Background measurement for 12 days in HH mode. The measurement was made successively after the lifetime measurement.

HH mode. Background value for the detector A and the detector B were determined from this figure to be 103.9 and 96.1 counts, respectively.

4. Analysis.

4.1 Ratio of summed decay curves.

Changing source position, the HT mode measurements and the HH mode measurements were carried out alternatively. Measurements of the decay curve and the background in the HT mode were performed. The results were very similar to the one's in HH mode shown in Fig. 3 and Fig. 4 except that in the HT mode the detector A collected the Al source events and the detector B recorded the Au source events. The Au source events recorded by the counter A in HH mode and by the counter B in HT mode were summed after background subtraction. Then a ratio of the summed decay curve of Au source to the summed curve of Al source was calculated as shown as a function of time in Fig.5. The time range is from 0 to 175 hour. Resolving time of the counting system was roughly estimated to be 2.5 ± 1.0 μs. Correction for resolving time was made. However magnitude of the correction was too small, it was found that the contribution to final result was negligible.

4.2 Difference of decay constants.

A technique of weighted least-squares fit was employed to determine difference of decay constants. Fitting the ratio to a straight line of time as a function of $C_0 + C_1 \times t$, values for C_0 and C_1 were obtained as

$C_0 = 1.57402 \pm 0.00073$ and

$C_1 = (2.51 \pm 1.89) \times 10^{-5}$.

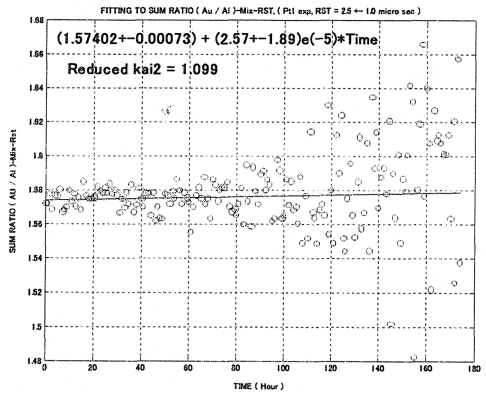

Fig.5 The ratio of the summed Au source event to the summed Al source event. Weighted least-squared fitting was made for the ratio

Experimentally obtained ratio R(t) is expressed as

$$R(t) = (N_0 \times \exp(-\lambda t)) / (N_0' \times \exp(-\lambda' t))$$
$$\cong (N_0 / N_0') - (N_0 / N_0') \times (\lambda - \lambda') \times t,$$
$$\cong C_0 + C_1 \times t.$$

where, λ is decay constant for Au source and λ' is for Al source, respectively. Employing C_0 and C_1 values, the difference $(\lambda - \lambda')$ is given as

$\lambda - \lambda' = -(1.6 \pm 1.2) \times 10^{-5}$

5. Conclusion.

Since the standard deviation ($\sigma = 1.2 \times 10^{-5}$) is relatively large, sign of the difference $(\lambda - \lambda')$ is essentially important. Confidence level for $-1.6 \times 10^{-5} \pm 1\times\sigma$ is 68.2 %. If we accept confidence level of 99.7 %, we have to take error as $\pm 3\times\sigma$. This means that

$\lambda - \lambda' = -(1.6 \pm 3.6) \times 10^{-5}$

$= (-5.2 \text{ to } +2.0) \times 10^{-5}$.

As seen, the sign ambiguity certainly exists for this confidence level. Therefore we may conclude that the absolute value of the difference of decay constant is

$|\lambda - \lambda'| < 5.2 \times 10^{-5}$.

Further experimental efforts should be paid to reduce the standard deviation.

References.

(1) T. Ohtsuki, et al. Phys. Rev. Lett., 93, 112501 (2004)

(2) M. Jaeger, et al., Phys. Rev., C54,423 1996)

(3) E. B. Norman, et al., Phys. Lett., B519, 15 (2001)

(4) Edited by C.Michael Lederer and Virginia S.Shirley, Table of Isotopes,1978,John Wiley & Sons.

Transmutation Test in Discharge Experiment with Pd/CaO/Pd Multi-layered Cathode

S.Narita*, H.Yamada, D.Takahashi, M.Yamamura, Y.Wagatsuma, M.Itagaki, S.Taniguchi

Department of Electrical and Electronic Engineering, Iwate University

Morioka, Iwate, 020-8551, JAPAN

* narita@iwate-u.ac.jp

ABSTRACT

We performed discharge experiment in deuterium atmosphere using cathode with multi-layered structure of Pd/CaO/Pd on which Cs are deposited, and the possibility that the transmutation reaction of Cs to Pr just as being observed in the permeation experiment was investigated. In addition, a search for newly produced elements over the wide mass range resulting from nuclear reaction was made by ICP-MS and TOF-SIMS analysis. In this primary study, we have not seen the clear evidence for the transmutation. In the current experimental condition, it was supposed that the deuterium fluence was not sufficient enough to induce the reaction significantly.

Keywords : Discharge, Multi-layered sample, Pd/CaO/Pd, Nuclear transmutation, ICP-MS, TOF-SIMS, Gamma rays

1. Introduction

Among the experimental approaches for the study of low energy nuclear reaction in condensed matter, permeation of D through Pd/CaO complex sample is widely recognized as well-established technique in which some specific transmutation reactions (e.g. Cs→Pr) have been observed [1]. Although the reaction mechanism has not been clarified theoretically, it has been claimed that sufficient D flux in the permeation through the sample and the multi-layered structure of the sample, especially for existing CaO layer, are necessary for triggering the phenomenon in the method.

Besides the permeation method, we have demonstrated the possibility of inducing low energy nuclear reaction by exposing Pd or Pd deuteride to the discharge in deuterium atmosphere. For example, the detection of nuclear products and anomalous gamma ray emission have been reported [2,3].

In this study, considering those experimental results, we performed the discharge in deuterium gas using cathode with multi-layered structure of Pd/CaO/Pd on which Cs are deposited and searched for peculiar phenomena which suggest occurring nuclear reactions, especially for Pr production by the transmutation reaction of Cs just as observing in the permeation experiment.

2. Experiment

The multi-layered sample was prepared in the following procedure. The Pd foil (12.5mm x 12.5mm x 0.1mm in size, >99.95% in purity) was washed with acetone and aqua regia. On the foil, ~2nm CaO and ~40nm Pd layers were formed by Ar ion beam sputtering. For now, the thickness of each layer is just adjusted by changing sputtering time and the surface condition is not always uniform, so it does not seem to be controlled. Improving sample quality should be considered in the future study since deuteron dynamics in the sample can be strongly affected by the sample condition.

Then, Cs was deposited on the surface of thin Pd layer by electrolysis. Pd/CaO/Pd cathode and Pt anode were put into 0.5mM of Cs_2CO_3/H_2O solution, and a 1V was applied the electrodes for 30 seconds.

After Cs deposition, the multi-layered sample was placed on the Au stand as the cathode in the discharge cell. The cathode was surrounded by a quartz cylinder to prevent movement during the discharge. The cell made of Pyrex glass has a spherical shape with a volume of ~1500cm^3. The thickness of the glass is 5mm. The cell is connected to a vacuum system through the port on the upper part of the cell so that we can drive out the gaseous impurities in the cell and control the pressure inside the vessel. An Au foil (0.1mm in thickness) hung on an Au wire was used as the anode. The gap distance between the two electrodes was ~10mm.

It is possible that the elements on the cathode surface are diffused by sputtering in the discharge, so that small amount of the elements produced by the

nuclear reactions almost can be flown away. In order to detect such elements, two pieces of Au foil (5mm x 10mm x 0.1mm) were place around the cathode hung by Au wire. One of the surfaces of each foil faced to the cathode to received elements sputtered. The Au foil is called "Au side-foil" hereafter in this paper.

After evacuating the cell to 10^{-2}-10^{-3}Torr, deuterium gas was supplied until the inside pressure became 1Torr. Then, DC voltage was applied to expose the sample to discharge with currents of 1-4mA and voltage of 400-600V. This condition was standard glow discharge. In order to discuss the time dependence for the detection efficiency, we performed some experimental runs with different duration periods of the discharge, 1hour, 3hours and 7days. For reference, we made discharge in nitrogen gas instead of deuterium for 1hour.

Two NaI(Tl) scintillation counters (76mmϕ x 76mm and 25mmϕ x 25mm in cylindrical crystal size, respectively) were used to detect gamma rays from the experimental system. They were placed perpendicularly ~10mm away from the side wall of the cell. The photons from the scintillation counter were detected by a photomultiplier tube (PMT). The signal from the PMT was amplified and the pulse height distribution was obtained using a multi-channel analyzer (ORTEC ScintiPack), then it was converted to an energy distribution of the gamma rays. These counters have independent power supply and data acquisition system, foreign electric noise and accidental noise can be distinguished from the real signal by checking coincidence signal of two counters.

The multi-layered cathode and one of the Au side-foils were analyzed by inductively coupled plasma mass spectroscopy (ICP-MS) (SEIKO INSTRUMENTS INC.:SPQ9000). The sensitivity of ICP-MS is so high that the quantitative analysis for Cs and Pr is enabled precisely. Also, the qualitative analysis over wide mass range can be made. For the analysis, sample solution introduced to the ICP-MS was prepared by soaking multi-layered cathode or Au side-foil in high purity HNO_3 solution for 30s.

For the other Au side-foil, the surface was analyzed by time-of-flight secondary ion mass spectroscopy (TOF-SIMS) (ULVAC-PHI:TFS-2100). As well as good sensitivity for detecting a small amount of elements on the surface with high mass resolution, TOF-SIMS is capable of analyzing all the elements including their isotopes. Then, we investigated qualitative analysis over all elements and anomaly in the isotopic abundance for the elements detected.

3. Results

3.1 ICP-MS analysis

Electrolysis Time [s]	Cs density [ppb] ([ug/g])	
	sample-1	sample-2
10	56.9	87.8
50	47.9	29.4
100	7.6	63.7

Table 1: Deposited Cs density of the Pd/CaO/Pd cathode measured by ICP-MS

Condition	Pd/CaO/Pd [ppb]		Au side-foil [ppb]	
	Cs	Pr	Cs	Pr
D_2 1hr	44.3	1.6	2.0	1.6
D_2 3hr	4.4	8.9	0.7	1.5
D_2 7dy	1.3	1.3	0.5	1.3
N_2 1hr	44.7	6.1	2.2	1.6

Table 2: Cs and Pr density measured by ICP-MS for the Pd/CaO/Pd sample and Au side-foil for each experimental condition.

Condition	Pd/CaO/Pd	Au side-foil
D_2 1h	Pd, Cs	Cu, Pd
D_2 3h	Li, Sc, Ti, Mn, Fe, Cu, Zn, Rb, Sr, Ru, Pd, Cs	Li, Sc, Fe, Cu, Zn, Pd, Pb
D_2 7d	Li, B, Sc, Fe, Cu, Zn, Ru, Pd, Cs	Sc, Fe, Cu, Zn, Pd
N_2 1h	Pd, Cs	N/D

Table 3: Candidates of element with mass on which peak was observed in ICP-MS spectrum.

At first, the quantity of Cs deposited onto the sample was evaluated. Table 1 shows the Cs concentration measured by ICP-MS for different duration time of electrolysis. It turned out that the quantity was not always constant and could not be controlled well by changing electrolysis time. It is supposed that our electrolysis method for Cs deposition has not been well-established. In this study, we temporarily made the electrolysis time 30sec. In this condition, the Cs quantity was estimated to be 50-100ppm, and it corresponded to a few mg per gram of cathode sample.

After the discharge, the quantitative analyses for Cs and Pr were made for multi-layered cathode and Au side-foil for various experimental conditions, and the results are shown in Table 2. For every experimental condition, we did not observe clear Pr signals exceeding background level of mass spectroscopy for both multi-layered cathode and Au side-foil samples. It can be seen that the longer we made the discharge duration, the less the Cs density for the multi-layered sample became. This is thought to be the effect of sputtering in discharge.

In ICP-MS analysis, we also surveyed peaks in mass spectrum qualitatively. We observed several peaks. Table 3 shows corresponding candidates of elements for such signals. Note that some of these are signals by interference of molecules. Other than these elements, major considerable impurities, i.e. B, Na, Mg, Al, Si, P and K were detected in all samples. The Pd signals were found for Au side-foil, and they are considered to be diffused from the cathode by sputtering as well as Cs.

As shown in Table 3, more signals were found for the experiment with longer discharge period.

There are two possibilities, that is, integrating contamination or transmutation products in longer experiment. Actually, we found that the inside pressure of the cell become 20Torr after 1week discharge although it was set to be 1Torr at the beginning of the experiment. There was apparently gas leak. It might affect the purity of the inside of the cell. So we would say these elements originated from impurities from environment rather than nuclear products. The sealing and pressure control should be considered for further study.

3.2 TOF-SIMS analysis

One of the Au side-foils was analyzed by TOF-SIMS. Figure 1 shows the results of TOF-SIMS analysis for samples for different discharge time. There are clear Cs signals on mass 133, while no Pr signals are found on mass 141. As observed in ICP-MS analysis, more materials including both elements and the fragments of molecules are likely to be detected for longer discharge samples. As described in ICP-MS results, they were possibly originated from contaminations from environment.

In ICP-MS analysis, several candidates of elements were detected, then, we investigated if those elements were also detected in TOF-SIMS. Table 4 shows elements detected in both ICP-MS and TOF-SIMS. Some of the elements listed in Table 4 were detected with their isotopes and their abundances were consistent with natural ones. Most of these are detected for the reference sample (i.e. sample exposing discharge in N_2), however Boron was detected only in D_2 discharge samples although the abundance of the isotopes were not clearly different from natural one as the signal statistic was poor. It can be a candidate of element produced during the discharge, although it is not a rare element.

The peaks which correspond to Sc, Rb, Sr, Ru and Pb were found only in ICP-MS analysis for the sample exposed to the discharge for 1 hour and/or 3 hours. Since sensitivity and mass resolution of ICP-MS and TOF-SIMS are different, we cannot say these elements really exist. If they do, it is quite interesting in terms of transmutation reaction. Further study is desirable.

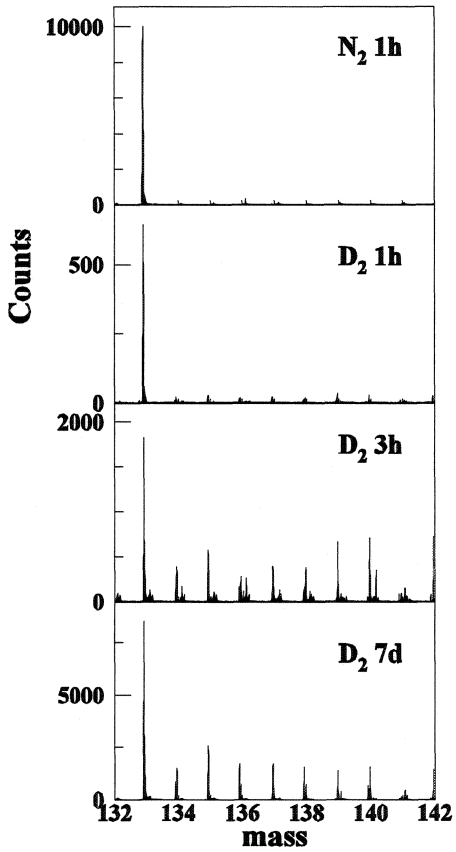

Figure 1: TOF-SIMS mass spectrum for the sample used in different discharge conditions.

Condition	Elements detected
D_2 1h	Li, B, Fe, Cu
D_2 3h	Li, B, Fe, Cu
D_2 7d	Li, B, Fe, Cu
N_2 1h	Li, Fe, Cu

Table 4: Elements detected in TOF-SIMS analysis.

3.3 Gamma ray measurement

The gamma ray spectra observed by the detectors during the discharge for each experiment are shown in Figure 2. In all spectra, including reference experiment with nitrogen, there are suspicious peaks around 20-30keV for detector-2. The peak looked like growing as time passed. For 1 week experiment, we suspended the data acquisition after 6 days passed, then, it was resumed again. Even in the data for resumed run, the peak was observed again. After stopping the 1 week discharge, the gamma ray

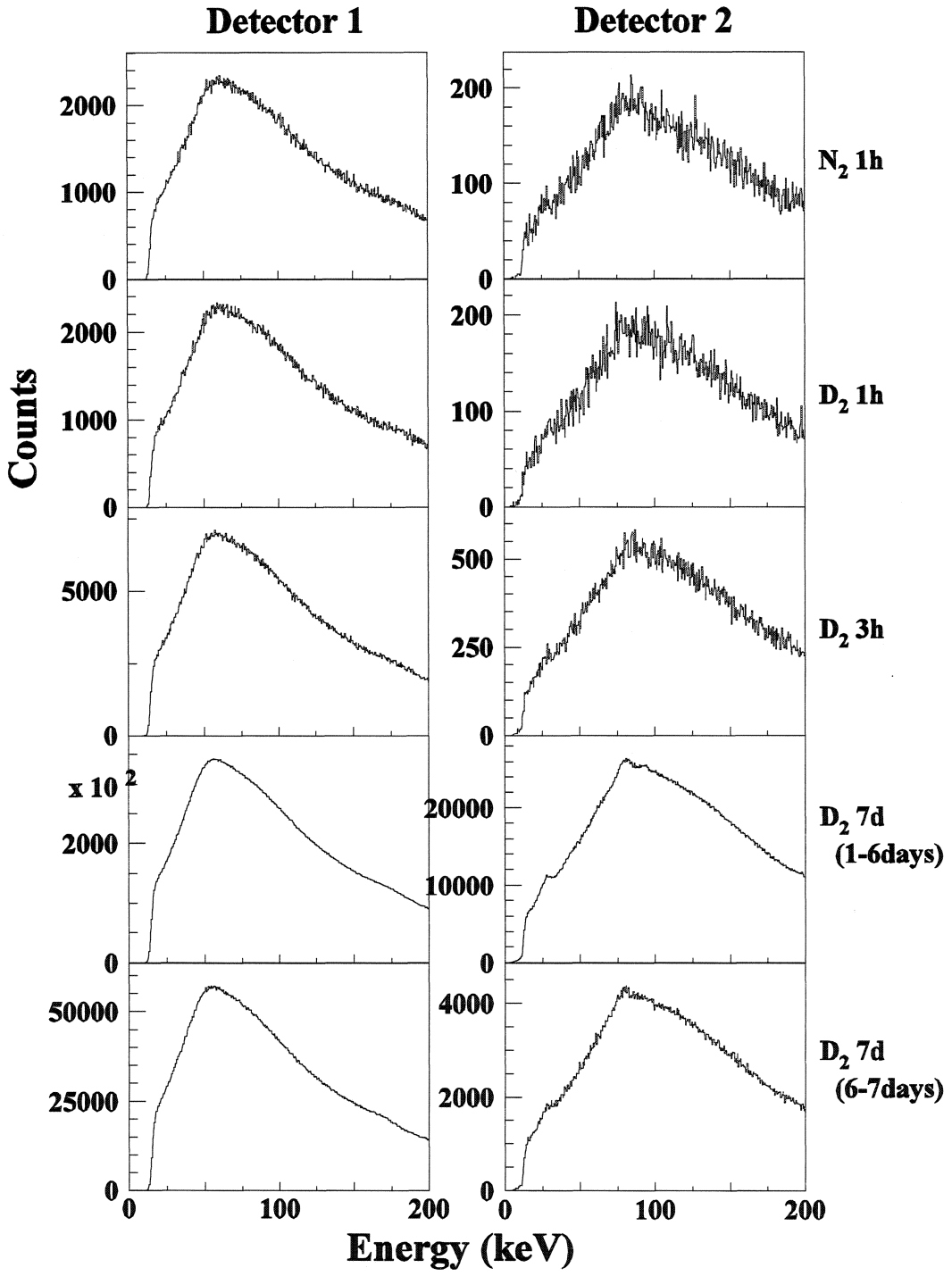

Figure 2: Gamma ray spectra of two NaI(Tl) detectors for each experimental condition

detection was performed and the suspicious peak was still shown (Figure 3). For the detector-1, such peak was not observed at all. If these signals are originated from gamma ray emission from just like short-lived radio isotopes which are assumed to be produced in nuclear reactions, some symptom should be seen in the spectra of detector-1. In addition, since the peak was detected even in the nitrogen experiment, it was

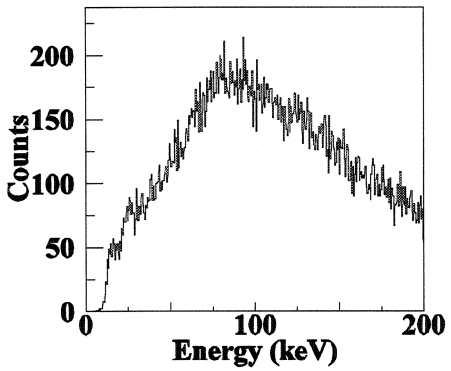

Figure 3: Gamma ray spectrum of Detector-2 after stopping 7days discharge.

definitely different from the anomalous gamma peak which we previously reported [3]. In the previous experiment, it was observed only in hydrogen system. Therefore, we cannot conclude these are the evidence for the nuclear reactions, for now.

4. Discussion

As described above, we did not observe the evidence of nuclear reaction such as the transmutation of Cs to Pr in this study. According to MHI reports, in permeation experiment, a sufficient deuterium flux irradiating to the sample is an important factor for determining conversion rate of nuclear transmutation. Now we discuss the difference in that point between two experimental methods.

MHI group has estimated the cross section of the reaction of Cs to Pr and its conversion rate assuming the deuterium flux permeating through the sample being equivalent to deuterium beam irradiation. They found that the conversion rate is proportional to average flow rate and they obtained ~0.3 for irradiating ~$3x10^{23}$ deuterium atoms [4]. In our experiment, DC current on the cathode was 1-4mA and the cathode area being exposed to the discharge was ~$1cm^2$. Using these values the number of D ions irradiated to the cathode a second was roughly estimated to be ~$10^{16}cm^2$. This value is much smaller than that for permeation experiment by MHI group. If we try to enhance the yields significantly under the current discharge condition, the discharge time has to be made much longer. Increasing discharge current may be possible way to induce the reaction, however the sample surface can be damaged and the elements produced on the surface are more likely to be diffused in such heavy discharge condition. It is not desirable condition for detecting a small amount of element.

From the point of view for improving transmutation efficiency, additional techniques should be considered. One considerable method is irradiating laser. According to recent reports, it is supposed to initiate and amplify the nuclear effect [5,6]. The other one is merging the key technologies of permeation and discharge methods. In practice, electric field is utilized to force deuteron to permeate to the sample. We will apply these techniques to our current method.

Using another kind of multi-layered sample systematically is also interesting in terms of understanding the mechanism of low energy nuclear reaction in condensed matter. There are some reports of anomalous enhancement of the cross section of nuclear reaction in various experimental methods [7,8].

We are now planning to accomplish a modified experiment considering these ideas.

5. Summary

We have attempted to induce a transmutation reaction in discharge method using Pd/CaO/Pd multi-layered sample deposited the target element, and no clear evidence for the transmutation reaction was observed in ICP-MS or TOF-SIMS analysis, this time. Comparing with permeation method, some problems were found out in our experiment, that is, quality of the sample and the deuterium fluence to the sample. The experimental technique will be modified considering those problems. We will continue to investigate the possibility of discharge method for the study of condensed matter nuclear reaction, and try to improve transmutation efficiency obtained in the current experiment.

References

1. Y. Iwamura et al., Jpn. J. Appl. Phys. (2002) 4642.
2. A. Arapi et al., Jpn. J. Appl. Phys. (2002) L1181.
3. S. Narita et al., Proc. of JCF5 (2004) 14.
4. Y. Iwamura et al., Proc. of JCF5 (2004) 60.
5. D. Letts, Proc. of ICCF10, in press.
6. V. Violante et al., Proc. of ICCF11, in press.
7. Y. Awa et al., Proc. of JCF5 (2004) 6.
8. A.G. Lipson et al., Proc. of ICCF9 (2003) 218.

SEARCH FOR TRANSMUTATION PRODUCTS ON PD-FOIL SURFACE AFTER HIGHLY PRESSURIZED DEUTERIUM PERMEATION

H. YAMADA, S. NARITA, S. TANIGUCHI, T. USHIROZAWA, S. KURIHARA, M. HIGASHIZAWA H. SAWADA, M. ITAGAKI and T. ODASHIMA*

Department of Electrical and Electronic Engineering, Iwate University, Ueda 4-3-5, Morioka, 020-8551 Japan *yamadahi@iwate-u.ac.jp*

* Department of Chemical Engineering, Ichinoseki National College of Technology, Hagiso, Takanashi, Ichinoseki, 021-8511 Japan *odashima@ichinoseki.ac.*

Abstract: Time-of-flight secondary ion mass spectroscopy (TOF-SIMS) and inductively coupled plasma mass spectroscopy (ICP-MS) were employed for elemental analysis of plain palladium foil surface. Increase in count intensity of B and Mg was found after deuterium permeation by TOF-SIMS. ICP-MS has revealed increase in amounts of elements B, Mg, Zn and Ba. These elements could have been produced by some nuclear transmutation. The results suggest that the reaction occurs on/in plain Pd foil as well as on/in Pd film complexes.
Keywords: Pd-deuteride, Deuterium permeation, Transmutation, TOF-SIMS, ICP-MS, Surface analysis

1. Introduction

The phenomena on nuclear reactions at low temperature in solid-state has been widely investigated for these sixteen years. Among several experimental methods for the reaction, the gas permeation method is one of the promising methods. Iwamura et al.[1] has studied using this method with Pd film complexes, which consist of thin Pd layers, a CaO layer and a bulk Pd. They have recently found a certain rule of nuclear transmutation, that is, 8 mass number and 4 atomic number increase in the process. The phenomenon has been observed with good reproducibility. While, we have been taking account of the possibility of nuclear transmutation not only in such Pd film complexes but also in plain Pd foil by hydrogen gas permeation at room temperature. We have performed an elemental analysis on the Pd-foil using time-of-flight secondary ion mass spectroscopy (TOF-SIMS) and have reported that increase in count intensity of several elements including Ag was found after hydrogen permeation [2]. The count intensity of Fe has been sometimes observed to increase significantly after the permeation of highly pressurized hydrogen gas through Pd samples of 0.1 and 0.3 mm thickness. This result would show a pressure effect on the reaction of transmutation. Furthermore, the isotopic ratio of Ti and Cr has been observed to differ from the natural one for those elements. These results have suggested that several elements were produced by a nuclear transmutation and that the reaction could occur in hydrogen system as some researchers have claimed in various experiments [3, 4].

In this present study, we have performed a deuterium permeation experiment by highly pressurized deuterium gas using plain Pd foil without any additional layer, and have searched for the products as a result of low energy nuclear reaction. The method has an advantage of involving less contamination in the palladium sample in contrast to other methods; the method is preferably used in investigating small amount of elements. We employed TOF-SIMS and inductively coupled plasma mass spectroscopy (ICP-MS) for the elemental analysis. This study would provide us information to understand transmutation process systematically.

2. Experiment

The experimental set-up is basically same as that used previously [2]. The Pd foil (99.95% pure) sample of

0.1×12.5×12.5mm in size was rinsed with acetone and pure water, then washed by aqua regia to remove impurities on the sample surface. No deuterium gas was loaded to the sample before deuterium permeation experiment. The Pd foil was set into a stainless steel holder placed between two chambers. The upper chamber was filled with deuterium gas at a pressure up to 1 MPa, and the lower was evacuated by a diaphragm (or diffusion) pump to prevent the Pd sample being contaminated from the atmosphere. The gas atoms were driven through the Pd sample to the evacuated chamber by the pressure gradient at 70 ℃. The gas was kept flowing for about 1 week, then the sample ("Sample after permeation") was taken out from the holder. Before the element analysis, the sample was not treated for purging the deuteron atoms remaining in. The sample surface of gas-filled side was analyzed by TOF-SIMS (ULVAC-PHI: TFS-2100). Next, the samples were analyzed by ICP-MS (Seiko Instruments Inc.: SPQ9000).

TOF-SIMS has a good sensitivity for a small quantity of the elements on the sample with high resolution in mass number although it is difficult to deduce the absolute quantities from its output data alone. The primary ion in TOF-SIMS was Ga^+ and measured area was 40×40 micron square. Since TOF-SIMS is not capable of analyzing total amount of elements, we also tried semi-qualitative analysis of the Pd samples using ICP-MS to obtain roughly the total amount of elements on/in it. In pre-processing of ICP-MS analysis, the Pd sample was immersed in 1 cc of ultra pure nitric acid for 30 sec to dissolve most of all the impurity elements on the Pd surface in the nitric acid. Then pure water was added to the nitric acid solution to be totally 50 cc of more weak acid solution for the processing ICP-MS. All the elements with mass number from 6(Li) to 238(U) can be detected in a run of the ICP-MS with high sensitivity (ppb). In our analysis, the signal stands out when the corresponding element exists with the density above 0.1 ppb. In order to take into account the contamination from the environment, we prepared the control sample ("Control sample"), which was set into the holder for the same period of 1 week as that for "After permeation sample" without flowing the deuterium gas. Comparing the composition of the elements on the surface of "Control sample" with that of "After permeation sample", we specified newly produced and increased elements during the deuterium gas permeation.

3 Results and Discussion

3.1 Time behavior of D_2 flow rate

Iwamura et al. have reported that the production amount of Pr is nearly proportional to the deuterium gas flow rate during a fixed permeation period using Pd film complexes [5]. Though a plain Pd foil was used in this study, similar condition of higher deuterium flow rate is thought to be essential for the reaction of transmutation. Further, the flow rate seems to be strongly affected by contamination at the deuterium gas flow pass of the test system. Thus, we investigated the difference of the flow rate between the cases with and without baking important parts of the gas flow system. We also investigated the difference of the flow rate between the cases using diffusion and diaphragm (dry) pumps, which were used to evacuate the inside of gas flow system.

First, we used a diaphragm pump to evacuate the upper and lower sides of chamber, and then only filled the upper chamber with deuterium gas at 0.5 MPa. Fig. 1 shows a time behavior of deuterium flow rate without baking. The rate was over 0.8 SCCM at the beginning of the deuterium gas flowing, followed by a decreasing the rate with time to the value below 0.1 SCCM after 200 min from the beginning. The pressure was again increased to 0.5 MPa after 550 min, resulted in increasing the rate from the value below 0.1 to ~0.5 SCCM. However, the rate soon became low as a value less than 0.1 SCCM, as seen in Fig. 2. Fig. 3 shows a similar time dependence of flow rate for deuterium gas pressure of 1.0 MPa. No clear pressure effect on the rate was observed between the tests for 0.5 and 1.0 MPa. Since contaminants such as water molecules could be removed from the inner

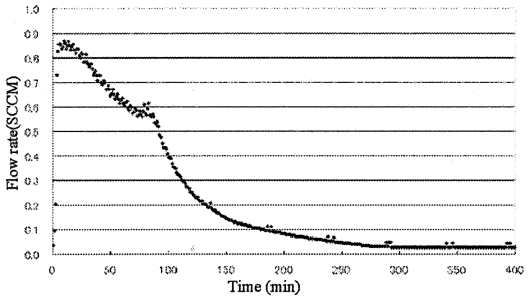

Fig. 1 Time behavior of D_2 flow rate for 0.5MPa without baking.

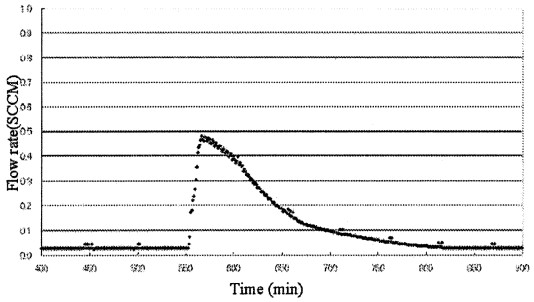

Fig. 2 Time behavior of D_2 flow rate for 0.5MPa without baking

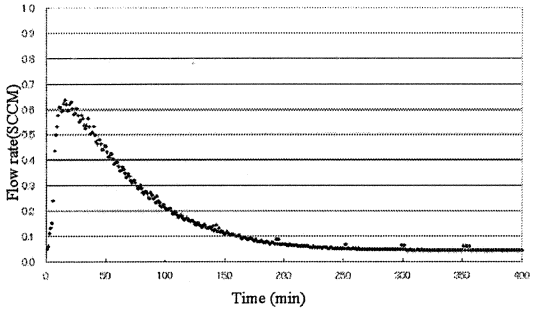

Fig. 3 Time behavior of D_2 flow rate for 1.0MPa without baking

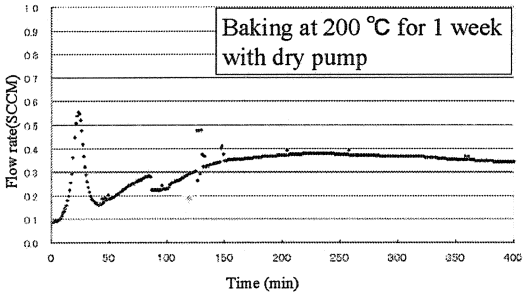

Fig. 4 Time behavior of D_2 flow rate for 0.5 MPa with baking.

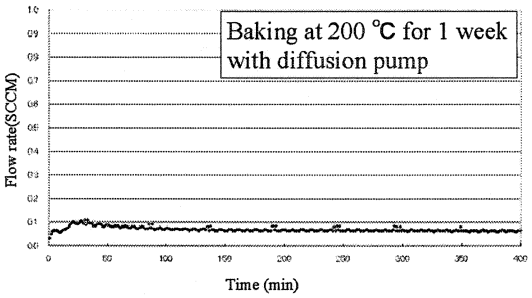

Fig. 5 Time behavior of D_2 flow rate for 0.5 MPa with baking.

surface of flow system by increasing temperature, we baked important parts of the flow system at 200 ℃ for 1 week. This procedure gave the flow rate above 0.3 SCCM for 400 min, as seen in Fig. 4. The result might imply that when the system without baking is used, water molecules covering the surface inside of chamber would move to the sample surface and would prevent the deuterium gas from flowing through the bulk of Pd sample.

Next, we changed the diaphragm pump to a diffusion pump and baked the same important parts of system at 200 ℃ for 1 week. Though the pressure inside of system was lower than that obtained using the diaphragm pump, the rate below 0.1 SCCM was continuously observed from the beginning, as seen in Fig. 5. It is likely that gaseous organic molecules with high molecular weight from the diffusion pump would close the pass of deuteron on the surface of Pd sample.

3.2 Possible elements production

In TOF-SIMS analysis, we performed on three randomly selected areas (40 μ m×40 μ m) of each sample. The TOF-SIMS system is capable of removing the uppermost surface layers of the Pd sample by Ga sputtering for surface cleaning. Of many detected as counts by the TOF-SIMS system, some parts of them are considered to correspond to impurities included in the Pd foil.

In the TOF-SIMS analysis, we do not discuss absolute quantities of the elements, since we have difficulties in quantitative analysis using the TOF-SIMS. Instead, we

	Control			After permeation		
	C1	C2	C3	P1	P2	P3
^{11}B	4	1.5	1.6	32	27	35
^{24}Mg	10	11	1.7	240	157	324
^{64}Zn	—	—	—	—	—	—
^{106}Pd	1241	329	471	258	264	351
^{138}Ba	—	—	—	—	—	—

Table 1. The intensities of ^{11}B, ^{24}Mg, ^{64}Zn, ^{106}Pd and ^{138}Ba,defined as the count of secondary ions of these elements divided by that of ^{69}Ga and multiplied by 10^4, obtained using TOF-SIMS.

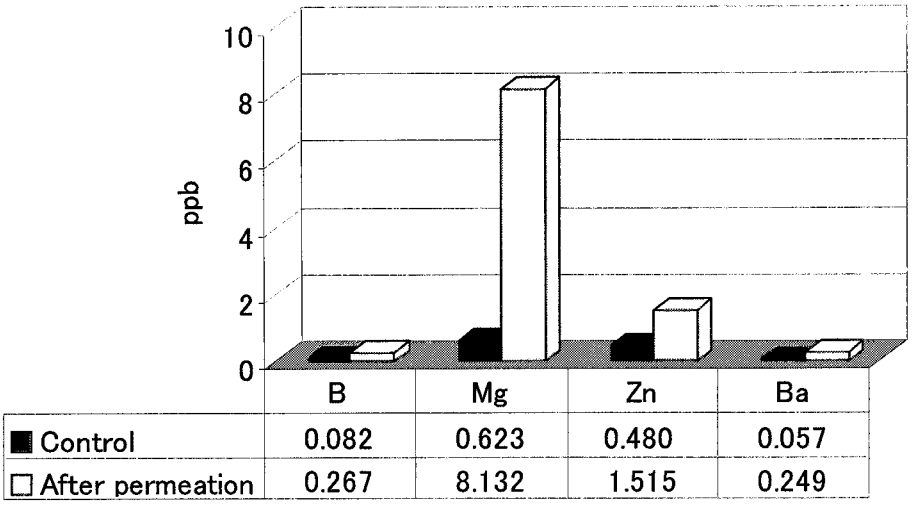

Fig. 6 Increase in count intensity of ICP-MS for B, Mg, Zn and Ba, after the deuterium permeation.

use an intensity that is defined here as the count of secondary ions of each element divided by that of ^{69}Ga and multiplied 10000. We did not find any significant difference in the mass spectrum for every selected area of the Pd samples at a fixed test condition.

Table 1 presents count intensities of ^{11}B, ^{24}Mg, ^{64}Zn, ^{106}Pd and ^{138}Ba for "Control sample" and "Sample after permeation" at gas pressures 1 MPa. These intensities were obtained from each three randomly selected areas of 40×40 micron square. Here, C1, C2, C3 refer to the place of these three areas of the "Control sample", P1, P2 and P3 do those of "Sample after permeation", respectively. Increase in the count intensity for elements ^{11}B and ^{24}Mg has occurred during the permeation. In particular, marked increase in the intensities of ^{24}Mg was found in "Sample after permeation". While, a little difference in counts is seen in Table 1 for ^{106}Pd between "Control sample" and "Sample after permeation". No count of ^{64}Zn and ^{138}Ba was detected by the TOF-SIMS.

The density obtained by ICP-MS was rough value as mentioned above. To compare the amount of an element in a solid sample with that in another solid sample using the ICP-MS, dissolved amount of Pd in 1 cc pure nitric acid for one sample is desirable to be almost same as that for another one. Furthermore, when a density value of an

element in one solution sample" is compared with that in another solution, processing ICP-MS for the solutions is desirable to be performed in a same working run of the ICP-MS. Thus, we processed the ICP-MS for the solution of "Control sample" at first and immediately followed by that of "Sample after permeation". Density of Pd was 5.384 ppm in the solution of "Control sample" and 4.225 ppm in the solution of "Sample after permeation", respectively. The small differences in density between two solutions indicates that the amount of Pd dissolved in the nitric acid solution for "Control sample" was almost same as that for "Sample after permeation". Of other detected as counts, some elements such as Na might be impurities introduced into ICP-MS from environment. The density of Na was 14.157 and 17.387 ppb for "Control sample" and "Sample after permeation", respectively. The impurity of Na is considered to originate mainly from beakers that were used to contain the solutions in the pre-processing of ICP-MS analysis. The density of Na in the solution of "Control sample" fairly equals that in the solution of "Sample after permeation". This means total amount of contaminants in solution of "Control sample" is almost same that of "Sample after permeation".

Fig. 6 illustrates densities of B, Mg, Zn and Ba in the solutions for two samples. The densities of these elements in the solution of "Sample after permeation" are seen to considerably increase after the permeation. In particular, that of Mg has increased markedly after the permeation. This feature of increasing in density of Mg agrees with that found by TOF-SIMS analysis. It should be noted that ICP-MS for "Control sample" was followed by that for "Sample after permeation". This implies that contamination by the processing ICP-MS for "Control sample" had little affect on the result of the next processing for "Sample after permeation". In other words, these increases were unlikely due to contaminants from balk of Pd sample and environment. These results suggest that elements B, Mg, Zn and Ba could have been produced in the deuterium gas permeation process.

4. Conclusion

Elements analysis on the Pd foil were performed for a sample after deuterium permeation experiment and for a control sample using TOF-SIMS and ICP-MS. TOF-SIMS revealed increase in count intensity of elements ^{11}B and ^{24}Mg after the deuterium gas permeation. While, the analysis using ICP-MS has presented the increase in amount of elements B, Mg, Zn and Ba after the permeation. The amount of Mg was observed to increase markedly among the elements. These four elements might be produced during permeation of highly pressurized deuterium through plain Pd foil by some nuclear transmutation occurring in/on Pd foil. The results are of storong positive evidences of the nuclear transmutation and suggest that the reaction occurs on/in plain Pd foil as well as on/in Pd film complexes.

References:

1) Y. Iwamura, T. Itoh and, M. Sakano, Jpn. J. Appl. Phys., 41, 4642 (2002).
2) H. Yamada, S. Narita, H. Onodera, H. Suzuki, N. Tanaka, T. Nyui and T. Ushirozawa, Proceedings of the 5-th Meeting of Japan CF Research Society, pp. 69-73, 2004
3) Deform, D. Murat. X. Dufour and J. Foos, Proceedings of 8-th International Conference on Cold Fusion, p. 153 (2000).
4) T. Ohmori, H. Yamada, S. Narita and T. Mizuno, Proceedings of 9-th International Conference on Cold Fusion, p. 284 (2002).
5) Y. Iwamura, T. Itoh, M. Sakano, S. Sakai and S. Kuribayashi, Proceedings of the 5-th Meeting of Japan CF Research Society, pp. 60-64, 2004

Possible Coexistence of Electron and Electron Neutrino in Nucleus and Its effect on D-D Cold Fusion into Helium in Pd

Mikio Fukuhara
Tohoku University
E-mail: fukuhara@imr.tohoku.ac.jp

Abstract

We investigate a possibility of coexistence of an electron and an electron neutrino in nucleus, based on weak interaction in β decays. Physical roles of electron and neutrino for cold fusion of helium in solid lattice were investigated in terms of elemental particle physics. The fusion requires massive photon bonding with 5.2 keV for confinement of deuteron pairs in solid lattice. The electron and neutrino in nucleus enhances the fusion reaction as well as a catalytic effect of neutral pions.

1. Introduction

In a previous paper,[1] elastic parameters (Young, shear and bulk moduli, Lamé parameter, Poisson's ratio and Debye temperature) and shear damping anomalies accompanied by generation of excess heat (not less than 6 W) were observed between 116 and 190 K in the deuterated palladium, $PdD_{0.719}$. We interpreted the dynamic interaction as a mixture effect of the result of condensation of deuterons into octahedral interstitial sites by electrolysis and contraction of the deuteron octahedral around the $Pd^{10-\delta}$ atom with the help of the electron-photon charge-density wave (CDW) coupling.[2]

In the following paper,[3] we showed that the formation of helium nucleus from two deuterons, *i.e.*, fusion, requires necessarily a direct force due to exchange of two neutral pions which do not actually compose the deuteron nucleus.

$$D^2 + D^2 + 2\pi^0 = He^4 \qquad (1)$$

The neutral pion is provided by two photons, which are produced by emission of excited collective electrons derived from the palladium atoms. The introduction of the pions makes possible to reduce remarkably an internuclear distance, enhancing fusion rate for helium formation. For a significant role for nuclear fusion by neutral pion, we explained that the pion could easily enter within effective nuclear force field of deuteron pairs at close proximity, because the neutral pion does not experience a Coulomb barrier.[4]

On the other hand, nitrogen in the earth's atmosphere was interpreted by endothermic nuclear transmutation of carbon and oxygen nuclei confined in carbonate lattice of the mantle, with help of electropionic attraction effect due to the excited electron and plenty of neutrinos.[5] However, it is not necessarily clear physical role of the electron and electron neutrino for nuclear fusion yet.

Our next interest lies in a possibility of coexistence of electrons and electron neutrinos

neutrinos for nuclear cold fusion, in addition to catalytic effect of neutral pions.

2. Tight bonding of Pd lattice for confinement of the deuterons

In our model, a tight bonding of Pd lattice for contraction of the deuterons is necessary condition. We first consider how the deuteron link to each other for fusion in interstitial Pd sites. One way to understand the origin of the attractive interaction between the deuteron atom pair is to imagine the existence of a virtual particle, which mediates the spherically symmetrical deuteron confined in lattice. Since the mass of the field quantum determines the range of potential and force, the maximum distance L that the virtual particles is allowed to travel by the Heisenberg uncertainty relation is given by the Yukawa formula[6]:

$$L \leqq c\,\Delta t \approx h/m_p c \qquad (2)$$

where c is the velocity of light, and t is time. We calculate the mass m_p of the postulated quantum from eq. (1), using the close proximity radii of deuteron, 0.038 nm in the previous paper.[3] The mass of 5.2 eV, being around 1/1000 times of the mass, 0.511 MeV, of the electron.

In order to maintain gauge invariance, it is necessary to introduce a gauge field which couples the conserved charge · · · in this case, the electromagnetic field. This result suggests the possibility of the mediation of a massive photon or a new particle. It is probably the former, although it is believed that the photon is a particle without mass in free space. Indeed, photons in superconductors are massive, because Cooper pairs are condensate in ground state of superconductor.[7] Therefore nuclear fusion in solid lattice requires massive photon bonding for confinement of deuteron pairs. This interaction for deuterium atom pairs is schematically shown in Fig.1, along with charge pion mediated *pn* interaction in deuteron. Thus, the Pd lattice with the tight bonding plays the same role as magnetic field confinement in hot nuclear fusion. In fact, the palladium *fcc* lattice has strong rigidity because the dynamic interaction does not occur in solids lacking shear strength.[2]

3. Physical role of electrons and electron neutrino for nuclear fusion

In the previous paper[8], we reported a possible coexistence of an electron and an electron neutrino in nucleus, based on weak interaction in β-decay. Provided that the electron of atom takes one's share of both electromagnetic and weak ones according as the zone ratio, we can see that one electron and one neutrino exist in proton and neutron, respectively. The electron and the neutrino are coupled as an *s*-wave boson in nucleus.

When a helium atom is formed two deuterons, quarks, electrons and neutrinos must be mediated by charged and neutral intermediated bosons, **W** and $\mathbf{Z^0}$ (Fig.2), respectively, as a result of mediation of charged and neutral pions.

$$u + e^- \leftrightarrow d + \nu \qquad (3)$$

$$e^+ + \bar{\nu} \leftrightarrow e^- + \nu \qquad (4)$$

$$e^- + \nu \leftrightarrow e^- + \nu \qquad (5)$$

From Fig.2, an addition of neutral pions is

equivalent to the double addition of eq.(5), *i.e.*, two e^- - ν pairs. Thus the addition of e^- and ν pairs enhances the fusion reaction.

4. Creation of electron and neutrino pairs

Last we consider how the pairs create before fusion reaction. When palladium nuclei with even atomic number exist, there is a possibility that double β decay, which is the second order β process, occurs [9].

$$(Z, A) \rightarrow (Z+2, A) + 2\,e^- + 2\,\nu, \qquad (6)$$

where Z and A are atomic and mass numbers, respectively. Eq.(6) is non-equilibrium equation. Since palladium in nature has five isotopes with even atomic number, *i.e.*, ^{102}Pd, ^{104}Pd, ^{106}Pd, ^{108}Pd and ^{110}Pd of 0.96, 10.97, 27.3, 26.7 and 11.8%, respectively, [10] the corresponding element sets for eq.(6) are ^{106}Pd→^{106}Cd, ^{108}Pd→^{108}Cd and ^{110}Pd→^{110}Cd. For starting elements, ^{106}Pd, ^{108}Pd and ^{110}Pd are plausible. As far as we know, no previous research has been done on physical role of electron and neutrino for nuclear reaction, except for nuclear reaction of excited electron and neutrino in solids [5]. This interesting area needs for further work.

5. Conclusion

We investigated necessary and sufficient conditions for cold fusion of helium in solid lattice in terms of elementary particle physics. The Pd lattice for confinement of deuteron pairs plays the same role as magnetic field confinement in hot nuclear fusion, because the attractive interaction between deuterium atom and electron is mediated by massive photon with 5.2 keV. Introduction of s-wave coupled electron and neutrino enhances cold fusion. The electron and neutrino pair may come from double β decay formation of helium,

$$(Z, A) \rightarrow (Z+2, A) + 2\,e^- + 2\,\nu. \qquad (6)$$

In this non-equilibrium equation, ^{106}Pd, ^{108}Pd and ^{110}Pd are plausible in nature.

References

1. H.Numata and M.Fukuhara, Fus.Tech., **31**, 300(1997).
2. M.Fukuhara, Fus.Tech., **34**, 151(1998).
3. M.Fukuhara, Fus.Sci.Tech., **43**, 128(2003).
4. D.F.Measday and G.A.Miller, Am. Rev. Nucl. Phys., **29**, 121(1979).
5. M.Fukuhara, Nuovo Cimento, **C27**, 99 (2004).
6. H.Yukawa and S.Sakata, Proc. Phys. Math. Soc. Jpn., **19**, 1084(1937).
7. G.Takada, Elementary Particle (in Japanese), Shokabo, Tokyo, 1987, p.189.
8. M.Fukuhara, unpublished
9. T.D.Lee and C.S.Wu, Weak Interactions, Ann.Rev.Nucl.Sci., **5**, 381(1965).
10. IUPAC, Element by element review of their atomic weights, Pure Appl.Chem.,**56**, 695(1984).

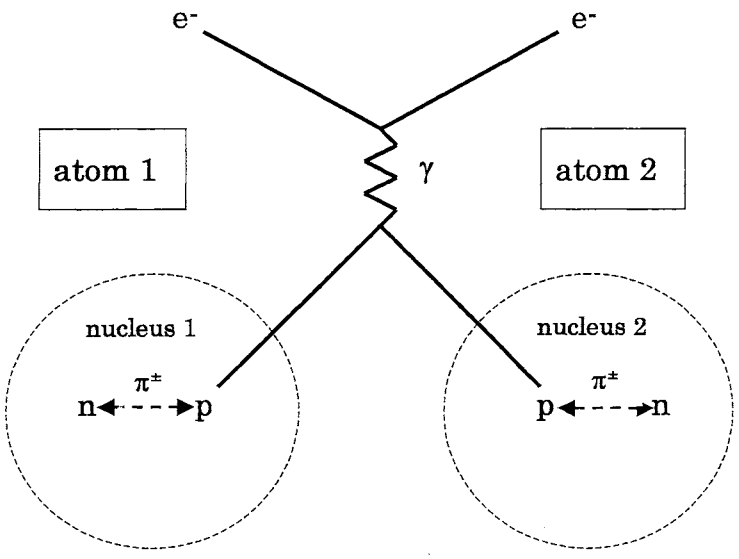

Fig.1 Schematic representation of electromagnetic interaction, $p+e^- \leftrightarrow p+e^-$, mediated by photon γ for two deuterium atoms, D_2, where p and n are proton and neutron, respectively.

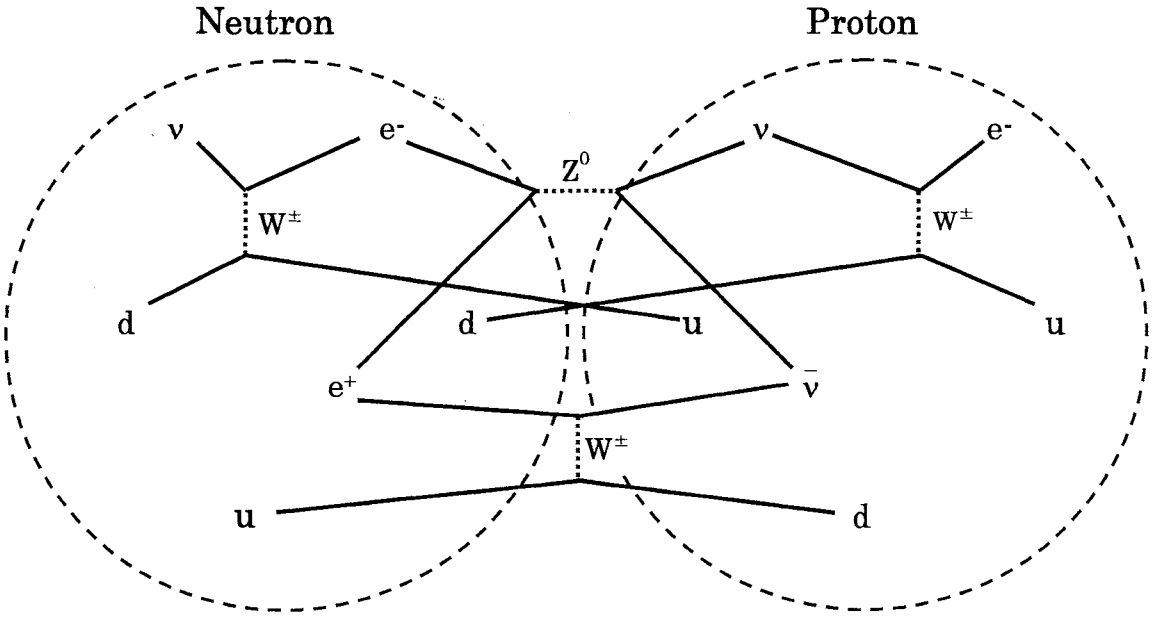

Fig. 2 Schematic representation of elementary particle interactions, $d+\nu \leftrightarrow u+e^-$ and $e^- + \nu \leftrightarrow e^+ + \bar{\nu}$, mediated by W and Z^0 bosons in proton and neutron deuterium atom, respectively, where u and d are up and down quarks, respectively. The reaction, $e^- + \nu \leftrightarrow e^- + \nu$, is eliminated.

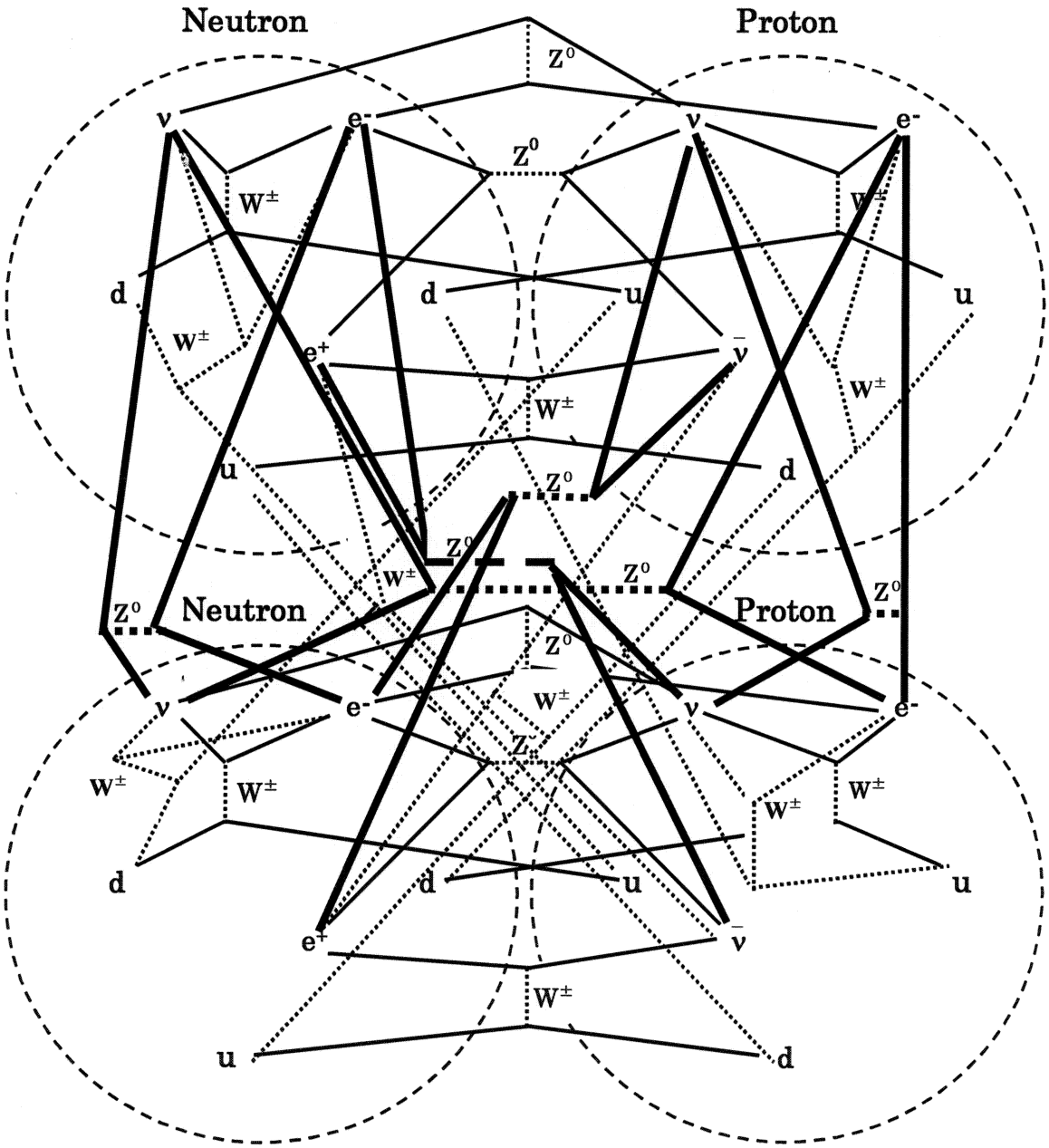

Fig. 3 Schematic representation of elementary particle interactions, $d+\nu \leftrightarrow u+e^-$, $e^+ + \bar{\nu} \leftrightarrow e^- + \nu$ and $e^- + \nu \leftrightarrow e^- + \nu$, mediated by W and Z^o bosons in proton and neutron of deuterium nucleus, respectively, where u and d are up and down quarks, respectively. The black lines are W and Z^o mediated interaction between proton and neutron. W and Z^o mediated interactions among protons and neutrons are dotted and broad lines, respectively.

An Explanation of Earthquake by Anomalous Explosion of Hydrogen Dissociated from Water in Mantle

Hiroshi Yamamoto, Free Journalist
3110-17, Tsuzuki, Mikkabi-Cho, Inasa-Gun, Shizuoka-Pref. Zip:431-1402, Japan
e-Mail: hughy@aqua.ocn.ne.jp

ABSTRACT: The mechanism of earthquakes is currently explained by the plate-tectonics theory which claims the earth's surface is covered with a series of crustal plates that can store elastic energy caused by relative movement of each plate. But recent observations of slow slip of crustal plates dismiss the capability of elastic energy storage in it. It was reported [1] that very powerful explosions of hydrogen and oxygen mixture dissociated from water due to nuclear irradiation at nuclear power plants can be explained by R. Mills' BlackLight process which claims that atomic hydrogen can release energy somewhat between chemical and nuclear reaction[2]. It is known that water injection into deep well can cause earthquake. Water can be dissociated into atomic hydrogen by metals in a very hot condition at the mantle. It was concluded that after accumulation of atomic hydrogen gas over 1GPa and 1500 Celsius degree and subsequent pressure drop due to cracks of the surrounding rocks triggers the BlackLight process, resulting in huge energy release, namely, earthquake.

Key words: hydrogen explosion, atomic hydrogen, BlackLight process

1. INTRODUCTION

It seems there are two ways to generate excess energy from hydrogen and its isotope. One is fusion and the other is to drop the electron in hydrogen atom from the ground state to the lower one. The later one is quite controversial to the current quantum physics and very few scientists in cold fusion research paid attention to it, but it was shown that later one can explain anomalous combustion phenomena such as very powerful explosions of hydrogen and oxygen mixture dissociated from water due to nuclear irradiation at nuclear power plants [1]. The mechanism of earthquakes is currently explained by the plate-tectonics theory which claims that the earth's surface is covered with a series of crustal plates that can store elastic energy caused by relative movement of each plate. But recent observations of slow slip of crustal plates by GPS (Global Positioning System) dismiss the capability of elastic energy storage in it and more plausible explanation is requested. If one can not find the cause of earthquakes, then, the next step is to study how human activities induced earthquakes and then to deduce a possible mechanism of earthquakes from the correlations between what was done and what happened.

2. EARTHQUAKES INDUCED BY HUMAN ACTIVITY

In 1961, a deep well was drilled at northeast of Denver Colorado U.S.A for disposal of nuclear waste fluids. Injection was commenced March 1962, and shortly after that, an unusual series of earthquakes erupted in the area. Injection had been discontinued and the number of quakes decreased dramatically. When the injection was resumed, quakes increased accordingly and the link between the fluid injection and earthquakes was established[3]. The most notable experience in this series of earthquakes is that many people heard extremely loud, explosive-like earth noises. Lately Japan experienced 2 large earthquakes, Niigata-Ken-Chuestu and Fukuoka-Ken-Seihouoki. There is a sharp contrast between two in the distribution pattern of epicentre. Fukuoka-Ken-Seihouoki has a slender rectangular pattern on the extension line of the Kego fault that seems a typical pattern of earthquakes induced by faults. But, the Niigata-Ken-Chuestu has a round shape distribution pattern of epicentre which suggests that the CO_2 injection into old gas well located near-by the epicentre of the first major earthquake and subsequent water permeation into mantle might have initiated the earthquake.

3. GENERATION OF ATOMIC HYDROGEN

The Earth's crust is divided into several separate solid plates. Subduction occurs when two plates collide and the edge of one dives beneath the other. The crust contains water and when it contacts with hot magma, metals in magma such as iron produce atomic hydrogen according to the following reaction.

$$3\,Fe + 4\,H_2O \rightarrow 8\,H + Fe_3O_4 \quad \text{-----(1)}$$

"H" designates atomic hydrogen.

Once atomic hydrogen is produced and if there is no heat sink at the collision point, just a collision of atomic hydrogen for a instance,

$H + H \rightarrow H_2$ (molecular hydrogen) wouldn't take place but just elastically repulse each other. This suggests that atomic hydrogen can exist much longer than normally expected. The pressure and temperature at 30km bellow the surface of the earth would be around 1GPa and 1500 Celsius degree. When the reaction (1) takes place at this condition and atomic hydrogen gas builds up, the pressure of the atomic hydrogen gas would be getting higher and higher and finally there would be cracks at the surrounding rocks of the hydrogen gas, resulting in pressure drop of the hydrogen gas.

4 ANOMALOUS ENERGY RELEASE FROM HYDROGEN ATOM

Randlle Mills demonstrated that hydrogen atoms can achieve lower states than ground state by a resonant collision with a near by atom or combination of atoms having the capability to absorb the energy to effect the transition, namely, an integer multiple of the potential energy of the electron at atomic hydrogen, m×27.2eV (m=integer) (2) . He named this shrunken hydrogen atom "Hydrino" and claims that this Hydrino can be a catalyst to shrink other hydrinos to further lower states. He named this reaction the BlackLight Process. Fig 1 illustrates the BlackLight Process. Based on his hypothesis, he succeeded in generating energy somewhat between chemical and nuclear reaction.

The author postulated that 3 body reaction of atomic hydrogen and oxygen can make the BlackLight Process because ionization energy of hydrogen and oxygen is very close as is shown below.

Hydrogen =13.598 eV, Oxygen =13.618 eV

It can be expected that the following reactions can take place:

$O + O + H \rightarrow H[n=1/2] + 2\,O^+ + 2\,e^-$ ----(a)

$H + H + O \rightarrow H[n=1/2] + H^+ + O^+ + 2e^-$ ----(b)

$H + H + H \rightarrow H[n=1/2] + 2\,H^+ + 2\,e^-$ ----(c)

H[n=1/2] designates a hydrogen whose electron orbit is shrunken to 1/2 the radius of a normal one and these will be shrunken further to lower orbits as reaction continues.

Ions and electrons thus produced will recombine, resulting in generation of energy.

It is reported that the BlackLight Process can produce up to 200W/cm3 at 700mTorr(4). If the Black-Light Process takes places at atmospheric pressure, the power density is about 300kW/cm3. There have been a couple of mysteriously powerful explosions in the experiment of cold fusion and in the nuclear power plants. The explosion of a cold fusion cell at SRI International in Menlo Park, California in 1992 is the most memorable one in the history of cold fusion research. The detonating cell (only 2 inches in diameter and 8 inches long), not only killed one researcher but peppered three other researchers in the lab with debris. The author analyzed these anomalous explosions and came up with a postulation that these explosions are due to the BlackLight Process (1).

5 WHAT TRIGGERS HYDROGEN EXPLOSION

High pressure molecular hydrogen gas up to 70MPa is now being used for fuel cell cars but almost no technical information on the stability of high pressure atomic hydrogen gas is available because it's almost impossible to make such a gas here on the ground. Only information available concerning the initiation of the BlackLight Process is the one carried out by BLACKLIGHT POWER Inc., but these are limited at very low pressure. The Black-Light Process is quite sensitive to the pressure and it can be expected that the same characteristic curve as is the case for the self ignition curve of the stoichiometric mixture of hydrogen and oxygen shown in Fig2.

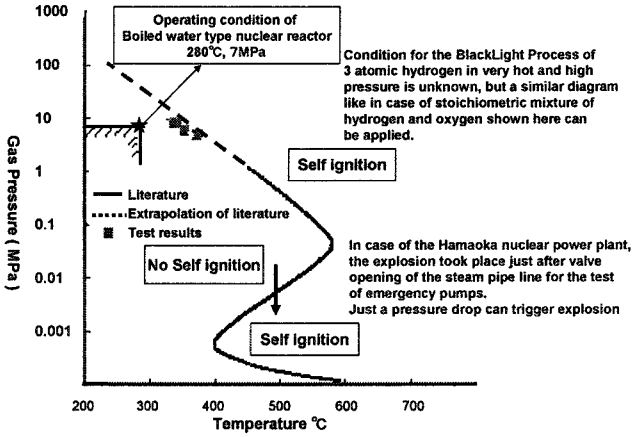

Fig. 2 Self Ignition Area of Stoichiometric Mixture of Hydrogen and Oxygen

Source:Chubu Electric Power Company:
Reactor Manual Shutdown Caused by Pipe Rupture in Residual Heat Removal System at the Hamaoka Nuclear Power Station Unit-1 (Final Report), April 2002 (in Japanese).

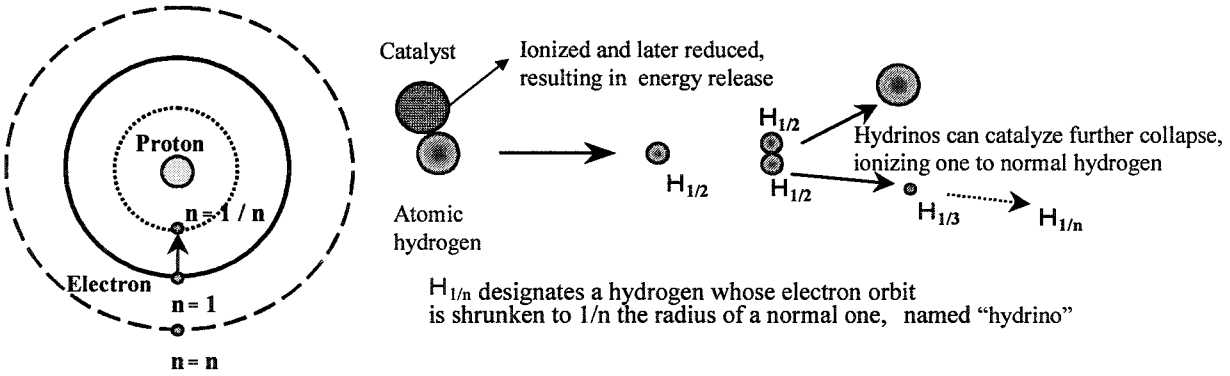

Fig. 1 Mechanism of "hydrino " generation and energy release

When the gas pressure of atomic hydrogen reaches such a high pressure that surrounding rocks can not sustain, gas leakage starts and the atomic hydrogen gas plunges into the area of the BlackLight Process. The power density of atomic hydrogen gas over 1 GPa, typical pressure at 30km beneath the surface of the Earth, would be almost equivalent to nuclear bombs, or enough power to shake the earth.

At BLACKLIGHT POWER Inc. magnetic wave is utilized to induce the BlackLight Process. This implies that an electro-magnetic fluctuation due to solar activities might induce the explosion.

6 SUMMARY

In the past, it could have been hardly imagined atomic hydrogen gas can explode but the Black-Light Process by R. Mills opened the way to investigate the cause of anomalous explosion of hydrogen from a new standpoint of view. Considering the very powerful explosion caused by atomic hydrogen and oxygen during cold fusion experiments and at nuclear power plants that can not be explained by current combustion theory but can be explained by the Black-Light Process and the relationship between water injection into deep well and occurrences of earthquakes, it can be reasonably concluded that earthquakes are caused by the explosion of atomic hydrogen gas dissociated from water that is bought deep in the earth by subduction of crustal plates.

REFERENCES

(1) Hiroshi, Yamamoto, Revisiting Anomalous Explosion of Hydrogen and Oxygen Mixture from a View of Cold Fusion, Proceedings of the 5th Meeting of Japan CF Research Society, p89-92, 2003

(2) R.L. Mills, P. Ray, B. Dhandapani, R.M. Mayo, J. He, Comparison of Excessive Balmer Alpha Line Broadening of Glow Discharge and Microwave Hydrogen Plasmas with Certain Catalysts, Journal of Applied Physics, Vol. 92, No. 12, (2002), pp. 7008-7022

(3) Nicholson, Craig and Wesson, R.L., Earthquake Hazard Associated with Deep Well Injection--A Report to the U.S. Environmental Protection Agency: U.S. Geological Survey Bulletin 1951, 74 p.

(4)http://www.blacklightpower.com/pdf/ItalyTech%20Paper%203.27.03.pdf

Fusion by 4d/TSC or 6d/OSC

Akito Takahashi (Osaka University); akito@sutv.zaq.ne.jp

Model mechanisms for 4D and 6D fusion by tetrahedral and octahedral symmetric condensate in metal-deuterium systems is proposed and some numerical results are shown.

1. Introduction

Mechanisms of deuteron cluster fusion in metal-deuterium/hydrogen systems have been modeled by EQPET/TSC theories[1,2] which gave consistent explanations to major experimental results of LENR/CMNS. In this study, more simple treatment of semi-classical models is extended for minimum size state of squeezing motion for 4d/TSC(Tetrahedral Symmetric Condensate) and fusion rates are given by STTBA (Sudden Tall Thin Barrier Approximation). Maximum 4D fusion rate for PdD lattice was estimated as 23 keV/Pd-atom and 46 MW/cc-Pd, which is comparable to 24.8keV/Pd-atom by the super-wave electrolysis experiment by El Boher et al[3].

Defect/Void of Pd atom in PdD lattice may provide site for formation of 6d/OSC(Octahedral Symmetric Condensate). Semi-classical modeling of squeezing motion for 6d/OSC is shown. 6D to $^{12}C^*$ to $^4He + ^4He + ^4He + 71.4MeV$ (hence 23.8 MeV/^{4}He) is the predominant fusion process for 6d/OSC in PdD lattice with defect/void. And 6d/OSC may be seed for M + 6D capture to make A+12 and Z+6 transmutation as Iwamura reported[4].

Ash of 4d/TSC or 6d/OSC fusion is predominantly amount of ^{4}He and reaction rate is high enough to explain major excess heat plus helium results claimed by CMNS experiments.

2. 4d/TSC fusion

There are remained open questions about where TSC is formed. We have proposed two mechanisms.

A) In the near surface region of PdDx cathode, deuterium full loading (x=1; PdD) may be attained by electrolysis, gas discharge or gas-permeation, at least locally. No experimental techniques have been developed to measure local distribution of x-value, although we know that it should be key information. With very small density (namely 1 ppm was assumed in our paper[8]) PdD_2 states may exist.

Trapped D in Bloch potential has discrete energies with 32 meV ground state and 64 meV one phonon energy for excited states. Over 0.22 eV, all D-ions in lattice diffuse out of solid. By exciting with external UV or EUV laser, due to classical Drude model, transient cluster of TSC can be formed with certain probabilities[8].

B) We know surface of metal is complex and fractal with ad-atoms, dimers and corner-holes, for example, as illustrated in Fig.2. Somewhere, for instance in corner holes, incident D_2 molecules are trapped by dangling bonds. Free D_2 molecule has freedom of rotation and vibration. Trapped D_2 would lose freedom of rotation, but can vibrate for changing distance between pairing two deuterons, and waiting for incoming D_2 molecule.

When incoming D_2 molecule meets near to trapped D_2, incoming D_2 rotates with 90 degrees maximum against waiting D_2 molecule to neutralize charge (minimize Coulomb repulsion energy) and form an orthogonally coupled two D_2 molecules when there meets coherence in vibration modes and electron-spins are anti-parallel for counter part electrons. In this way, TSC may be formed on surface. Since the scenario is still very speculative, we need further substantiating studies.

In this paper, we have considered that the squeezing motion of TSC can be more simply treated by a semi-classical model, because of the three-dimensionally constrained motion of 4d and 4e particles in TSC into the central focal point. **Figure-1** illustrates the feature of the semi-classical treatment. Every particle in TSC can make central squeezing motion with same velocity, to keep charge neutrality of total TSC system – in other words to satisfy minimum system energy state (as calculated by the variational

principle of quantum mechanics). Therefore this squeezing motion can be treated as Newtonian mechanics until when 4 deuterons get into the range (about 5 fm) of strong nuclear interaction.

Life time of TSC is estimated to be about 60 fs by its linear Newtonian motion to reach strong interaction range.

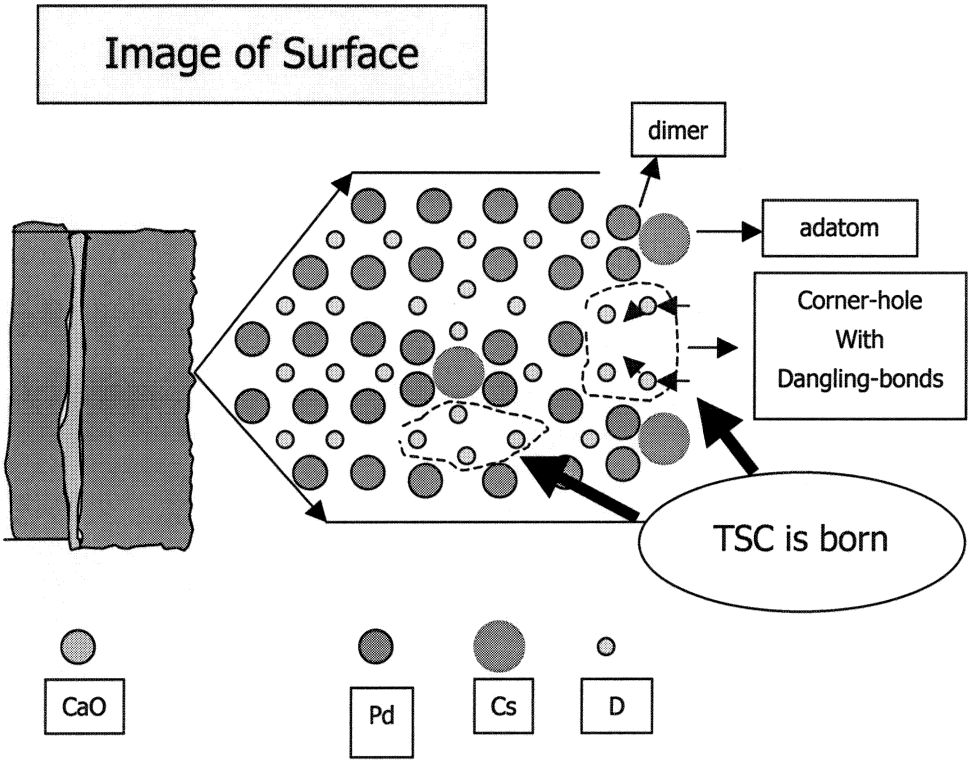

Fig.1: Image of Pd-complex surface

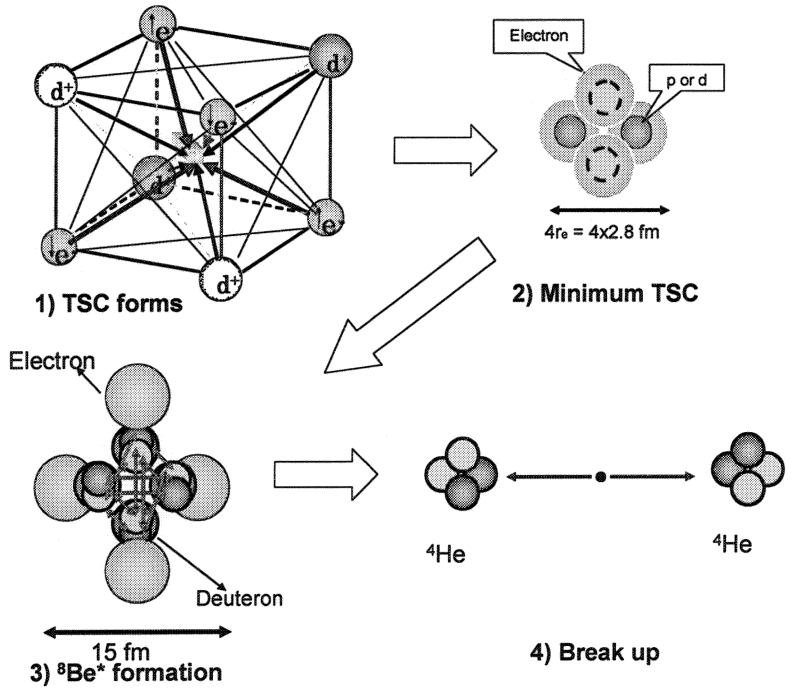

Fig.2: Semi-classical view of squeezing motion of TSC, <e> = (e ↑ + e ↓)/2 for 4 electron centers in QM view.

In Fig.2, TSC will form in the near surface region of condensed matter by the mechanism A) or mechanism B) as discussed in Session 2, with certain probability depending on methods of experiments and near-surface physics of condensed matter :Step-1): (TSC forms). Then TSC starts Newtonian squeezing motion to decrease linearly its size from about 100 pm radius size to much smaller size and reaches at the minimum size state: Step-2): (Minimum TSC). Classical squeezing motion ends when 4 deuterons get into the strong force range (5 fm) and/or when 4 electrons get to the Pauli's limit (about 5.6 fm for e-e distance). Here for the Pauli's limit, we used the classical electron radius of 2.8 fm, which is determined by equating the static Coulomb energy (e^2/R_e) and the Einstein's mass energy (m_ec^2) to obtain,

$$Re = e^2/(m_ec^2) = 2.8 \text{ fm} \quad \text{; classical electron radius} \qquad (14)$$

Since the range of strong interaction (about 5 fm) is comparable to the classical electron diameter (5.6 fm), as shown in Fig.2-2), the intermediate nuclear compound state ^{8}Be* will be formed just after the minimum size state ("over-minimum" state); Step-3): ^{8}Be* formation. Immediately at this stage, 4d-cluster shrinks to much smaller size (about 2.4 fm radius) of ^{8}Be* nucleus, and 4 electrons should go outside due to the Pauli's repulsion for fermions. Shortly in about few fs or less (note; Life time of ^{8}Be at ground state is 0.67 fs), ^{8}Be* will break up to two ^{4}He particles, each of which carries 23.8 MeV kinetic energy; Step-4): Break up.

When 4 electrons start to separate, 4 deuterons suddenly start to *feel* mutual Coulomb repulsion. Nuclear interaction at this stage can be approximately treated by STTBA (Sudden Tall Thin Barrier Approximation). Gamow integral of STTBA[9] is given by,

$$\Gamma_{nd} = 0.218(\mu^{1/2})\int_{r0}^{b}(V_B - E_d)^{1/2}dr \qquad (15)$$

And bare Coulomb potential is,

$$V_B(r) = 1.44Z_1Z_2/r \quad \text{; in MeV and fm units} \qquad (16)$$

And barrier penetration probability is,

$$P_{nd}(E_d) = \exp(-n\Gamma_{nd}) \qquad (17)$$

For $V_B >> E_d$,

$$\Gamma_{nd} \simeq 0.523(Z_1Z_2\mu)^{1/2}(b^{1/2} - r0^{1/2}) \qquad (18)$$

Using b = 5.6 fm and r0 = 5 fm, we obtained; P_{4d} = 0.77 with V_B = 0.257 MeV and

Using S_{4d} value in Refefences-8 and 9, we obtained: λ_{4d} = 2.3E-4 f/s/cl. This microscopic fusion rate is 1E+7 times larger value than one given in Table-3. We consider therefore that EQPET model gave significant underestimation for 4D fusion rate when rigid constraint of motion in three dimensional space is attained as shown in Fig.2.

Macroscopic reaction rate with N_{4D} = 1E+22 (1/cc) is then given as Y_{4D} = 4.6E+18 f/s/cc-Pd, which is equivalent to 46 MW/cc-Pd and 23 keV/Pd-atom.

In ICCF11, El Boher et al reported[5] very intense excess power for about 17 hours, by their super-wave D_2O/Pd-thin-pate electrolysis technique, to give 24.8 keV/Pd-atom. This experimental value is close to 23 keV/Pd-atom by the over-minimum state 4D fusion by 4d/TSC. El Boher et al did not measure helium, and gave no information about nuclear mechanism behind. If they will find corresponding level of helium atoms, we can say very good agreement between experiment and theory.

If we apply λ_{4d} = 2.3E-4 f/s/cl for modal fusion rates in Table-3, neutron production level drops to the order of 1E-17 of ^{4}He production rate and tritium production rate also drops to the order of 1E-9 of ^{4}He production rate. These results are nearer to experimentally observed levels of neutrons and tritium-atoms in CMNS studies.

3. 6d/OSC Fusion

Iwamura et al reported[4] transmutation from ^{137}Ba to ^{149}Sm, namely mass-12 and charge-6 increased transmutation. This may be M + 6D capture process.

We considered 8D fusion process emit ^{12}C nuclei with

high kinetic energy and M + ^{12}C capture process can be considered as secondary reaction. The second and more plausible process is direct 6D capture by OSC (octahedral symmetric condensate) for 6D cluster occupying 6 peaks of regular octahedron orthogonally coupled with 6 electrons which also occupy heads of regular octahedron, as shown in **Fig. 3 and Fig.4**. The squeezing motion of 6d/OSC can be modeled in analogous way to Fig.1, although we need to treat three-dimensionally more complex system (cuboctahedron or dodecahedron).

Self fusion of 6d/OSC may be 6D fusion as shown in **Fig.5**.

$$6D \rightarrow {}^{12}C^* \rightarrow {}^{4}He + {}^{8}Be + 71.3\ MeV$$
$$\rightarrow {}^{4}He + {}^{4}He + {}^{4}He + 71.4\ MeV \quad (5)$$

And transmutation by M + 6d/OSC is

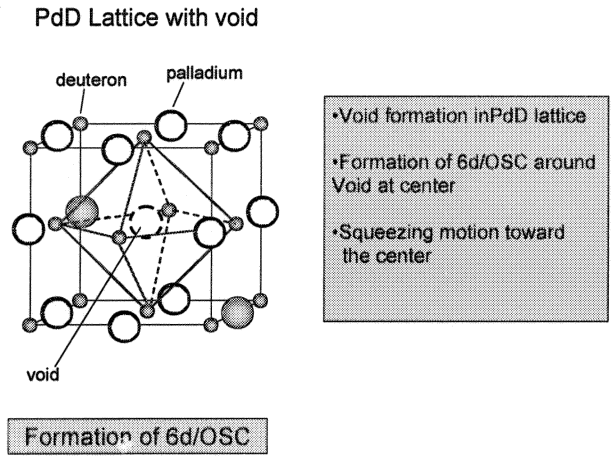

Fig.3: Formation of 6d/OSC seed by a central void in PdD lattice

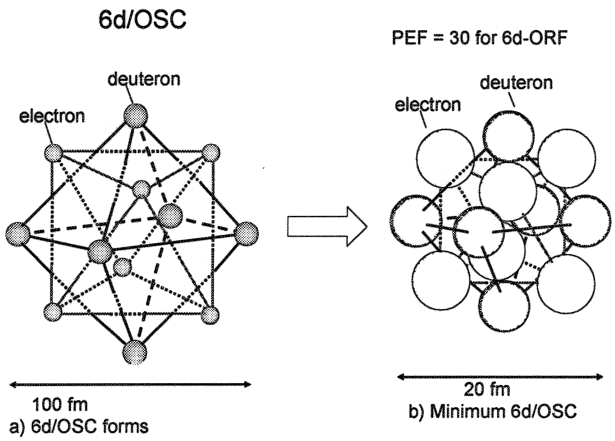

Fig.4: Formation of 6d/OSC

$$M(A, Z) + 6d/OSC \rightarrow M(A+12, Z+6) \quad (6)$$

For example,

$$^{137}Ba + 6D\ (\text{or } ^{12}C^*) \rightarrow {}^{149}Sm + Gamma(68.23\ MeV) \text{ or fission} \quad (7)$$

Detail analysis for this process is expected. Approximate estimation of reaction rates are as follows. Microscopic 6D fusion rate for minimum state 6d/OSC is given as,

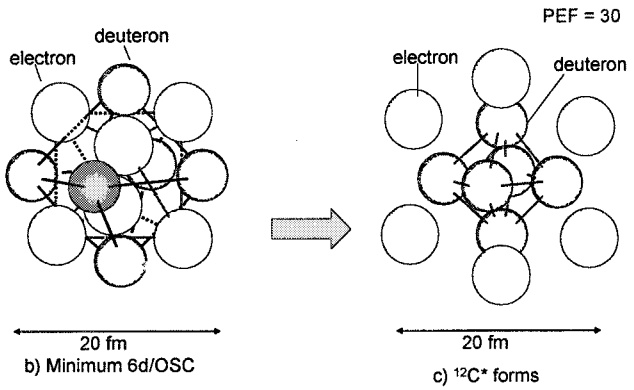

Fig.5: Formation of $^{12}C^*$ by 6d/OSC fusion

$$\lambda_{6d} = (S_{6d}(E)\ v/E)\exp(-6\Gamma_{STTBA}) = 4.8E\text{-}2\ (f/s/cl) \quad (8)$$

Using PEF = 30 for 6d fusion,

$$S_{6d}(E) = 1E+14\ keVbarn \quad (9)$$

$$\Gamma_{STTBA} = 0523(b^{1/2} - r_0^{1/2}) = 0.31 \quad (10)$$

Here we used $b = r_{ddmin} = 8$ fm and $r_0 = 5$ fm.

Application of EQPET analysis to 6d/OSC is expected. The electronic quasi-particle e*(6,6) is composed of three Cooper pairs coupling orthogonally in 3-dimensional rectangular axes, and its screening energy for d-d pair is 9,600 eV which is just near to that of muon.

1. Conclusions

TSC (tetrahedral symmetric condensate) of 4D cluster can squeeze very small as 10 fm in diameter at its minimum-size state, and will make self-fusion of 4d/TSC cluster to produce helium-4.

However, the present modeling of TSC mechanisms is still primitive and we need further elaboration. Especially, formation mechanisms near surface of host-metal complex is interested for further studies.

Formation of 6d/OSC and 6D fusion in defect (void) of PdD lattice was proposed, although we need more detailed modeling of mechanism inducing central squeezing motion of 6 deuterons around central defect. The 6d/OSC fusion will produce also helium-4 with average kinetic energy of 23.8 MeV.

Time-dependent EQPET analysis of TSC is under way.

Acknowledgments

The author is grateful to Dr. Y. Iwamura, Mitsubishi Heavy Industries Co. and Dr. F. Celani, INFN Frascati for their kind discussions. The author thanks Dr. M. Ohta, PNC Japan, for providing fission product calculations for Ni + 4p system

References:

1. A. Takahashi: $^3He/^4He$ production ratios by tetrahedral symmetric condensation, Proc. ICCF11, Marseilles, November 2004, see http://www.iscmns.org/
2. A. Takahashi: Deuteron cluster fusion and related nuclear reactions in metal deuterium/hydrogen systems, Recent Developments in Physics, Transworld Research Network, India, 6(2005): ISBN 81-7895-171-1
3. El Boher et al: Proc. ICCF11, Marseilles, November 2004, see http://www.iscmns.org/
4. Y. Iwamura, et al: Proc. ICCF11, ibid.

Transmutations by Metal plus TSC or OSC

Akito Takahashi (Osaka University); akito@sutv.zaq.ne.jp

A model of direct nuclear reaction between host-metal-nucleus and deuterium or hydrogen cluster of TSC or OSC is proposed and some numerical results are given.

1. Introduction

TSC(Tetrahedral Symmetric Condensate) and OSC(Octahedral Symmetric Condensate) may squeeze as small as 10-20 fm diameter at minimum size state[1-3], and can make penetration, like "neutron", through electron clouds of host-metal nucleus to approach and make direct nuclear reactions with host-metal nucleus.

Transmutation reactions by 4p/TSC + M(host-metal nucleus) interaction are analyzed for Ni + H systems. Reaction rates and products are shown for Ni + p to Ni + 4p reactions with various nickel isotopes. Especially, Ni + 4p capture goes out to fission of very clean products.

Transmutation reactions by 4d/TSC + M interaction are analyzed for Cs + 4d (or ^{8}Be*) reactions. Transmutation rate for Cs-to-Pr is estimated for the condition of Iwamura experiment[4]. Transmutation reactions for radio-active Cs isotopes (^{135}Cs and ^{137}Cs) are discussed.

Transmutation reactions by 6d/OSC + M interaction are briefly discussed. Defect/void of PdD lattice will incubate 6d/OSC and its squeezing motion to reach at minimum size of about 20 fm in diameter and form ^{12}C* compound nucleus. Then M + ^{12}C* capture process is foreseen.

2. TSC + Metal Interaction

2.1 Barrier Penetration

TSC squeezes from about 100 pm size to its minimum-size with about 10 fm diameter and behaves as charge-neutral pseudo-particle. Life time of TSC is estimated as time difference from 100 pm size state to minimum size with velocity of the order of 1E+5 cm/s; we obtain about 60 fs. During its life, TSC as charge-neutral pseudo-particle may approach to host-metal nuclei with some probability, as illustrated in **Fig.1**.

Time-averaged density of TSC in metal-deuteride (MDx) or hydride (MHx) is given in our previous papers[1,2]:

Macroscopic reaction rate Y (f/s/cc) for M+TSC reaction is given by

$$Y = N_{M+TSC}\lambda \qquad (2)$$

Here we have to estimate the density N_{M+TSC} of "united molecule" M+TSC in atomic level.

$$N_{M+TSC} = \sigma_A N_M N_{TSC} v \tau_{TSC} \qquad (3)$$

N_M is the host metal atom density, N_{TSC} the time-averaged TSC density, σ_A the atomic level cross section (about 1.0E-16 cm^2) for M+TSC combination, and τ_{TSC} the mean life of TSC (about 60 fs), respectively. If we can assume N_M = 1E23 (per cc) and N_{TSC} = 1E20 (per cc), we obtain roughly N_{M+TSC} = 1E19 (per cc).

2.2Sudden Tall Thin Barrier Approximation

TSC around with its minimum-size may approach closely to the interaction range of strong force between protons (deuterons) of TSC and host-metal nucleus. The situation is shown in **Fig.2**.

When protons (or deuterons) start to make strong interaction by exchanging charged pions with nucleons of host-metal nucleus, charge-neutrality of TSC starts to break and electrons should go outside, since electron does not make strong interaction but weak interaction. Field coupling constant for weak interaction is very small as on the order of 1E-14 of coupling constant (1.0) of strong interaction. According to Fermi's golden rule, reaction cross section is proportional to square of transition matrix element which is proportional to field coupling constant.

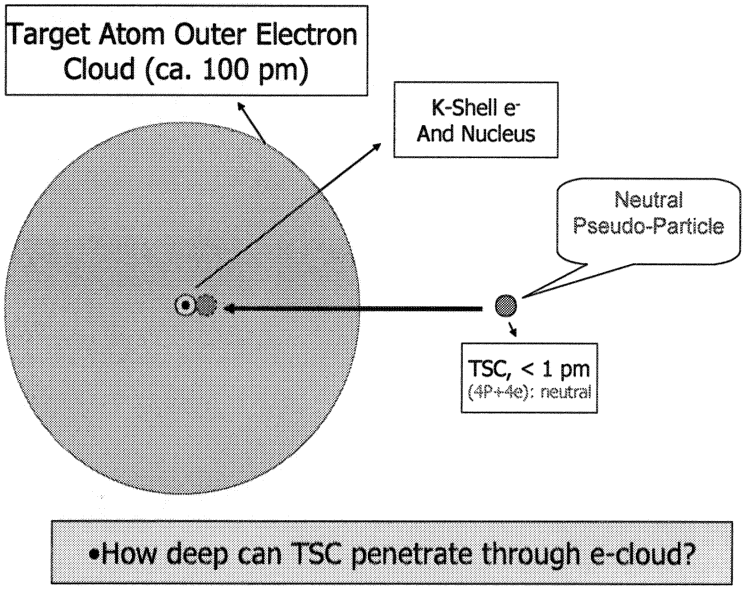

Fig.1: Illustration for TSC and host-metal atom interaction

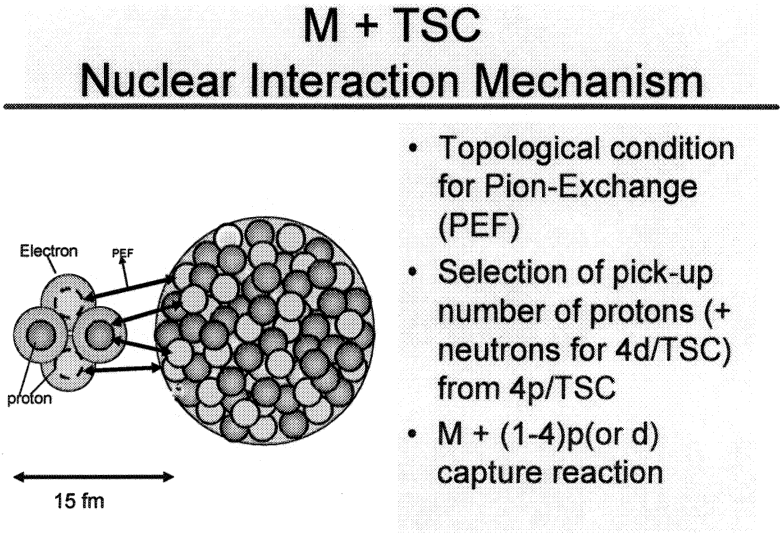

Fig.2: Feature of strong nuclear interaction, for closely approached TSC + M-nucleus united molecule

Therefore, weak interaction between electrons and host-metal nucleons is neglected. PEF (Pion Exchange Force) unit is relative measure of effective surface for very short range (about 2-5 fm) force of strong interaction.

Since electrons should go out of the interaction domain of strong force, protons (or deuterons) in TSC should *suddenly feel* Coulomb repulsion with host-metal nucleus, and also among protons (and deuterons) in TSC itself. The feature of stage is illustrated in **Fig.3**. We derived the Sudden Tall Thin Barrier Approximation[1,2], for calculating reaction rate in this stage.

2.3 Ni + 4p/TSC Reactions

Miley-Patterson[5] reported production of anomalously large foreign elements in their electrolysis experiments with Ni-H systems. Piantelli et al[6] also reported large

excess heat, anomalous foreign elements and about 660 keV gamma-ray peak. There are many other reports which claimed anomalous heat events and foreign elements production. Most authors claimed *cold transmutations* in condensed matter.

The author applied STTBA for estimating reaction rates of Ni + 4p/TSC nuclear reactions, which are competing process of Ni + p, Ni + 2p, Ni + 3p and Ni +4p reactions.

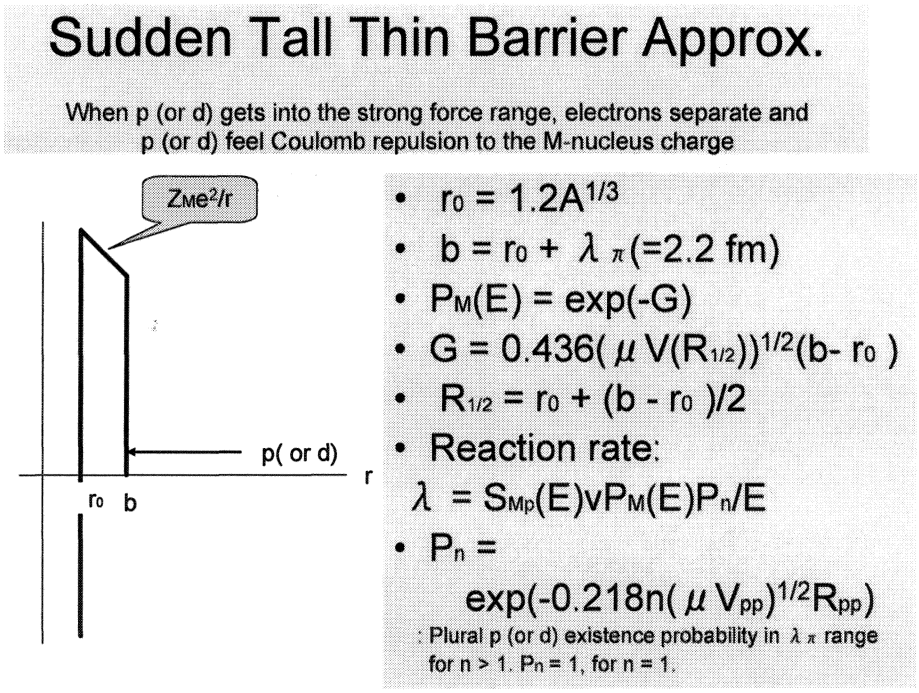

Fig.3: Sudden Tall Thin Barrier Approximation (STTBA) for TSC + M system

Calculated reaction rates are shown in **Table-1**. We obtained considerably large values for microscopic reaction rates, and macroscopic yield 1E+8 f/s/cm^2 with assuming N_{TSC+M} density = 1E+16 (1/cm^2)in 10 nm area of Ni sample surface. Especially, Ni + 4p capture reaction rate 1E-8 (f/s/pair) is large enough to explain claimed foreign elements as fission products of Ni + 4p to Ge* process. Before showing fission products, The excited compound state Ge* has enough excited energy (19 to 29 MeV, for ^{60}Ni + 4p to ^{64}Ni + 4p) to induce fission. Fission products are calculated by the SCS (Selective Channel Scission) model[7]. Calculations were done for all nickel isotopes. FP distribution for averaged natural abundance is shown in **Fig.4**.

We see good agreement, although low-Z elements (C, N, O) were not given in the experiment, probably due to contaminants in low mass region.

Typical fission products (FP) are shown in **Table-2**. Major contribution of FP is from Ni + 4p fission for higher mass isotopes of nickel. Most interesting point is that most FPs are stable isotopes and radioactive products are very weak. Therefore, this fission process is much cleaner than known fission of uranium. However the opening of neutron emission channel is possible, although weight is small. Some FPs are decaying by electron capture (EC) process, in few cases of which there are small portion of gamma-ray emission.

Table-1: Calculated reaction rates for Ni + 4p/TSC and Ni + 4d/TSC nuclear reactions

---

Results by STTBA calculation; M = Ni

- $P_{Mp}(E) = 9.2E-2$
- $P_{Md}(E) = 3.5E-2$

Reaction Rates:

- $\lambda_{Mp} = 3.7E-8$ (f/s/pair)
- $\lambda_{Md} = 2.1E-7$ (f/s/pair)
- $\lambda_{M4p} = 1.0E-8$ (f/s/pair)
- $\lambda_{M4d} = 3.4E-9$ (f/s/pair)
- <Macroscopic Reaction Rate> = $\lambda \times N_{M+TSC}$
- With N_{M+tsc} = 1.0E+16 in 10nm area, Rate = 1E+8 f/s/cm2 and Y = 1E+14 in 1E+6 sec.

$V_{pp} = 1.44/6 = 0.24$ MeV
$P_{2p} = 0.527$
$P_{2d} = 0.404$

$S_{Mp}(0) = 1.0E+8$ kevb
$S_{Md}(0) = 1.0E+9$ keVb

$\lambda_{4d} = 4.9E-5$

FP Elements by SCS vs. Miley Exp.

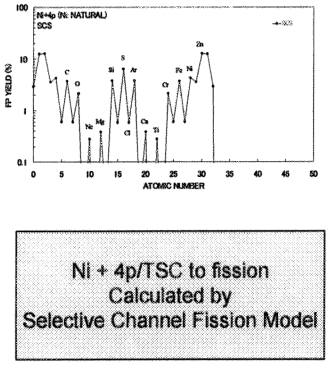

Ni + 4p/TSC to fission
Calculated by
Selective Channel Fission Model

G. Miley and J. Patterson
J. New Energy, 1996, 1, p.5

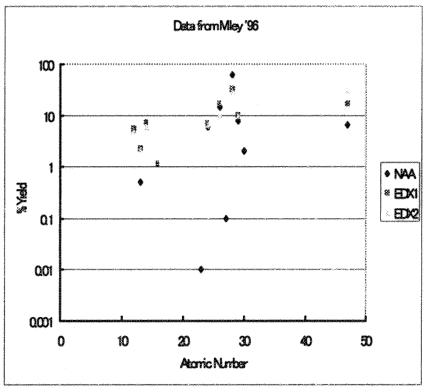

Fig.4: Comparison of calculated FP distribution (left figure) and Miley-Patterson experiment (right figure), for Ni + 4p to fission process.

2.4 M + 4d/TSC Reactions

In the minimum-size stage of 4d/TSC, 4 deuterons fuse, by exchanging charged pions, to $^{8}Be^{*}$ compound state with about 2 fm radius. And electrons are kicked outside of the range of strong interaction (see Fig.1). Therefore, M + 4D interaction becomes M + $^{8}Be^{*}$ capture reaction, as illustrated in **Fig.5**

Iwamura et al reported[8,9] selective transmutations;

$$M(A, Z) + 4D \text{ (or } ^{8}Be) \rightarrow M(A+8, Z+4) \quad (4)$$

They added ^{133}Cs or Sr atoms on surface of Pd-complex and permeated D_2 gas through the sample complex. They observed repeatedly transmutations; ^{133}Cs to ^{141}Pr or ^{88}Sr to ^{96}Mo with total transmuted amount of the order of 1E+14 to 1E+15 atoms per week.

The author applied STTBA analysis for modeled Pd(Cs)/D system to estimate transmutation rate. Results are shown in **Table-3**. Calculated rate 4.6E+14 (atoms per week) for Cs-to-Pr transmutation showed considerable agreement with those by Iwamura experiments.

Table-2: Fission products from Ni + 4p reactions

Major Fission Channels from Ni + 4p

(1) ^{58}Ni(68%) + 4p → ^{62}Ge(Ex=11.2MeV)

→ 8.8MeV + ^{4}He +^{58}Zn(EC)^{58}Cu(EC)^{58}Ni
→ 8.8MeV + ^{28}Si + ^{34}Ar(EC)^{34}Cl(EC)^{34}S

(2) ^{60}Ni(26.2%) + 4p → ^{64}Ge(Ex=19.1MeV)

→ 16.4MeV + ^{4}He +^{60}Zn(EC)^{60}Cu(EC)^{60}Ni
→ 13.6MeV + ^{8}Be +^{56}Ni(EC)^{56}Co(EC)^{56}Fe
→ 13.0MeV + ^{12}C +^{52}Fe(EC)^{52}Mn(EC)^{52}Cr
→ 12.2MeV + ^{16}O + ^{48}Cr(EC)^{48}V(EC)^{48}Ti
→ 13.5MeV + ^{24}Mg + ^{40}Ca
→ 16.4MeV + ^{28}Si + ^{36}Ar
→ 16.7MeV + ^{32}S + ^{32}S
→ 6.5MeV + ^{36}Ar + ^{26}Si(EC)Al(10^{5}y)

(3) ^{61}Ni(1.1%) + 4p → ^{65}Ge(Ex=21.3MeV)

→ 18.9MeV + ^{4}He+ ^{61}Zn(EC)^{61}Cu(EC)^{61}Ni
→ 15.9MeV +^{12}C+^{53}Fe(EC)^{53}Mn(3.7x10^{6} y)
→ 11.0MeV + ^{20}Ne + ^{45}Ti(EC)^{45}Sc
→ 17.4MeV + ^{28}Si + ^{37}Ar(EC)^{37}Cl
→ 12.0MeV + ^{27}Si(EC)^{27}Al + ^{36}Ar
→ 17.5MeV + ^{32}S + ^{33}S

Note:
• Green shows stable isotope.
•Average Kinetic Energy of Fission Product = 9.7 MeV for Ni-natural

M + 4d/TSC Nuclear Interaction Mechanism

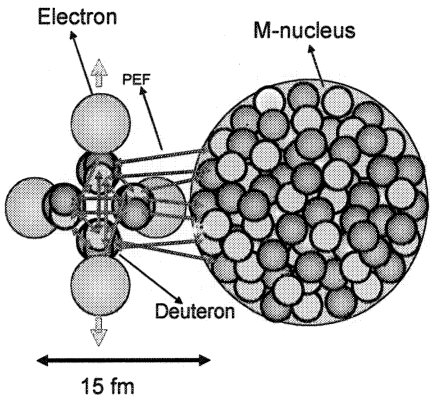

- Over-minimum sate of 4d/TSC
- Admixture of 4d/TSC to form ^{8}Be*
- M + ^{8}Be* capture reaction
- Strong force exchange (PEF) between M and ^{8}Be*

Fig.5: Strong interaction for M + 4d/TSC

Table-3: Cs-to-Pr transmutation rate estimated by STTBA model for M + 4d/TSC reaction

STTBA Prediction for Cs-to-Pr

- S_{Mp} = 1E+8 kevb
- S_{Md} = 1E+9 keVb
- λ_{Mp} = 8.4E-10 f/s/tsc
- λ_{M4p} = 2.3E-10 f/s/tsc
- λ_{Md} = 2.8E-8 f/s/tsc
- λ_{M4d} = 7.6E-9 f/s/tsc
- Where combination probability of anti-parallel spin was used for 4p/TSC.

- Suppose N_{M+tsc} = 1E+17 in 10 nm layer of surface
- Macro Yield = λ xN_{tsc} = 7.6E-9 x 1E+17 = 7.6E+8 (f/s/cm^2)
- Cs-to-Pr rate = 4.6E+14 (atoms per week) per cm^2

3. Conclusions

Deuteron or proton cluster as TSC or OSC state can become very small charge neutral pseudo-particle, penetrate almost freely through electron clouds of host-metal atom, and approach very close to host-metal nucleus to make strong interaction and transmutation reactions. A model is proposed in this study to make numerical study for estimating reaction rates and products.

Acknowledgment:

The author thanks Dr. Y. Iwamura, MHI, Japan and Dr. F. Celani, INFN Frascati, Italy, for their discussions to this work.

References:

1. A. Takahashi: ^{3}He/^{4}He production ratios by tetrahedral symmetric condensation, Proc. ICCF11, Marseilles, November 2004, see http://www.iscmns.org/
2. A. Takahashi: Deuteron cluster fusion and related nuclear reactions in metal deuterium/hydrogen systems, Recent Developments in Physics, Transworld Research Network, India, 6(2005): ISBN 81-7895-171-1
3. A. Takahashi: Fusion by 4d/TSC or 6d/OSC, this meeting
4. Y. Iwamura, et al: Jpn. J. Appl. Phys., 41(2002)4642
5. G. Miley, J. Patterson: J. New Energy, 1(1996)5
6. E. Campari, et al: Surface analysis of hydrogen loaded nickel alloys, Proc. ASTI5 Meeting, Italy, March 2004, see http://www.iscmns.org/
7. A. Takahashi, et al: Jpn. J. Appl. Phys., 41(2001) 7031

The Cold Fusion Phenomenon as a Complexity (1)
– Complexity in the Cold Fusion Phenomenon –

Hideo Kozima
Cold Fusion Research Laboratory, 421-1202, Yatsu, Aoi, Shizuoka 421-1202, Japan
E-mail; cf-lab.kozima@nifty.com, Website; http://www.geocities.jp/hjrfq930/

Abstract

The science of complex systems treats such problems as **why** simple particles organize themselves spontaneously complex structures like stars, galaxies, hurricanes, and Coulomb lattices of neutron and proton clusters surrounded by a dilute neutron gas in the neutron star matter, as **what** is the cause of $1/f$–fluctuation, and as **what** means the edge of chaos.

The cold fusion phenomenon (CFP) has revealed such nature of many-particle effects as a complexity as shown by various experimental results as the "**stability effect**" in the nuclear transmutation and the "**inverse-power law**" in the excess power generation. The complexity of the cold fusion phenomenon originates in the non-linear interactions between millions of agents (component particles in the cold fusion materials) and is magnified by enormous energy difference (about an order of 10^8) of the cause (atomic) and the effect (nuclear). Existence of complexity in the cold fusion phenomenon is explained in this paper.

1. Introduction

The cold fusion phenomenon (CFP) was explicitly announced its discovery in 1989 by Fleischmann and Pons [1] as huge excess heat accompanying tritium and neutron productions in an electrolytic system with Pd metal anodes and Pt wire cathodes in the electrolytic solution D_2O + LiOD. The motivation of their experiments was the Fleischmann's hypothesis that the Pd lattice gives enormous effect on the *d-d* fusion reactions in the transition-metal deuteride PdDx ($x \simeq 1$), [2] which the name "cold fusion" originates from.

The history of CFP research in the past 16 years revealed, however, that the Fleischmann's hypothesis should not be essential to CFP as a whole due to following facts; CFP occurs not only in deuterium systems but also in protium systems, there are too various events [4] and too various nuclear products to be explained by simple *d-d* fusion reactions. Furthermore, numerical relations between amounts of products [4] contradict with those expected from the *d-d* fusion reactions known in nuclear physics. It has been known that existence

of the ambient thermal neutrons is one of necessary conditions for CFP. Therefore, the name "cold fusion phenomenon" (CFP) should be used as one to signify a phenomenon including nuclear reactions and accompanying events occurring in solids with high densities of hydrogen isotopes (H and/or D) in ambient radiation when dynamical conditions are imposed on them.

Fields and products of CFP observed by now are tabulated in Table 1. [3] In this table, matrix substances and agent nuclei comprise the field where occurs CFP. It is not designated in the table but should be emphasized that CFP occurs more frequently in dynamical, stationary, or non-static conditions than in the static one.

The TNCF (trapped neutron catalyzed fusion) model proposed by the author in 1994 [4] has been one of successful approaches to qualitative and semi-quantitative explanations of several events in CFP and has given several numerical relations between amounts of products consistent with experiments. Basic assumptions of the model are based on the many-particle nature of the CF system where occurs CFP. Existence of the trapped thermal neutrons in CF materials, one of the basic assumptions in the TCNF model, is clearly a result of many-particle interactions in the solids if the assumption has any reality behind it. [5]

Table 1. Matrix Substances, Agent nuclei, Direct and Indirect Evidence of nuclear reactions in cold fusion phenomenon (CFP). Q is for the excess heat and NT for the nuclear transmutation. Dependences of products on energy ε and position r, decay time shortening of radioactive nuclides, and fission-barrier lowering of compound nuclides give direct information of nuclear reactions in CFP.

Matrix Substances	Transition metals (Ti, Ni, Mo, Pd, Pt, etc.), Proton Conductors ($SrCeO_3$, $REBa_2Cu_3O_7$, $AlLaO_3$), Ferroelectrics (KD_2PO_4, TGS, etc.), Others (C, Na_xWO_3, Stainless Steel, etc.)
Agents	${}_0n$, ${}_1H$, ${}_2H$, (${}_8O$), ${}_3Li$, ${}_5B$, ${}_{11}Na$, ${}_{19}K$, ${}_{37}Rb$, ${}_{37}Rb$, SO_4^{2-}, etc.
Direct Evidences	Neutron energy spectrum $n(\varepsilon)$, Gamma rays $\gamma(\varepsilon)$, Spatial distribution of NT products (${}^{A'}_{Z'}X(r)$), Decay time shortening, Fission barrier decrease
Indirect Evidences	Excess Heat Q, Number of neutrons N_n, Number of tritons N_t, Number of ${}_2He$ N_{He4}, Number of NT products N_{NT} (for NT_D, NT_F, NT_A, and NT_T), X-ray spectra $X(\varepsilon)$

These facts clearly show that CFP is a phenomenon conditioned by multi-component, dynamical and/or stationary properties of systems composed of transition metals and hydrogen isotopes

under influence of ambient thermal neutrons.

There are discovered a few characteristics and few laws in CFP. Following characteristics are essential factors in CFP to study its physics; qualitative reproducibility and sporadicity of events, favorable combinations of a cathode, a hydrogen isotope, and an electrolyte (e.g. Pd, D, Li; Ni, H, K). Two laws were recently discovered in CFP; the stability effect in the nuclear transmutation [3,6] and the inverse-power law of excess heat generation. [3,7]

These characteristics and laws in CFP show clearly that the entirety of CFP should be treated as a kind of complexity as explained below.

2. Many-particle Effects in CF Materials Resulting in Complexity

In this section, we explain a general nature of the complex system with non-linear interactions between its agents first and then explain the nature of the cold fusion phenomenon (CFP) in relation with complexity.

2.1 Complex System, Complexity and *1/f* Fluctuation

In a complex system (system composed of many components (agents) interacting with nonlinear forces), there occur various phenomena alien from those in simple systems that have been the main objects of modern science until 20th century. The science of the complex system has developed in recent twenty years and includes several new branches as synergetics, self-organization, fractals, chaos, emergence, complexity and so on named by pioneering scientists according to their points of view.

To make our discussion clear, we will use a terminology defined below referring to the Waldrop's book [8] as follows: the science of complex systems are divided into three classes; A. self-organization, B. chaos and C. complexity. These classes, A, B and C, correspond Wolfram's universality classes, I and II, III and IV, respectively, in relation with the cellular automata rules of S. Wolfram.

The Wolfram's classes are, on the other hand, characterized by the Langton's λ parameter in a von Neumann universe; Wolfram's classes, I and II, III and IV, correspond to λ's in following regions, $0.0 \leq \lambda < \lambda_c$ with a critical value $\lambda_c \simeq 0.275$, $\lambda_c < \lambda < 0.50$, and $\lambda \simeq \lambda_c$, respectively.

There is another interesting phenomenon, *1/f* fluctuations, closely related with CFP. The *1/f* fluctuations of the power spectrum in thermionic tube was discovered in 1925 by J.B. Johnson [9] and now recognized ubiquitous in many different phenomena. [10] It is interesting to notice that there is an attempt (self-organized criticality or SOC) to explain the *1/f* fluctuations in relation with a nonlinear process that

had fractal characteristics.[10] If this explanation applies to CFP, characteristics of CFP are explained in the frame of many-particle dynamics with nonlinear interactions among agents as investigated below.

These interesting features of the complex system may appear in the cold fusion phenomenon (CFP) if CFP is characterized by many-particle effects in the CF materials where observed various events, which will be classified similarly as phenomena in the complex system.

2.2 Cold Fusion Phenomenon (CFP) and Complexity

There are several evidences showing that CFP should be treated in the science of complex systems.

First of all, the irreproducibility and sporadicity of CFP events suggest chaotic nature of the process realizing CFP.

Second, there is an evidence of possible existence of self-organization in CFP. Negele and Vautherin [11] had shown that there appears a lattice of neutron-proton cluster, the Coulomb lattice, in a thin neutron star matter. In boundary and surface regions of CF materials, there occurs a situation where neutrons in a neutron band accumulate to form a high-density state due to the local coherence realized by a dispersion relation of the band. [12,13] The density of neutrons approaches to the lower limit of the density used in the simulation by Negele and Vautherin [11] showing possible self-organization of the Coulomb lattice in CF materials even if there are crystal lattices of the host elements (e.g. Pd) that does not exist in the neutron star matter. Existence of the crystal lattice may intensify the self-organization process.

Third, in addition to this theoretical analogy of CF material to the neutron star matter where many-particle effect plays essential role, there is experimental evidence showing many-particle effect of nucleons in CF materials; the stability effect in products of the nuclear transmutation in CFP, the first statistical law in CFP, discovered in 2003. [5,3] Counting a number of observations $N_{ob}(Z)$ of an element with an atomic number Z, from papers published in over ten years, we compared $N_{ob}(Z)$ with the logarithmic abundance of the element log $H(Z)$. [14] Even if the numerical values of $N_{ob}(Z)$ are small and the comparison is between $N_{ob}(Z)$ (not log $N_{ob}(Z)$) and log $H(Z)$, there is an excellent coincidence between them except few cases at several values of Zs with such reasonable explanations for discrepancies as follows; a large value of $N_{ob}(Z)$ at $Z = 47$ (Ag) next to Pd (a major element in the system) in the periodic table and absence of $N_{ob}(Z)$ for noble gases $Z = 10$, 18, 36 (Ne, Ar, Kr) which were not tried to detect intentionally without expectation. [5]

This coincidence of $N_{ob}(Z)$ and log $H(Z)$

clearly shows existence of a state where nucleons interact together to form stable groups as if they are in the process realized in the evolution of stars to produce elements in the universe from the lightest component, proton, up to the heaviest, uranium. Possible cause of this coincidence could be given by the above-mentioned self-organization in the cf materials with high-density neutrons.

Fourth, the inverse power law of the power spectrum of the excess heat generation, the second law in CFP, discovered in 2004, shows another evidence of the complex nature of CFP if SOC mechanism applies.[6,3] Referring to the explanation of *1/f* fluctuations in terms of the fractal, the inverse power law may also relate CFP with self-organization.

Fifth, the success of the TNCF (Trapped Neutron Catalyzed Fusion) model [4] shows complex nature of CFP on which the model based. There are numerical relations between numbers N_X of events X in CFP:

$N_t = N_Q$, $N_{NT} = N_Q$, $N_{He4} = N_Q$,

$N_n / N_t \simeq 10^{-6}$, $N_Q \equiv$ Q (MeV)/5 MeV,

where N_Q is defined as above. These relations were semi-quantitatively explained by the TNCF model that assumed thermal neutrons in CF materials based on many-particle nature.

3. Conclusion

From explanations of the complex system in general in subsection 2.1 and of the cold fusion phenomenon (CFP) in 2.2, we can guess that essential features of CFP may have close relation with the science of the complex system. These experimental facts explained in 2.2 (varieties of fields and products of CFP, numerical relations of numbers of events and two laws relating complex nature of CFP) clearly show that many-particle effects cause the cold fusion phenomenon in complex systems composed of transition metals, hydrogen isotopes, some minor elements appropriate for the transition metals, and/or hydrogen isotopes, and the background thermal neutrons.

The nature of complexity will give an explanation of the large value of the excess heat Q in CFP showing $1/f$ fluctuation. Usually, fluctuations of a physical quantity in a system composed of a large number of particles (agents) are negligibly small. The relative fluctuations of a quantity G will usually given by an equation of the type

$$(\langle G^2\rangle - \langle G\rangle^2)/\langle G\rangle^2 = 1/\langle G\rangle$$

where the $\langle\ \rangle$ indicate average values and will usually be very small due to a large value of $\langle G\rangle$ in the many-particle system.

However, it becomes very large near a critical point where $\langle G\rangle$ becomes very small as at the second-order phase transition. The Langton's critical parameter λ_c is another example to

specify a point where fluctuations become very large. This is one cause of large Q if CFP is a complexity.

It should be pointed out another cause to make the excess heat Q very large. There is a tremendous difference in energy of the cause (atomic) and the effect (nuclear); nuclear energy output is 10^8 times larger than atomic energy input. The small fluctuation in atomic processes that ignite nuclear reactions may induce a huge effect due to this difference. This is the second possible cause of the large Q that together with peculiar nuclear products troubled people to understand its nature for such a long period.

The nature of the complexity of CFP will be the main theme of the forthcoming investigation.

References

[1] M. Fleischmann, S. Pons and M. Hawkins, "Electrochemically induced Nuclear Fusion of Deuterium", *J. Electroanal. Chem.*, **261**, 301 (1989).

[2] M. Fleischmann, "Cold Fusion: Past, Present and Future", *Proc. ICCF7* pp. 119 – 127 (1998).

[3] H. Kozima, "Cold Fusion Phenomenon" *Rep. Fac. Science, Shizuoka University* **39**, 21 – 90 (2005).

[4] H. Kozima, *Discovery of the Cold Fusion Phenomenon - Evolution of the Solid State-Nuclear Physics and the Energy Crisis in 21st Century*, Ohtake Shuppan KK. Tokyo, Japan, 1998. ISBN 4-87186-044-2.

[5] H. Kozima, "Quantum Physics of the Cold Fusion Phenomenon" in *Developments in Quantum Physics,* ed. F. Columbus and V. Krasnoholovets, Nova Science, New York, 2005. ISBN 1-59454-003-9.

[6] H. Kozima, "CF-Matter and the Cold Fusion Phenomenon" *Proc. ICCF10* (Aug. 24 – 29, 2003, Cambridge, MA, USA) (to be published).

[7] H. Kozima, "Cold Fusion Phenomenon and Solid State-Nuclear Physics" *Proc. ICCF11* (Oct. 31 – Nov. 5, 2004, Marseille, France) (to be published).

[8] M.M. Waldrop, "Complexity – The Emerging Science at the Edge of Order and Chaos," Simon and Shuster, New York, 1992. ISBN 0-671-76789-5.

[9] J.B. Johnson, Phys. Rev. 26, 71 (1925).

[10] E. Milotti, "*1/f* noise: a pedagogical review" http://arxiv.org/ftp/physics/papers/0204/0204033.pdf

[11] J.W. Negele and D. Vautherin, "Neutron Star Matter at Sub-nuclear Densities" *Nuclear Physics*, **A207**, 298 – 320 (1973).

[12] H. Kozima, "Neutron Drop; Condensation of Neutrons in Metal Hydrides and Deuterides", *Fusion Technol.* **37**, 253 – 258 (2000).

[13] H. Kozima, "Excited States of Nucleons in a Nucleus and Cold Fusion Phenomenon in Transition-Metal Hydrides and Deuterides" *Proc. ICCF9* (May 19-24, 2002, Beijing, China), pp. 186 – 191 (2002).

[14] H.E. Suess and H.C. Urey, "Abundances of the Elements" *Rev. Mod. Phys.* 28, 53 – 74 (1956).

Bose-Einstein Condensation and Nuclear Reaction in Solids

Hiraku OKUMURA and Ken-ichi TSUCHIYA †

Department of Mathematics, Tokyo Institute of Technology,
2-12-1 Oh-okayama, Meguro-ku, Tokyo 152-8551, Japan
† Department of Chemical Science and Engineering, Tokyo National College of Technology,
1220-2 Kunugida, Hachioji, Tokyo 193-0997, Japan
e-mail: tsuchiya@tokyo-ct.ac.jp

Abstract: This paper shows the model for nuclear fusion induced by Bose-Einstein condensation in solids. Kim-Zubarev method is modified to calculate the quantum states of deuterons in Pd. The thermal conduction from the reaction center is also estimated by Fourier analysis.

1. Introduction

Many experimental results of the workers in the world suggest that the cold fusion may happen in the solids in room temperature. However, it is not completely understood now. The purpose of this study is to give a theoretical explanation for the mechanism of cold fusion. In the beginning, Bose-Einstein condensation (BEC) in solid is considered, because deuterons are highly condensed at defects in some metals. By using Kim-Zubarev theory [1], the wave function, the d-d fusion rate of condensed deuterons in crystalline solid and critical temperature Tc of BEC are obtained. [2] Furthermore, the thermal conduction from a reaction center is estimated as a function of position and time.

In section 2, Kim-Zubarev method is briefly shown and new approaches in solid state physics are described. In section 3, the methods how to calculate the nuclear reaction rate and the critical temperature of BEC are explained. In section 4, calculated results are discussed. In the last section, conclusions are described.

2. Kim-Zubarev Method and it's Application

In Kim-Zubarev theory, they assumed the potential for the ion trap device as an isotropic harmonic potential. Then the Hamiltonian of the system including N charged particle is

$$\mathcal{H} = -\frac{\hbar^2}{2m}\sum_{i=1}^{N}\nabla_i^2 + \frac{m\omega^2}{2}\sum_{i=1}^{N}\mathbf{r}_i^2 + \sum_{i<j}\frac{e^2}{|\mathbf{r}_i-\mathbf{r}_j|}, \quad (1)$$

where m is the rest mass of the particle and $\mathbf{r}_i$ is the position of an ion. The ground state of this many-body problem is written as

$$\Psi(\mathbf{r}_1,\mathbf{r}_2,.....,\mathbf{r}_N) \approx \frac{\phi(\rho)}{\rho^{(3N-1)/2}}, \quad (2)$$

where quantity ρ is defined as $\rho = \left(\sum_{i=1}^{N}\mathbf{r}_i^2\right)^{1/2}$. The wave function ϕ in eq.(2) satisfies

$$h = -\frac{\hbar^2}{2m}\frac{d^2}{d\rho^2} + \frac{\hbar^2}{2m}\frac{p}{\rho^2} + \frac{m\omega^2\rho^2}{2} + \frac{qe^2}{\rho}$$

$$h\phi(\rho) = E\phi(\rho), \quad (3)$$

where p and q are defined as $p = (3N-1)(3N-3)/4$ and $q = 2N\Gamma\left(\frac{3N}{2}\right)/3\sqrt{2\pi}\Gamma\left(\frac{3(N-1)}{2}\right)$. Generally, these differential equations for harmonic oscillators are rewritten by using nondimensional quantities $x = \sqrt{\frac{m\omega}{\hbar}}\rho$ and $\varepsilon = 2E/\hbar\omega$. As a result, eq.(3) is rewritten as

$$\left(-\frac{d^2}{dx^2} + x^2 + \frac{p}{x^2} + \frac{q'}{x}\right)\phi(x) = \varepsilon\phi(x). \quad (4)$$

In this equation q' are given by $q' = 2\alpha q\sqrt{mc^2/\hbar\omega}$, where $\alpha = e^2/\hbar c$ is the fine structure constant. The method described above is called equivalent linear two-body (ELTB) method.

Now we show the application of Kim-Zubarev method to the phenomenon in solid. The Hamiltonian of a system including N deuterons in solid consists of kinetic energy of deuterons, deuteron-deuteron interactions and deuteron-host ion interactions. Therefore, Hamiltonian of the N-deuteron systems in solid is written as

$$\mathcal{H} = -\frac{\hbar^2}{2m}\sum_{i=1}^{N}\nabla_i^2 + \sum_{ij}\frac{Ze^2\exp(-K|\mathbf{R}_j-\mathbf{r}_i|)}{|\mathbf{R}_j-\mathbf{r}_i|} + \sum_{i<j}\frac{e^2\exp(-k|\mathbf{r}_i-\mathbf{r}_j|)}{|\mathbf{r}_i-\mathbf{r}_j|}, \quad (5)$$

where $\mathbf{R}_j$ is the Bravais lattice vector of the host lattice and Z is the effective charge of a host ion. If a site $\mathbf{R}_j$ corresponds to the defect, it is omitted from the lattice summation. In eqs.(3) and (4) of Kim-Zubarev theory, harmonic term is the electro magnetically induced attractive potential in the ion trap device [1]. For the case of the problems in crystalline solids, this term corresponds to the repulsive interaction between positively charged host ions and positively charged impurity deuterons trapped in the defects. The second term of eq.(5) has the same role with the harmonic term in eqs.(3) and (4). The second and third terms of eq.(5) should be transformed into ρ space.

For the case of our Hamiltonian, eq.(4) is rewritten as

$$h = -\frac{d^2}{dx^2} + \sum_{m=2}^{M} A_{N,m} x^{2m-2} + \frac{p}{x^2} + \frac{q'}{x} f_{TF}$$
$$h\phi(x) = \varepsilon\phi(x), \qquad (6)$$

where coefficients $A_{N,m}$ and screening factor f_{TF} are defined as

$$A_{N,m} = \frac{K^{2m-4}(3N)!!\left(\frac{\hbar}{m\omega}\right)^{m-2}}{2^{m-2}(m-1)!(3N+2m-4)!!} \qquad (7)$$

and

$$f_{TF}(\rho) = 3(N-1)\int_0^{\pi/2} d\theta \sin\theta \cos^{3N-4}\theta \times \exp\left(-k\sqrt{2}\rho\sin\theta\right). \qquad (8)$$

In eq.(6), M is the cut-off of the summation for m. For the case of $M = 2$ and $k = 0$, it is completely consistent with eq.(4) of Kim-Zubarev theory. In practice, M should be selected to keep required accuracy. The screening factor is also defined for self-consistent non-linear screening potential. [2–4] In eq.(6), we consider only one defect. This means interactions between deuteron clucters are regarded as negligible contribution to the distribution of deuterons.

3. Nuclear Reaction Rate and Probability of Ground State Occupation

The ground state wave function Ψ for N identical charged Bose nuclei gives the nuclear reaction rate as

$$R = -\frac{2\sum_{i<j}\langle\Psi|ImV_{ij}^F|\Psi\rangle}{\hbar\langle\Psi|\Psi\rangle}, \qquad (9)$$

where imaginary part of Fermi pseudopotential V_{ij}^F [1] is written as $ImV_{ij}^F = -\frac{A\hbar}{2}\delta(\mathbf{r}_i - \mathbf{r}_j)$. The short-range interactions of nuclear forces between two Bose nuclei are introduced by using δ function [1]. This rate can be calculated by using numerical solution of eq.(6), because ϕ gives Ψ. The constant A is given by Bohr radius $r_B = \hbar^2/me^2$ and the S factor of the nuclear reaction between two nuclei as $A = 2Sr_B/\pi\hbar$.

If the ELTB solution is obtained, the critical temperature T_c of BEC is estimated by well known formula which is written as

$$T_c = \frac{h^2}{2\pi m k_B}\left(\frac{n}{\zeta(\frac{3}{2})}\right)^{2/3}, \qquad (10)$$

where n is the number density of Bose particles and $\zeta(z)$ is the Riemann's zeta function. This temperature gives probability of the ground-state occupation. It is written as

$$\Omega = 1 - \left(\frac{T}{T_c}\right)^{2/3} \quad for\ T < T_c\ . \qquad (11)$$

If we account the ground state occupation for $T < T_c$, the fusion rate is given by $R\Omega$. When $T \geq T_c$, no nuclear reactions have happened because $\Omega = 0$.

4. Thermal Conduction

If nuclear reactions happen in solid, heat generated from the reaction center is diffused. In this study, we only consider thermal conduction from the center of a DD reaction in Pd as a simplified model. Equation of the thermal conduction in solid is written as

$$\frac{\partial T}{\partial t} = k\nabla^2 T, \qquad (12)$$

where T and t mean temperature and time, respectively. In this equation, the constant k is defined as

$$k = \frac{K}{C\rho}, \qquad (13)$$

where K, C, and ρ mean thermal conductivity, specific heat and density of the solid , respectively. The origin of the temperature is selected as the equivalent value. Eq.(12) is divided into x, y, z and t as

$$T(x,y,z,t) = X(x)Y(y)Z(z)U(t). \qquad (14)$$

The periodic boundary condition we used for X is defined as

$$X(x) = \begin{cases} 0 & for\ 0 \leq x < \frac{1}{2}(L-d) \\ T_0^{1/3} & for\ \frac{1}{2}(L-d) \leq x \leq \frac{1}{2}(L+d) \\ 0 & for\ \frac{1}{2}(L+d) < x \leq L \end{cases} \qquad (15)$$

and

$$X(x) = X(x + L), \tag{16}$$

where parameter d corresponds the size of the deuteron cluster. The initial condition is written as

$$U(0) = 1. \tag{17}$$

The general solution using Fourier expansion is written as

$$T = \sum_{n_x,n_y,n_z=1}^{\infty} C_{n_x} \cos(\lambda_x x) e^{-k\lambda_x^2 t} \times C_{n_x} \cos(\lambda_y y) e^{-k\lambda_y^2 t} \times C_{n_x} \cos(\lambda_z z) e^{-k\lambda_z^2 t}, \tag{18}$$

where constants are written as

$$\lambda_i = \frac{2n_i\pi}{L} \tag{19}$$

and

$$C_{n_i} = (-1)^{n_i} \frac{2T_0^{1/3}}{n_i\pi} \sin\frac{n_i\pi d}{L}. \tag{20}$$

The parameter L means distance between two neighboring reaction centers. This parameter is obtained by well known formula for the concentration of Shottky defect in solid. It is written as

$$\frac{n}{N} = \exp\left(-\frac{w}{k_B T}\right), \tag{21}$$

where n, N and w mean the number of defect, the number of total atoms and vacancy formation energy, respectively.

The initial condition used for solving eq.(12)is described as follows. Inside of the d×d×d cubic including the center of a DD reaction, temperature is uniformly T_0. Outside of the cubic, T=0. The lattice constant of fcc Pd is 3.89Å. The initial temperature is obtained by

$$T_0 = \frac{E}{CM_0}, \tag{22}$$

where E and M_0 mean energy generated from a DD reaction and number of moles in the d×d×d cube, respectively.

The constants used for the calculation are $K = 75.5J/(sec\, m\, K)$, $C = 25J/(mol\, K)$, $\rho = 12.0g/cm^3$, $E = 23.8MeV$, $M_0 = 4/Avogadro\ number$ and $w = 1eV$.

5. Results and Discussions

We considered octahedral void shown in Fig.1 as an ion trap in Pd. Calculated results for some cases at an octahedral void (VacO) are shown in Table 1 and Fig.2. Seeing Fig.2, sharp peak exists at the potential well. Seeing Table 1 , T_c's are higher than room temperature for the case of non-linear screened d-d interactions. Nuclear reaction rates are extremely high.

Thermal conduction from a center of a DD reaction is plotted in Figs.3 and 4. The contour plot is also shown in Fig.5. The calculated results show the rapid temperature relaxation. Within $10^{-10} sec$, temperature outside of the reaction core is reduced to the initial value. When the void contains 5 deuterons, reaction rate is $10^9 sec^{-1}$. This means that temperature reduces to the initial value earlier than the inverse of the reaction rate. Therefore, continuous reaction will not make thermal explosions. If the number of deuteron clusters is very large, recovery from the initial temperature is not so rapid. However, if the temperature is higher than Tc, probability of the ground state occupation becomes zero. And the reaction will not continue.

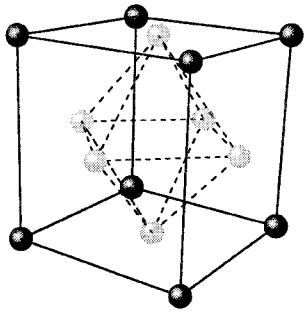

Fig. 1. The structure of VacO in fcc lattice. The black and gray circles mean occupied and unoccupied lattice points, respectively. These defects construct octahedral void.

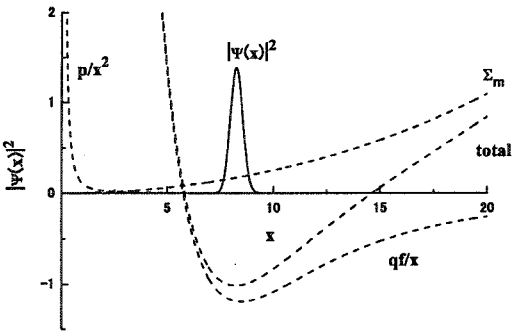

Fig. 2. The ELTB solution for the system including 5 deuterons in VacO in fcc Pd. Non-linear screening potential is used as the d-d interaction. The nondimensional quantity x is defined as $x = \sqrt{m\omega/\hbar}\ \rho$, where $\omega = 0.86 \times 10^{14} sec^{-1}$. The solid line means the ELTB solution. The dashed lines mean each potential in eq.(6) normalized by $|\varepsilon| = |-409|$.

Table 1
Nuclear reaction rate R $[10^7 sec^{-1}]$ and critical temperature T_c $[K]$ for the case of N deuterons in VacO in Pd.

		Thomas-Fermi screening				non-linear screening			
N	$\sqrt{N}R_v$	ρ_{max}	ρ_2	T_c	R	ρ_{max}	ρ_2	T_c	R
3	5.83	2.86	2.98	56	2.1	1.13	1.21	257	33.8
4	6.74	3.67	3.80	66	3.5	1.37	1.45	329	66.4
5	7.53	4.41	4.53	76	5.0	1.58	1.66	403	108.6
6	8.25	5.10	5.22	86	6.7	1.77	1.85	480	160.2
7	8.91	5.75	5.86	95	8.6	1.94	2.02	558	221.3

ρ_{max}: position of the peak in ELTB solution [Å]
ρ_2: position of the right foot of the peak [Å]
R_v: Radius of the spherical defect is 3.23[Å].

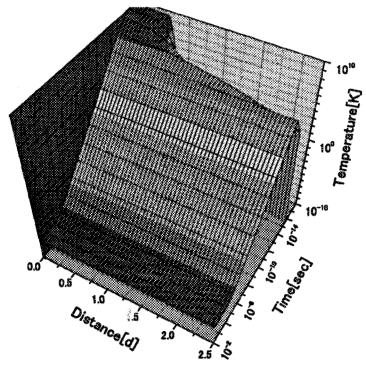

Fig. 3. Thermal conduction from a center of a DD reaction. Distance from a reaction center is normalized by the size of the deuteron cluster.

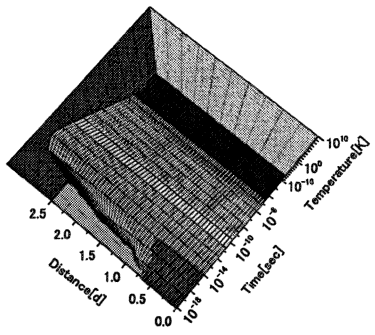

Fig. 4. Thermal conduction from a center of a DD reaction. (The same surface with Fig.3 viewing from another direction.)

6. Conclusions

Our calculations show that nuclear reactions are induced by BEC at defects in Pd in room temperature. The reaction rate is extremely high but explosions will not happen because of the rapid thermal decay in lattice. Even if the temperature increases, it will exceeds Tc and the ground state occupation Ω becomes 0. This means that the reactions will not continue.

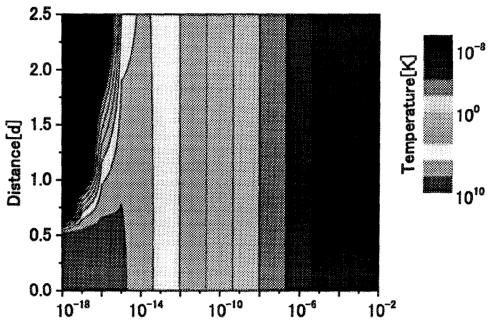

Fig. 5. The contour plot of thermal decay plotted in Figs. 1 and 2.

Acknowledgements

The author wishes to thank Professor H.Yamada of Iwate University for helpful discussions and encouragements.

References

[1] Y.E.Kim and A.L.Zubarev, "Nuclear Fusion for Bose Nuclei Confined in Ion Trap", Fusion Technology **37**(2000)151

[2] K.Tsuchiya, "Quantum States of Deuterons in Pd ", International Journal of Hydrogen Energy, **29**(2004)1513

[3] H.Hohenberg and W.Kohn, "Inhomogeneous Electron Gas", Phys.Rev. **136**(1964)B864.

[4] W.Kohn W and L.J.Sham, "Self-Consistent Equations Including Exchange and Correlation Effects", Phys.Rev. **140**(1965)A1133.

The Iwamura experiment and fusion chemistry

Norio YABUUCHI
High Scientific Research Laboratory
204 Marusen Building, 28-16 Marunouchi, Tsu City, Mie 514-0033, JAPAN
E-mail yabu333@lilac.ocn.ne.jp

Abstract

In the experiment conducted by Iwamura, et al., the passage of ^{2}D gas through a multilayered palladium membrane yielded the following two results:

$$^{133}Cs_{55} \rightarrow {}^{141}Pr_{59} + \Delta E \quad (1)$$

$$^{88}Sr_{38} \rightarrow {}^{96}Mo_{42} + \Delta E \quad (2)$$

That is to say, the experimental results indicate that elemental transmutation occurred at low energy levels, with the release of middle-level nuclear energy.

One possible explanation for these two facts is nuclear fusion by atomic nuclei having low binding energy. If this is so, the question then raised is, what are nuclei that have low binding energy? The answer is that they may be either halo nuclei or liquid-crystal nuclei. Such theoretical inquiry into the nature of nuclei can be expected to yield favorable results.

The author has previously described both halo and liquid-crystal nuclei in this paper those earlier observations are extended to the methods of Iwamura, et al.

The peripheral equipment which induces nuclear fusion is also discussed. Such equipment must enable the existence of a state having a field current of large amounts of deuterium caused by the passage of deuterium. A multilayered membrane of palladium, which serves as the deuterium-storage metal, must also be present. The paper describes how these two main features are what enable the equipment to function as a fusion device. The conclusion is reached that, as a result, radiation of middle-level nuclear energy and transmutation is brought about by low energy.

Key words: liquid crystal, nano-space, Platonic structure of atomic nucleus, block arrangement of atomic nucleus, subsidence of Coulomb barrier

1. Introduction

Firstly considering is of halo nuclei having low binding energy, one case of which is the isotope ^{11}Li, in which the neutrons in the outer shell exist at locations farther from the center of the nucleus. However, an isotope having many neutrons does not exist in the reported nuclear reaction, and so this is judged not to be suitable.

Next are liquid-crystal nuclei. In a molecular liquid crystal, the positional relationship of the arrangement of its constituent atoms remains unchanged, the spaces between the arranged atoms are large, and a high degree of freedom exists in the orientation of the atomic arrangement. In correspondence to this, in an atomic liquid crystal the positional relationship of the arrangement of its nucleons remains unchanged, the spaces between the arranged nucleons are large, and a high degree of freedom exists in their orientation. In a word, this could be termed an atomic nucleus that has undergone large expansionary change

with no alteration of its configuration. Accordingly, this can be regarded as a state intermediate between a coalesced solid and a liquid.

As a result of this, the radius of the atomic nucleus is enlarged and proton reaction on the periphery becomes small, and so it can be predicted that nuclear fusion will be facilitated. When the radius becomes large, however, Coulomb attraction grows weak and binding energy is diminished as well, and the release energy is smaller. It was predicted from these two points that the nuclear fusion in the Iwamura experiment was fusion by liquid-crystal nuclei. Now we turn to discussion of the type of fusion reaction that is produced.

2. Nuclear-chemistry Process of Nuclear Fusion

Firstly, the existence of the ^2D gas cannot be ignored. The fact must be admitted that during its passage through the multilayered membrane of palladium it combined with the cesium or strontium deposited on the surface of the palladium membrane and, as a result, underwent transmutation to praseodymium or molybdenum. The deuterium therefore participated in the nuclear reaction. Next there is the existence of cracks. Minute spaces equivalent to cracks exist between the seams in the multilayered membrane. It is possible that the fluid deuterium, which consists of Bose particles that have undergone Bose-Einstein condensation, is accelerated and collides with the cesium or strontium. Accordingly, it appears, because the Coulomb barrier is lowered by the widened radius of the nucleus, this acceleration causes the Coulomb barrier to be overcome with ease, and fusion occurs. Once this has been elucidated, the next step is to derive the nuclear chemical formulae.

Examination of reaction formulae (1) and (2) reveals that each atomic number increased by 4 and atomic weight by 8.

Accordingly, because the equipment brought about the reaction through the passage of deuterium, it is possible that the $2{\cdot}2^2D$ reacted immediately. Reaction by liquid-crystalline $^4He_2$, which has a weakly reactive, large nuclear radius, instead of $2{\cdot}^2D$ is also conceivable.

Reaction formulae (1) and (2) would thereby change as follows:

$$^{133}Cs_{55} + 2{\cdot}2\ ^2D\ (2{\cdot}^4He_2) \rightarrow\ ^{141}Pr_{59} + \Delta E \qquad (3)$$

$$^{88}Sr_{38} + 2{\cdot}2\ ^2D\ (2{\cdot}^4He_2) \rightarrow\ ^{96}Mo_{42} + \Delta E \qquad (4)$$

Next, although the life of a water-bubble in the air is short, the life of the same bubble when submerged in water is long. In the same way, the life of the compound-nucleus 2^2D in a sea of deuterium is long, and so fusion reaction is postulated as possible. The liquid-crystal nuclear reaction was described by the author in detail at JCF5. To amplify, firstly, the atomic nuclear structure is not a conventional Bohr-Sommerfeld membrane, but rather a Plato-Kepler membrane. Accordingly, the state of condensation is fundamentally one having a crystalline structure, but when it exists within the metal of a hydrogen-absorbing alloy, it is assumed to be in a liquid-crystal state, that is, one intermediate between a crystal and a liquid. Atomic nuclei having high atomic numbers all have a molecular structure, as has been described in past papers.

Following is the explanation of formula (3).

With reference to Fig. 1 and Fig. 2, it is believed that the (b) and (d) of the cesium respectively reacted with $2{\cdot}^2D$ or 2^4He_2 and were transmuted into

praseodymium.

Next is an explanation of formula (4).

With reference to Fig. 3 and Fig. 4, it is believed that the (a) and (c) of the strontium respectively reacted with $2 \cdot {}^{2}D$ or ${}^{4}He_2$ and were transmuted into molybdenum.

References

Norio YABUUCHI. Proc. JCF4, 82 (2002)
Norio YABUUCHI. Proc. JCF5, 93 (2003)
Yasuhiro IWAMURA, Mitsuru SAKANO, Takehiro ITOH. Jpn. J. Appl. Phys. Vol. 41 (2002) pp. 4642-4650

Figure 1 – Liquid-crystal nucleus structure of $^{133}Cs_{55}$

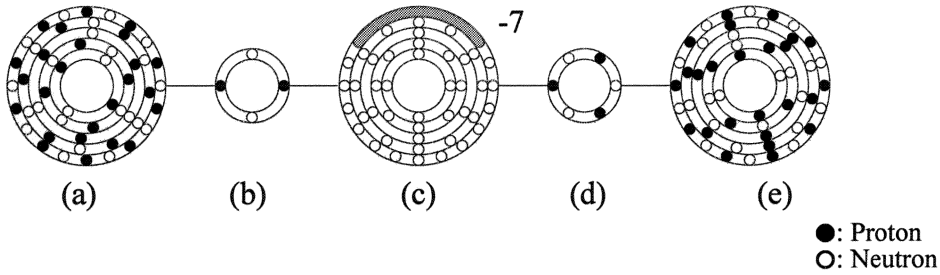

Figure 2 – Liquid-crystal nucleus structure of $^{141}Pr_{59}$

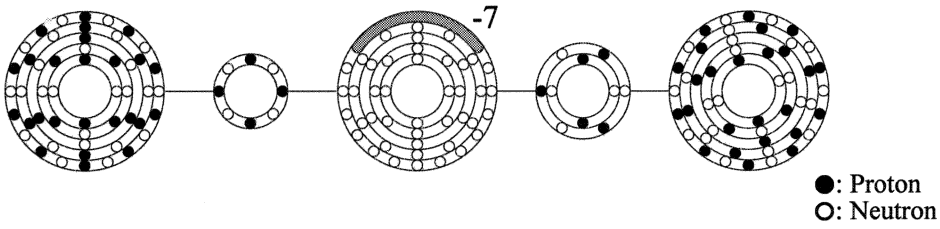

Figure 3 – Liquid-crystal nucleus structure of $^{88}Sr_{38}$

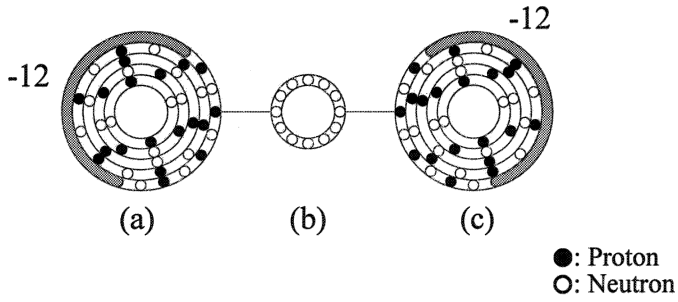

Figure 4 – Liquid-crystal nucleus structure of $^{96}Mo_{42}$

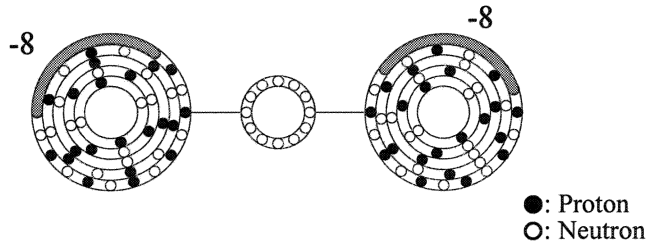

Cold fusion associated with three kinds of matter wave resonance

Masanobu BAN, Tokyo Metropolitan Industrial Technology Research Institute: Masanobu_Ban@member.metro.tokyo.jp

Abstract: It is watched that cold fusion is responsible for the configuration of deuterium atoms in solid condensates. We found that electric charge assists to form in line for deuterium atoms in crystals. The force, which is based on electron waves, gets free particles fall in. Electron resonance is one of phenomenon in electric discharge. There are three kinds of resonance. In this study, we investigate phase transition of resonance in views of a relation between cold fusion and matter wave resonance in direct current circuit.

Keyword: 1/f noise, soliton, transition probability, electron, tunnel effect, electron wave, cold fusion

1. Introduction

It is pointed out that cold fusion (CF) is responsible for the configuration of deuterium atoms in crystal.

The CF is connected to three kinds of resonance occurring in electron discharge. The CF is a type of electron resonance, which occurs in the dc circuit.

In the dc circuit, the charge causes the alignment of the free particle.[1)2)3)4)5)] We found a force that the electric charge assists to form in line for deuterium atoms in crystals.

In this study, we investigate a relation between matter wave resonance occurring in dc discharge current and cold fusion in view of variation of the resonance. For dc electric discharge three noises interchange in the same condition.(6)Fig.12, Fig.13)

The noise, which occurs in power spectral density, fluctuate white, 1/f square and 1/f noises. These noises are exchangeable.

We explain the relation for cold fusion, using change of resonance matter wave.[7)] Nano carbons, nano tubes and Fullerene are produced by dc discharge circuit.[8)] Since phase conversion of crystals awes to dc discharge, we consider phase conversion for cold fusion.

Maeda et al. successfully found that the noise component of 1/f and 1/f square was observed at discharge portion in graphite electrode[9)], and took out the noise of the electric discharge portion from demodulation controlled by the electric discharge distance. ([10)] p.2141) In this case, the two kinds of noise occur alternately in the circuit.

In general, it is well known that the white noise always exists as JB-Johnson Noise. Indeed, the three kinds of noises occur continuously and alternately at least. This is responsible for tunneling in discharge at part of discharge.

Thus the tunneling occurs alternately three states; free electrons in discharge are emitted from metal surface into the air by tunneling, and the matter wave in tunneling consists of standing and traveling waves for electrons, because free electrons and matter waves coexist in tunneling.[7)]

In other words, existence of the standing and traveling waves make assist to form in line for deuterium atoms in crystals, leading to cold fusion.

Such phenomena, plasma crystal occurs in plasma dust of direct current glow discharge. [1)] Furthermore, since dust being line up becomes crystal, phase change exists in resonance of the de Broglie wave.

2.White noise and 1/f square noise

An expectation of energy can be obtained from a transition probability of quantum mechanics. When analogy of a fluid and the electricity of direct current is used, the formula of electric current can be made from a variable of time.

That time it is possible to change the operational order of integral calculus and square root extraction, making use of orthogonality concerning integral calculus of the section where orthogonal basis is squared. [7)] Then, the momentum calculates from the square root of power. Equation 9 of the paper[7)] is displayed equation (1).

$$i(t)=\varepsilon\rho_{vol}S\sqrt{\frac{2h}{m\pi}}\int_{-\infty}^{\infty}\frac{\sin\omega}{\omega}e^{i\omega t+\theta(t)}d\omega \qquad (1)$$

The 1/f square characteristic of a power spectrum density appears in the expression. Because it is a linear algebra, the same power spectrum density as the expression cannot be shown at the same time by other expressions. The current of 1/f square was decided to this expression.

However, the electron makes the white noise when generated from the cathode, and the signal of the Poisson distribution becomes Rayleigh distribution.

And, when the signal is 1/f square characteristic, the following electron should synchronize phase θ(t).

Let's pay attention to 1/f square noise having been against nature of this Rayleigh distribution. In Rayleigh distribution, amplitude strength R is normal distribution p(R) because of the random probability process. The formula is shown in the following equations 2,3.

$$p(R)=\frac{2R}{\Omega}\exp\left(-R^2/\Omega\right) \tag{2}$$

$$i(t)=C(t)\cos\{\omega_0 t+\theta(t)\} \tag{3}$$

The current of narrowband i(t) is expressed with alternating current and the feature is in a random jump change of initial phase theta (t). However, when initial phase θ(t) of the electron is synchronized for a long time, the quantum resonance makes 1/f square noise of expression 1. Therefore, 1/f square can conclude the character of the quantum resonance.

The discharge part is put to the potential barrier of well type by the electrode. In the row of the potential barrier of the well type, whenever the quantum propagates, 1/f square noise must be made.[11]

If the freedom of the phase is excluded, then 1/f square can be considered to be a basic character of the electrical discharge circuit.

3. 1/f noise

The 1/f noise to be explained from now on the 1/f square noise was used as the foundation and it is done.

There is a well type potential in the discharge region. Electron wave includes wave packet and standing wave in well type potential.

From the harmonic that have the quality of 1/f in amplitude, the wave is synthesized inside the well as Fig. 1. Function sin x/x is used for the harmonic component because it is a character that the amplitude is in inverse proportion to the frequency at the phase proportional to wave number. It is a condition that there is wave number of nπ in a basic wave between the cathode and the anode discharging electricity.

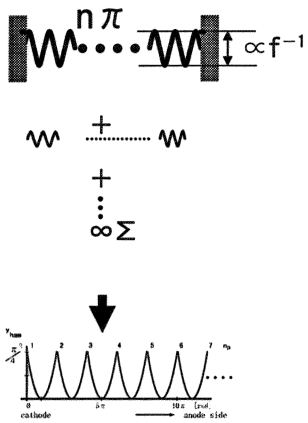

Fig. 1 Synthesis of harmonic

Then, the row of the subdivided small well can be made in the bottom in a big well of inter electrode.

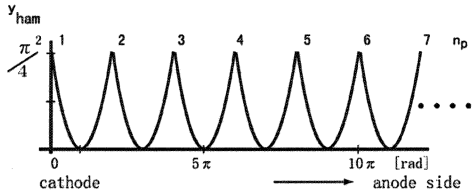

Fig. 2 Synthesized Electron wave

The existence probability is set to the electrode side high. When the harmonic component of the standing wave is synthesized on an easy condition, the line of the particle is found from the free particle group.[7] When harmonic of the standing wave are synthesized, the free particle getting together, it lines up.[1] Alignment appears at Y_{ham} in Fig. 2 and the electron wave builds the aligned power.

From 1/f square and next, with synthesis as 1/f noise trying, the line was completed also. And in our paper[7], the power of the electron wave was settled in simple equation 4.

$$\eta\frac{dk}{dt}=F \tag{4}$$

This is thought from the relational expression when the electron propagates in the semiconductor.

$$\frac{1}{m}=\frac{1}{\eta^2}\frac{d^2E(k)}{dk^2} \tag{5}$$

$$dE(k) = \eta v_g dk \quad (6)$$

$$dE(k) = (F \bullet v_g) dt \quad (7)$$

The equation 4 is made from equation 6 and equation 7.

The free particle following to the power becomes the line of the position where Y_{ham} is shown in Fig. 2.

It is the cause this designating 1/f square quality as basic character of the discharge circuit. The repetition of a barrier as Fig. 2 makes the resonance of tunnel phenomenon.[11]

However, because this row is a crystal, it is row of the harmonic oscillator. The wave packet, which is spread to the harmonic oscillator output, is integrated because of Virial theorem. The meaning of integration is a low-pass filter if it is explained as working of the electric circuit.

As a result, as for the signal of propagating wave packet, it is turned integral calculus into 1/f from the 1/f square. However, working might not work constantly and continuously. There will be such a resonance, and the resonance changes.

The structure of a repetition is increasing resonance. Accordingly resonance of electron wave of 1/f power may be promoted by surface structure of an electrode. For instance, it can be expected that a graphitized layer structure promotes the resonance.

For example, as promoting factor of resonance it can expect the type of stratified structure of graphite. As the case, the resonance is invited by negative resistance that came when perylene is observed with STS.[12]

Negativity resistance of that is considered to be a part of character in which resonance is attracted.

There is an electrode where the resonator which promotes resonance, induces phenomenon had stratified crystalline structure.

The phenomenon is going to be induced by a resonator, and the cold fusion can expect it, too.

4. A characteristic of resonance

Power spectral density P is in inverse proportion to frequency f in 1/f noise. If we display in formula, it becomes P(f)=C/f. C is constant, but when we rewrite, it becomes the relationship to which power is distributed equally in the product, P(f)f =C, as white noise P(f) =C.

Since $1/f^2$ noise is $P(f)=C/f^2$, it can be written to $P(f)f^2$ =C.

There is always the feature of P(f) f^m =C in resonance like the law of energy partition. There is always an equation P(f) f^m =C that it looks like the equation P(f) f^0 =C of the oscillator at Planck's black body radiation.

5. Conclusion

Free electron is discharged by tunneling at the time of electric discharge to the air by the cathode. Therefore free particle and matter wave exist in tunneling.

And at least three kinds of resonance exist in electron wave in one dimension of boundary condition. When it fluctuates alternately with 3 interspecific, phase change occurs in plasma crystal of the electron wave.

When a free particle is contained in the material placed between the electrodes, the material wave is the same condition even if it is not an electrical discharge.

For example, if the tunnel phenomenon has occurred in a solid solution, a semiconductor, electrolysis liquid, and gas, a phenomenon of same class will occur.

In electric discharge of a direct current, the feature of a phase transition is found in many examples.[13]

The conduction of heat with a sudden temperature change occurs to the electrical discharge as an example of the phase transition at the electrostatic cooling phenomenon.[14]

Carbon graphite is changed into fullerene or the crystal structure of a tube. [13]

There is nanotechnology that controls only one atom when the atom is transported with the tunnel microscope. [15] Similarly, the plasma Crystal is made from the gravitation of the electron wave.

These cases prove the feature of the phase transition.

Acknowledgement

I appreciate that Dr. Hiroo Numata gave me aid. The paper is possible with the help of JCF.

References:

1) http://annex.jsap.or.jp/hokkaido/yokousyuu39th/B-29.pdf, in Japanese.

2) H.M.Thomas and G.E.Morfill,Nature(London)379,806,(1996).

3) F.Melandso, Phys. Plasmas 3,3890(1996).

4) S.V. Vladimirov and O.Ishihara, Phys. Plasmas 3,444(1996).

5) S.V. Vladimirov, P.V. Shevchenko and N.F. Cramer., Phys. Plasmas 5,4(1998).

6) S. Sugita, Y. Mera, K. Maeda: Origin of low frequency noise and 1/f fluctuations of tunneling current in scanning tunneling microscopes, J. Appl. Phys.,Vol. 79, No. 8, pp.4166-4173, 15 April 1996.

7) M. Ban: COMPOSITION OF 1/F AMPLITUDES ELECTRON WAVE AND A WORK OF ONE DIMENSION OF LATTICE, Proceedings of the 4th Meeting of Japan CF-Research Society, Morioka, October 17-18, 2002,p.90-94.

8) Y. Hayashi: Dusty Plasmas and Carbon Fine Particles, J. Plasma Fusion Res., Vol.78., No.4, (2002)pp.320-324. in Japanese

9) S. Sugita, Y. Mera, K. Maeda: Origin of low frequency noise and 1/f fluctuations of tunneling current in scanning tunneling microscopes, J. Appl. Phys.,Vol. 79, No. 8, pp.4166-4173, 15 April 1996.

10) K. Maeda , S. Sugita, H. Kurita, M. Uota, S.Uchida, M. Hinomaru, Y. Mera: Spatial variation of 1/f current noise in scanning tunneling microscopes, J. Vac. Sci., Technol. B 12(3),pp.2140-2143, May/Jun.

11) T. Haga, Y. Takane and K. Nakamura: $1/f^2$ Law in One-dimensional Quantum Transport: an Example of Weak Chaos in Quantum Systems, Chaos Solutions & Fractals, Vol. 5, No. 7, pp. 1077-1083, 1995.

12) Okuda, Inaba, Naitou, Ehara, Takagi: Negative resistance of the organic membrane with STS, IEICE, TECHNICAL REPORT OF IEICE, OME 93-56 (1994-03), in Japanese.

13) N.Sato, R.Hatakeyama, T.Hirata: Applicatins of Dusty Plasma: Fullerene Plasmas, J. Plasma Fusion Res., Vol.73., No.11, (Nov.1997)pp.1252-1256. in Japanese.

14) K. Kisi, H. Eda: Electrostatic cooling, Journal of IEIC, 9/'77, vol. 60, no. 9, pp. 1044-1046, Sep. (1977), in Japanese.

15) D.M. Eigler, E.K. Schweizer: Positoning single atoms with a scanning tunneling microscope, NATURE, Vol.344, 5, ,pp.524-526.Apr.(1990)

Brief Review of EQPET/TSC Theory Versus Experiments

Akito Takahashi (Osaka University); akito@sutv.zaq.ne.jp

Brief review of theoretical results by EQPET (Electronic Quasi-Particle Expansion Theory) and TSC (Tetrahedral Symmetric Condensate) are given in comparison with major experimental results of CMNS (Condensed Matter Nuclear Science).

1. Introduction

A series of elaborated theories on deuteron cluster fusion model is reviewed in two papers[8,9]. The EQPET (Electronic Quasi-Particle Expansion Theory) model was proposed and applied for numerical analyses of D- and H/D-mixed cluster fusion in PdDx systems. Formation and squeezing of TSC (Tetrahedral Symmetric Condensate) were modeled with numerical estimations by STTBA (Sudden Tall Thin Barrier Approximation)[9]. Obtained numerical results could explain major claims of CMNS experiments.

In this paper, we review short summary of theoretical models, in comparison with key experimental results, as briefly listed in **Table-1**. We have seen very consistent agreements between key experimental results[1-7] and numerical estimations by EQPET/TSC models.

Table-1: Summary Results, experiment vs. theory

Item	Experiment Author/ Method / Results	EQPET/TSC Models
Screening of d-d fusion	Kasagi/ D-beam, PdDx/Us= 310+-30eV Takahashi/3D,TiDx/ <dd> =1E9 in range	Us=360eV, by dde*(2,2) (1E13)τ with τ = 0.1 ms
$^4He/^3He$ production	McKubre/Electrolysis/ 30 +- 13 MeV/^4He Arata/nano-Pd, El./ $[^3He]/[^4He]$=0.25	23.8 MeV/^4He by $4D \rightarrow {}^4He + {}^4He$ +47.6MeV $[^3He]/[^4He]$=0.25, for H/D=0.6
Max. Heat	El Boher/ Super-wave El./ 24.8 keV/Pd Gain = 25	23 keV/Pd 46 MW/cc-Pd by 4d/TSC
Transmutation	Iwamura/ Pd-complex, gas/ Cs to Pr Miley/Ni-H, electrolysis/ fission-like FP	4d/TSC or ^8Be capture FP by Ni+4p/TSC

2. Screening Effects for d-d Fusion in Condensed Matter

When low energy d-beam is implanted into condensed matter, e.g., PdDx, incident d^+ picks up and conveys an electron which is quasi-free in Incident d gives same velocity to convey electron, which has therefore enough momentum of 180 degree opposite direction to another electron with target deuteron. We easily expect two electrons form a Cooper pair e*(2,2) with 50% weight for anti-parallel arrangement of spins.

In our previous paper[8], numerical (graphical) result of screened Coulomb potential for d-d interaction Vs (r) is given using the formula, for dde*(m,n) EQPET molecules,

$$Vs(r) = e^2/r + Vh + (J+K)/(1+\Delta) \quad (1)$$

$$Vh = - 13.6Z^2/(me/m^*) \quad \text{(in eV unit)} \quad (2)$$

conduction band of PdDx lattice to make charge neutralization. A target D-atom (d + e) is waiting for incoming (d + e).

By defining b0-parameter to satisfy,

$$Vs(b0) = 0 \quad (3)$$

We obtain screening energy Us by

$$Us = - e^2/b0 = - 1.44/b0 \quad \text{(in eV and nm unit)} \quad (4)$$

Calculated b0-parameters and screening energies are listed in **Ta**ble-2.

Table-2: Screened energies for various EQPET molecules

e*(m*/me, e*/e)	Screening Energy Us (eV) dde*	dde*e*	b0 (pm) dde*	dde*e*
(1, 1) ; Normal electron	36	72	40	20
(2, 2) ; Cooper pair	360	411	4	2
(4, 4) ; Quadruplet	4,000	1,108	0.36	1.3
(8,8) ; Octal coupling	22,154	960	0.065	1.5
(208, 1) ; muon	7,579	7,200	0.19	0.20

Kasagi et al[1] gave Us = 310 +- 30 eV for Pd target with 1-10 keV d-beam irradiation, by measuring proton yield from d + d to the p + t + 4.02 MeV reaction channel. Huke et al[10] gave 320 eV for similar beam target experiments. These experimental values considerably agree with theoretical value 360 eV by dde*(2,2), namely EQPET dd molecule with Cooper pair. These values for screening energy are very large, compared to 72 eV for ddee (D_2).

3. Formation of TSC

We have proposed multi-body deuteron fusion process by formation of TSC (Tetrahedral Symmetric Condensate) and OSC (Octahedral Symmetric Condensate)[8,9]. Some numerical results were given by EQPET analyses, which could explain 3-78 W/cc power with 1E11 f/s/cc to 1E13 f/s/cc of ^{4}He-atoms production by 4D and 8D fusion reactions, with less than 10 n/s/cc neutron production.

There are remained open questions about where TSC is formed. We have proposed two mechanisms.

A) In the near surface region of PdDx cathode, deuterium full loading (x=1; PdD) may be attained by electrolysis, gas discharge or gas-permeation, at least locally. No experimental techniques have been developed to measure local distribution of x-value, although we know that it should be key information. With very small density (namely 1 ppm was assumed in our paper[8]) PdD_2 states may exist.
Trapped D in Bloch potential has discrete energies with 32 meV ground state and 64 meV one phonon energy for excited states. Over 0.22 eV, all D-ions in lattice diffuse out of solid. By exciting with external UV or EUV laser, due to classical Drude model, transient cluster of TSC can be formed with certain probabilities[8].

B) We know surface of metal is complex and fractal with ad-atoms, dimers and corner-holes, for example. Somewhere, for instance in corner holes, incident D_2 molecules are trapped by dangling bonds. Free D_2 molecule has freedom of rotation and vibration. Trapped D_2 would lose freedom of rotation, but can vibrate for changing distance between pairing two deuterons, and waiting for incoming D_2 molecule.
When incoming D_2 molecule meets near to trapped D_2, incoming D_2 rotates with 90 degrees maximum against waiting D_2 molecule to neutralize charge (minimize Coulomb repulsion energy) and form an orthogonally coupled two D_2 molecules when there meets coherence in vibration modes and electron-spins are anti-parallel for counter part electrons. In this way, TSC may be formed on surface. Since the scenario is still very speculative, we need further substantiating studies.

4. 4D Fusion by 4d/TSC Itself

Trial to explain excess heat with ^4He production based on d + d two-body fusion in condensed matter has two intrinsic difficulties to overcome;

(1) Maximum level of d-d fusion rates should saturate on the order of 10 mW/cc (1E+9 fusion/s/cc), due to the constraint of trapped deuterons in Bloch potential and not large S(0) value (1.1E2 keVbarn) enough to increase power level[11].
(2) The dreamed scenario of d + d to ^4He + lattice-energy (23.8MeV) has no reason supported by nuclear physics – see Appendix.

Macroscopic reaction rate (yield) of two-body and multi-body fusion rate with D-cluster condensates as TSC and OSC is given by,

$$Y = N_{nd}\lambda_{nd} \quad (5)$$

Here, N_{nd} is the time-averaged nD-cluster (n=2, 4, 8) density and λ_{nd} is the microscopic modal fusion rate[8,9], given by

$$\lambda_{nd} = v(S_{nd}(E)/E)\exp(-n\Gamma_{nd}) \quad (6)$$

$S_{nd}(E)$ is the astrophysical S-factor and Γ_{nd} is Gamow integral for d-d interaction in nD-cluster system. The microscopic modal fusion rate for 4D cluster is defined by EQPET as,

$$\lambda_{nd} = a_1^2\lambda_{nd(1,1)} + a_2^2\lambda_{nd(2,2)} + a_4^2\lambda_{nd(4,4)} \quad (7)$$

Here EQPET assumes that the total wave function Ψ_{4D} of 4D-cluster is approximated with linear combination of partial wave functions for EQPET molecules, $\Psi_{(1,1)}$, $\Psi_{(2,2)}$ and $\Psi_{(4,4)}$, for normal electron (1,1) state, Cooper pair (2,2) state and quadruplet state (4,4), respectively.

$$\Psi_{4D} = a_1\Psi_{(1,1)} + a_2\Psi_{(2,2)} + a_4\Psi_{(4,4)} \quad (8)$$

In our previous papers[8,9], we have given calculated microscopic fusion rates for EQPET molecules, dde(1,1), dde*(2,2) and dde*(4,4), using,

$$\lambda_{nd(m,Z)} = v(S_{nd}(E)/E)\exp(-n\Gamma_{nd(m,Z)}) \quad (9)$$

And the Gamow integral for dde*(m,Z) EQPET molecule is given by,

$$\Gamma_{nd(m,Z)} = \int r_0^b (Vs(r) - E)^{1/2} dr/((h/\pi)/(2\mu)^{1/2}) \quad (10)$$

Some numerical results are re-listed in **Table-3**.

Table-3: Typical results by EQPET/TSC for fusion rates, power level and products, for TSC in PdDx, assuming N_{4D} = 1E+22 (1/cc)

Multi-body	Microscopic fusion rate (f/cl/s)	Macroscopic Yield (f/s/cc) , Power (W/cc)	Ash (fusion products)
2D	1.9E-21	1.9E+1 (f/s/cc), 1.9E-11(W/cc)	Neutron; 10 n/s/cc
3D	1.6E-13	1.6E+9 (f/s/cc), 1.6E-3 (W/cc)	Tritium; 8E+8 t/s/cc
4D	3.1E-11	3.1E+11(f/s/cc), 3.1E+0 (W/cc)	Helium-4; 3E+11 h/s/cc

Here typical break-up channels of reactions are;

$$2D \rightarrow n + {}^3He + 3.25 \text{ MeV } (50\%), \quad p + t + 4.02 \text{ MeV } (50\%) \quad (11)$$

$$3D \rightarrow t + {}^3He + 9.5 \text{ MeV} \quad (\text{about } 50\%) \quad (12)$$

$$4D \rightarrow {}^4He + {}^4He + 47.6 \text{ MeV} \quad (\text{almost } 100\%) \quad (13)$$

This calculation (Table-3) shows that 4d/TSC fusion is clean with ^{4}He main ash with very low neutron production (less than 1E-10 order of ^{4}He rate), although power level (about 3 W/cc-Pd) is rather low. Tritium production rate (1E-3 order of ^{4}He rate) is however rather high.

Modal fusion rate given by Eq.(7) for 4D fusion is attributed almost 100% to the quadruplet EQPET molecule dde*(4,4) sate. Therefore, the accuracy of this model is closely related to what the minimum size sate of 4d/TSC is.

Later[9], we have considered that the squeezing motion of TSC can be more simply treated by a semi-classical model, because of the three-dimensionally constrained motion of 4d and 4e particles in TSC into the central focal point. **Figure-1** illustrates the feature of the semi-classical treatment. Every particle in TSC can make central squeezing motion with same velocity, to keep charge neutrality of total TSC system – in other words to satisfy minimum system energy state (as calculated by the variational principle of quantum mechanics). Therefore this squeezing motion can be treated as Newtonian mechanics until when 4 deuterons get into the range (about 5 fm) of strong nuclear interaction.

In Fig.1, TSC will form in the near surface region of condensed matter by the mechanism A) or mechanism B) as discussed in Session 2, with certain probability depending on methods of experiments and near-surface physics of condensed matter :Step-1): (TSC forms). Then TSC starts Newtonian squeezing motion to decrease linearly its size from about 100 pm radius size to much smaller size and reaches at the minimum size state: Step-2): (Minimum TSC). Classical squeezing motion ends when 4 deuterons get into the strong force range (5 fm) and/or when 4 electrons get to the Pauli's limit

(about 5.6 fm for e-e distance). Here for the Pauli's limit, we used the classical electron radius of 2.8 fm, which is determined by equating the static Coulomb energy (e^2/R_e) and the Einstein's mass energy (m_ec^2) to obtain,

$$Re = e^2/(m_ec^2) = 2.8 \text{ fm}$$
; classical electron radius (14)

Since the range of strong interaction (about 5 fm) is comparable to the classical electron diameter (5.6 fm), as shown in Fig.1-2), the intermediate nuclear compound state ^{8}Be* will be formed just after the minimum size state ("over-minimum" state); Step-3): ^{8}Be* formation. Immediately at this stage, 4d-cluster shrinks to much smaller size (about 2.4 fm radius) of ^{8}Be* nucleus, and 4 electrons should go outside due to the Pauli's repulsion for fermions. Shortly in about few fs or less (note; Life time of ^{8}Be at ground state is 0.67 fs), ^{8}Be* will break up to two ^{4}He particles, each of which carries 23.8 MeV kinetic energy; Step-4): Break up.

When 4 electrons start to separate, 4 deuterons suddenly start to *feel* mutual Coulomb repulsion. Nuclear interaction at this stage can be approximately treated by STTBA (Sudden Tall Thin Barrier Approximation)[14].

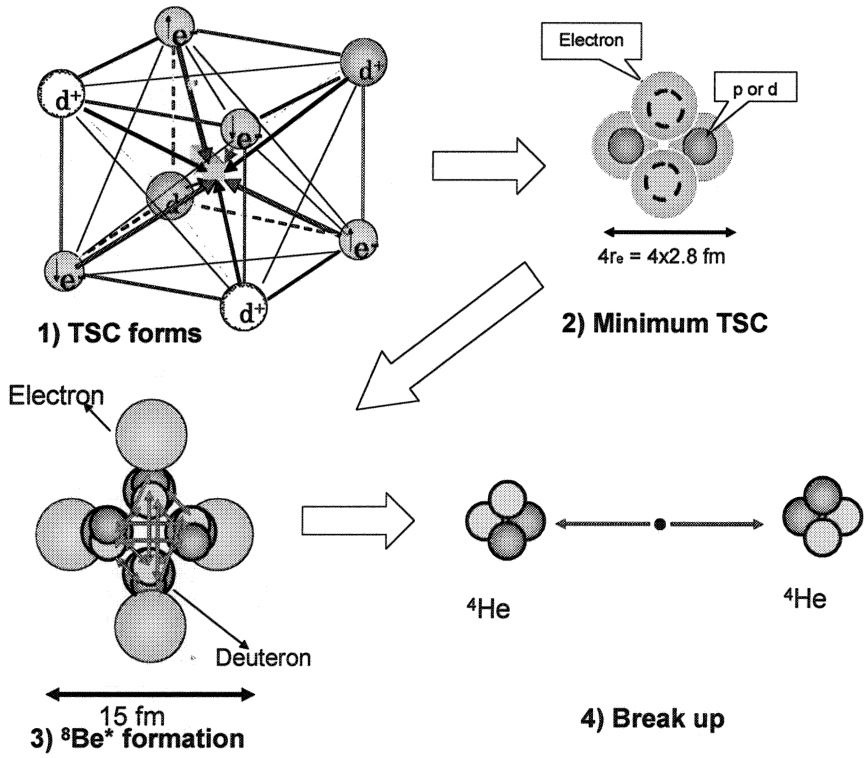

Fig.1: Semi-classical view of squeezing motion of TSC

Gamow integral of STTBA[9] is given by,

$$\Gamma_{nd} = 0.218(\mu^{1/2})\int_{r0}^{b}(V_B - E_d)^{1/2}dr \quad (15)$$

And bare Coulomb potential is,

$$V_B(r) = 1.44Z_1Z_2/r, \quad \text{in MeV and fm units} \quad (16)$$

And barrier penetration probability is,

$$P_{nd}(E_d) = \exp(-n\Gamma_{nd}) \quad (17)$$

For $V_B >> E_d$,

$$\Gamma_{nd} \simeq 0.523(Z_1Z_2\mu)^{1/2}(b^{1/2} - r0^{1/2}) \quad (8)$$

Using b = 5.6 fm and r0 = 5 fm, we obtained; P_{4d} = 0.77 with V_B = 0.257 MeV and

Using S_{4d} value in Refefences-8 and 9, we obtained: λ_{4d} = 2.3E-4 f/s/cl. This microscopic fusion rate is 1E+7 times larger value than one given in Table-3. We consider therefore that EQPET model gave significant underestimation for 4D fusion rate when rigid constraint of motion in three dimensional space is attained as shown in Fig.1.

Macroscopic reaction rate with N_{4D} = 1E+22 (1/cc) is then given as Y_{4D} = 4.6E+18 f/s/cc-Pd, which is equivalent to 46 MW/cc-Pd and 23 keV/Pd-atom.

In ICCF11, El Boher et al reported[5] results of very intense excess power for about 17 hours, by their super-wave D_2O/Pd-thin-pate electrolysis technique, to give 24.8 keV/Pd-atom. This experimental value is close to 23 keV/Pd-atom by the over-minimum state 4D fusion by 4d/TSC. El Boher et al did not measure helium, and gave no information about nuclear mechanism behind. If they will find corresponding level of helium atoms, we can say very good agreement between experiment and theory.

If we apply λ_{4d} = 2.3E-4 f/s/cl for modal fusion rates in Table-3, neutron production level drops to the order of 1E-17 of ^{4}He production rate and tritium production rate also drops to the order of 1E-9 of ^{4}He production rate. These results are nearer to experimentally observed levels of neutrons and tritium-atoms in CMNS studies[12].

6. Conclusions

Some essential results of cluster fusion model for condensed matter nuclear effects were summarized in this work. Major experimental results as d-d screening effects, ^{4}He production without visible neutron emission, correlation of excess heat and ^{4}He production, very intense excess power level as 46 MW/cc-Pd, selective transmutations and fission-like products, were almost consistently explained by the EQPET/TSC models.

However, theories are still in primitive stage and further elaborations are expected. Some key conditions like TSC formation mechanism and places are speculative, and we need substantiation of problems in views of condensed matter and surface physics,

Acknowledgments

The author acknowledges Dr. Y. Iwamura, Mitsubishi Heavy Industries Co. and Dr. F. Celani, INFN Frascati for their kind discussions to this work

References

1. J. Kasagi, et al: J. Phys. Soc. Jpn. 71(2002)2881.
2. A. Takahashi, et al.: Physics Letters A, 255(1999)89.
3. M. McKubre, et al: Proc. ICCF10, Boston, 2003, see http://www.lenr-canr.org/
4. Y. Arata: Il Nuovo Aggiatore, Jan. 2005, p.66-71
5. El Boher, et al: ppt slide of ICCF11, Marseilles, November 2004, see http://www.iscmns.org/
6. Y. Iwamura, et al.: Jpn. J. Appl. Phys., 41(2002)4642
7. G. Miley, J. Patterson : J. New Energy, 1(1996)5
8. A. Takahashi: Deuteron cluster fusion and ash, Proc. ASTI5 WS, Italy, March 2004, see http://www.iscmns.org/
9. A. Takahashi: Deuteron cluster fusion and related nuclear reactions in metal-deuterium/hydrogen systems, Recent Research Developments in Physics,

Transworld Research Network, India, issued June 2005

10. A. Huke: Ph D thesis, Technical University of Berlin, 2004
11. A. Takahashi, et al.: Fusion Technology, 27(1995)71
12. see many papers in http://www.lenr-canr.org/
13. A. Takahashi, et al: Jpn. J. Appl. Phys., 41(2001)7031
14. A. Takahashi: TSC-induced nuclear reactions and cold transmutations, Proc. Siena Workshop on Anomalies in Metal-D/H Systems, 13-16 May 2005